Final Degree Project

**Bachelor's degree in Industrial Technology Engineering**

# Modeling and sizing of a hybrid powertrain for an industrial mobile robot

**REPORT**

**Author:** Tomàs Montobbio de Pérez-Cabrero

**Director:** Ramon Costa-Castelló

**Date:** January 2021


Escola Tècnica Superior
d'Enginyeria Industrial de Barcelona

# Abstract

The transition from conventional combustion engines to greener solutions without compromising the performance of the powertrain is one of the major challenges of today's industry. Fuel cells are receiving increasing attention when combined with an energy storage system to form a hybrid powertrain, as they have zero on-board emissions and present an interesting solution to the propulsion's dilemma. This is because they overcome the limitations of the present alternative propulsion systems while having a positive impact in the environment if they are adopted worldwide.

In this project a study of the modification of the powertrain of an industrial mobile robot is performed. From the actual plug-in battery electric powertrain, a battery-fuel cell hybrid configuration is proposed. Different hybrid configurations are modelled, sized and tested through simulation. The optimal solution is found through the comparison of different objective parameters that indicate the powertrain's performance in different battery charge levels. Although the passive configuration presents the best performance indicators, the impossibility to integrate its elements makes that the selected powertrain configuration is the semi-active one. A 150 W fuel cell is chosen, and a control system is modelled to manage the complementary contribution of the fuel cell and the actual 2200 mAh battery.

# Contents

# Abbreviations

**AC** Alternating current 9

**BEV** Battery Electric Vehicles 9

**BJT** Bipolar junction transistor 32

**CD** Charge-depleting 11

**CL** Catalyst Layer 21

**CS** Charge-sustaining 11

**D** Duty cycle 32

**DC** Direct current 9

**DOD** Depth of discharge 43

**EMS** Energy Management Strategy 58

**EoL** End of Life 44

**ESS** Energy Storage System 33

**FC** Fuel Cell 13

**FCHV** Fuel Cell Hybrid Vehicles 11

**GDL** Gas Diffusion Layer 21

**HB** Half-Bridge Converter 35

**ICE** Internal Combustion Engines 7

**IGBT** Insulated-gate bipolar transistor 32

**lpm** Liters per minute 42

**MOSFET** Metal–oxide–semiconductor field-effect transistor 32

**MPL** Micro-Porous Layer 22

**PEM** Proton-Exchange Membrane / Polymer Electrolyte Membrane 16

**PEMFC** PEM Fuel Cell 14

**PHEV** Plug-in Hybrid Electric Vehicles 11

**PLC** Programmable Logic Controller 100

**PM** Permanent-Magnet 9

**PWM** Pulse-Width Modulation 32

**SC** Supercapacitor 25

**SOC** State of Charge 11

**std lpm** Standard liters per minute 42

**ZEV** Zero-Emission Vehicles 8

# Chapter 1

# Introduction

## 1.1 Project's origin and motivation

This project is born from a proposal to collaborate with the Institute of Robotics and Industrial Informatics (IRI), an investigation center of the Polytechnic University of Catalunya (UPC). The project is the result of the union of two of the lines of work in which the center has been working for the past years: the implementation of hydrogen fuel cells in industrial applications and the investigation of autonomous industrial mobile robots that move objects in warehouses and other industrial plants.

Fuel cells represent a solution of increasing interest in the search of a green source of power for automotive and industrial applications, as in its reaction only water and heat are formed. As no pollutants that can be harmful for the environment are generated in its process to obtain electricity, it can become one of the major solutions to global warming if its drawbacks are overcome and fuel cells are adopted worldwide in expense of the sources of power based in petroleum. One of these drawbacks is the slow transient response of the fuel cells; for this reason, it is common that these devices incorporate an energy storage system that allows them to work alongside.

The starting point of the project is an autonomous industrial mobile robot that works with an electric powertrain consisting in a battery feeding an electric motor. The autonomy of the robot is not high, and its performance can be enhanced combining the

actual battery with a fuel cell acting as a second source of power. In this project, a study of the best way to implement this hybrid powertrain and its sizing will be done. To do so, different configurations will be considered and tested, and a comparison will be performed with objective parameters.

## 1.2 Previous requirements

This project is the Final Degree Project of a Bachelor's degree in Industrial Engineering, and in it, knowledge of several fields acquired throughout these 4 years is displayed. As a consequence, experience in these engineering areas is necessary in order to carry out this project. The two main engineering fields in between which this project sits are automation and electronics. Related to the automation field, knowledge in transfer functions, controllers and signal response is necessary. On the other hand, in the electronic field, knowledge of passive and active circuit components is needed, as well as in the power devices such as the batteries or fuel cells. Other engineering fields that will also be touched are, for example, thermodynamics, automotive systems or economics. Finally, in order to perform the study, knowledge in data processing and programming with *Python*, simulation with *Matlab's Simulink* and LaTeX writing is necessary.

## 1.3 Objectives and scope of the project

In this project, a comparison study will be performed between different implementations of a hybrid powertrain based in a fuel cell and a battery for an existing industrial mobile robot. The main objective of the project is, then, to model and size the optimal hybrid powertrain for the robot. In order to fulfill it, different and more specific objectives are set:

- To present the actual state of the automotive industry: the different types of propulsion systems available and its strengths and weaknesses.

- To present the fuel cell technology and why its introduction to the automotive industry can be beneficial.
- To model and size different fuel cell-battery hybrid powertrains and test them through simulation. Not only the power sources of the hybrid powertrain will be sized, but also all the other components found in the circuit and its control system.
- To find the optimal solution for the robot by analyzing its needs and comparing through objective parameters the performance given by every configuration proposed. This comparison will take into account constructive (correct integration of the system's components), performance (minimization of hydrogen consumption and maximization of the robot's autonomy) and component degradation aspects. The optimal powertrain should not only ensure the fulfillment of the electric motor's consumption needs and the industry requirements, but also minimize the initial cost of the powertrain and its energy consumption costs, as well as ensure safe operating conditions in order to enhance the fuel cell and battery's lifetime.
- To give an economic and environmental overview of the project and the cost of the proposed implementation.

The scope of the project is focused in helping the IRI-UPC institute with their research and their investigations in broader projects that can be beneficial for the industry, concerning the fuel cells' implementation in industrial equipment or the development of autonomous industrial robots. Also, the project has the intention of having a small impact in whoever it reaches, to increase the perception of the need to leave behind the conventional transportation systems and gain confidence in alternative propulsion ones.

# Chapter 2

# Introduction to alternative propulsion systems

## 2.1 From IC engines to electric powertrains

Although electrically-propelled vehicles first appeared in the 19th century, in the beginning of the 20th century they suffered a worldwide decline in their production and research in expense of the rise of the Internal Combustion Engines (ICE) vehicles. Several factors influenced in the stoppage of the development of such technology. In the first place, the price drop-down of ICE vehicles, thanks to the introduction of mass production of gasoline-powered vehicles by Henry Ford and the low price of the oil after worldwide discoveries of large petroleum reserves, made it impossible for the battery-electric vehicle to compete with the prices of the ICE vehicles. The high price of the lead-acid batteries used at the time made the electric car twice as expensive as the gasoline one. In addition, the batteries needed a long time to recharge and offered low top speed and much shorter ranges than the levels achieved by the more powerful IC engines.

After this brief initial time of electric propulsion systems' development, the gas-powered vehicles took over the control of the industry of transportation for over a century. It was with the energy crises of the 1970s and 1980s that the world became

perceptive of the need to promote the development of renewable energies and an alternative to gasoline-powered propulsion systems. Not because of its effectiveness, that was indisputable, but for its underlying problems. There are two key problems with continued use of fossil fuels [1]. The first one is that its amount is limited and sooner or later they will be depleted. It is believed that the production of fossil fuels has peaked its demand in 2019, where they meet about an 85% of the world's energy demand [2]. The crisis unleashed by the pandemic of Covid-19 has accelerated the time of this peak, where a combination of a drop on the energy demands and an increasing capacity of renewable energies will make it difficult for fossil fuel demands to recover its previous levels. It is expected that this demand will decline to a share between 20% and 65% of the world's total energy needs by 2050 [3]. The second problem with fossil fuels is that their combustion produces several of the most important pollutants responsible for the climate change: not only $CO_2$, nitrogen oxides ($NO_x$) and $SO_2$, but also volatile organic compounds and heavy metals. Environmental effects due to the increase of these greenhouse gases are serious problems, such as global warming, acid rains, pollution, ozone layer depletion and so on. It is estimated that the worldwide environmental damage adds up to five trillion dollars each year, approximately [1]. For this reason, electric powertrains have been developed in the past few decades, as they are the cleanest propulsion method available. Nevertheless, while the source of the electricity that feeds their system isn't fully renewable, we can't consider them Zero-Emission Vehicles (ZEV), as in the process of procurement of the electricity lots of greenhouse gases are produced.

## 2.2 Types of electric propulsion systems

An electric powertrain is a propulsion system that is powered through electricity. Electric vehicles have seen a resurgence thanks to technological developments and due to the need of finding alternative propulsion systems less pollutant than the conventional ones. These technologies have advanced through different fronts, so different types of electric powertrains can be found. However, for the purpose of this project, it is only

necessary introduce two major types: pure battery electric vehicles and different hybrid models.

### 2.2.1 Battery electric powertrain

The vehicles with this type of powertrain are called Battery Electric Vehicles (BEV). In this type of propulsion system, the only source of power is the chemical energy that a pack of rechargeable batteries contain and provide to an electric motor in form of electricity. Once the energy stored is used, the batteries can recharge when the vehicle is plugged-in, but they can also recover energy with a regenerative braking system. This type of powertrain replaces the IC engine with 3 main components (a basic battery electric powertrain is shown in Figure 2.1):

- *Pack of batteries*: stores the energy provided by an external connection to provide power to the vehicle. The early lead-acid batteries used in the beginning of the development of electrical powertrains have been replaced mostly by lithium-ion batteries. The battery pack consists on electrochemical cells that are put together in groups, which are then assembled in multiple modules that form the overall pack.

- *Electric motor*: is the element responsible for transforming the electric current in mechanical power to turn the drive shaft and the wheels. Traditionally, brushed DC electric motors were used, but recently it is more common to use brushless permanent-magnet (PM) AC motors or induction motors, as they are simpler to build and have no brushes that can wear out.

- *Motor controllers*: their mission is to coordinate in a predetermined manner the performance of the electric motor. They are responsible for starting and stopping the motor, selecting forward or reverse rotation and of regulating the amount of power needed in the motor to fulfill the torque needs, after receiving a signal of the different sensors and potentiometers. Besides, the controller converts the DC power supplied by the battery pack either in pulsed DC or AC, depending on the

motor type, and also manages regenerative braking. Finally, it can also perform various safety checks, as anomaly detection or protecting against overloads and electrical faults.

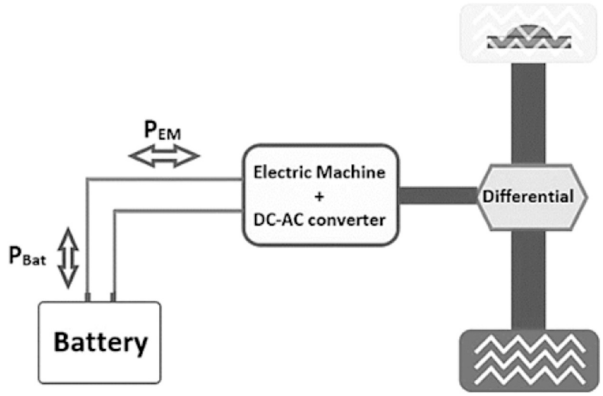


**Figure 2.1:** *Schematic of the main components of a Battery electric powertrain [4]*

Following the environmental concerns around conventional vehicles, BEV have aroused as the primary model of alternatively powered vehicles, as in operation they produce no greenhouse gases or other pollutants. The increasing amount of recharge stations and the possibility of having these at home make more and more people change to BEV. The main drawbacks of BEV's are the same they encountered in the beginning of its development: price and range. In order to increase the latter, a higher capacity of the batteries is needed, but as the capacity grows so does the price. A price of 250$/kWh is estimated for the battery [5]. For a BEV with 200 miles of range, the estimated increment in price with respect to an equivalent ICE vehicle is of 10 200$ [5].

The high price needed to achieve long range levels, makes it interesting to investigate into different types of alternative propulsion systems. The other major types of alternative powertrains are the hybrid configurations.

### 2.2.2 Hybrid powertrain configurations

A hybrid powertrain is a propulsion system that uses two or more different sources of power. Usually, and for the purpose of continuing the discussion of the previous section,

one of these sources is an electric battery. These types of powertrains are known as hybrid electric powertrains. The objectives followed when using hybrid powertrains are multiple and can vary depending on the type of configuration chosen. On overall means, hybrid configurations optimize the performance of the powertrain, meaning different things depending of the objective: a higher efficiency on different work modes, better fuel economy, lower emission levels or longer range. An energy management system through controllers becomes of high importance. Two major types of vehicles with hybrid electric powertrains will be discussed: Plug-in Hybrid Electric Vehicles (PHEV) and Fuel Cell Hybrid Vehicles (FCHV).

The plug-in hybrid electric powertrain combines a conventional ICE with electrical batteries, rechargeable when plugged-in to an external source of power. In this case, the introduction of the electric powertrain to the conventional one follows the intention to achieve better fuel economy, lower emission levels and a better performance when combining both powertrains.

Depending on the electric motor power different approaches are found: mild-hybrids' electric motor can't sustain the vehicle's propulsion on its own, as they aren't powerful enough, and are used to achieve better fuel consumption levels. Normally, the electric motor is used for producing torque and accelerating, when it is more efficient, while the IC engine is best used for maintaining high speeds. On the other hand, all-electric hybrids can be propelled solely with the electric powertrain. In this case latter, different control strategies can be found, depending on the moment where the electric motor is used. A good timing of the controller can bring great energy efficiency that translates in less fuel consumption and pollution. One of the major control tactics is to operate depending on the state of charge (SOC) of the battery, where two modes are found: the first is the charge-depleting (CD) mode, during which the battery powers the electric motor and discharges progressively. After reaching the end of its CD range, a PHEV will switch to charge-sustaining mode (CS), during which the average SOC of the battery is kept constant or the battery is charged, using regenerative braking and power from the engine [5]. The controller switches from CD to CS when the battery reaches a specified low SOC, and can turn again to CD mode if the battery charges up to a high specified

SOC. In this case, the ICE would act as a range extender of the electric powertrain. The most common configuration is the parallel one, where both sources of power are connected to the shaft and can deliver power individually or jointly. A schematic of a parallel configuration of a plug-in hybrid electric drivetrain is shown in Figure 2.2.

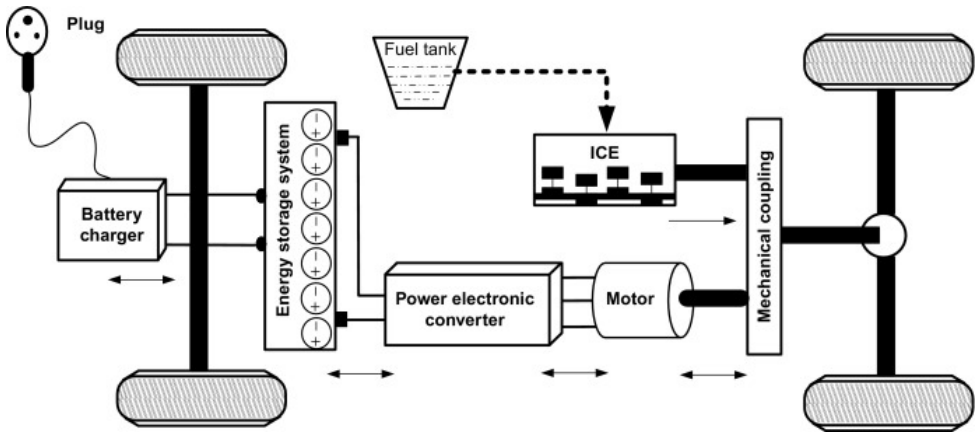


**Figure 2.2:** *Schematic of the main components of a Plug-in Electric powertrain [6]*

ICE-battery hybrid models are an intermediate point in between conventional and electric powertrains and present advantages of both models: they offer good performance and range, as well as a decrease in fuel consumption and the emission of greenhouse gases and other pollutants. However, they still present several drawbacks. Mainly, the use of a combustion engine as one of the sources of power still means that high levels of pollutants are produced (lower than in conventional vehicles, but still considerable). Nevertheless, this type of powertrain can act as a start point in the search of a drivetrain system that overcomes the limitations of the battery electric powertrain but produces no pollutants in operation.

One of the major candidates is the hydrogen fuel cell – battery/supercapacitor hybrid, as it combines the positive characteristics described for the plug-in hybrid, with the addition of using a power source of high efficiency and zero emissions (if the hydrogen is produced using energy from renewable sources) [4]. Nevertheless, before entering in the description of this hybrid architecture and the different control possibilities, technical aspects regarding the fuel cell will be discussed.

# Chapter 3

# Hydrogen fuel cells

## 3.1 Introduction to hydrogen fuel cells

A fuel cell (FC) is an electrochemical device that converts the chemical energy of a reaction directly into electrical energy, promising power generation with high efficiency and low environmental impact [7]. In the FC a redox reaction between two reactants takes place: a gaseous fuel and an oxidizing agent. Though fuel cells could, in principle, process a wide variety of fuels and oxidants, of most interest today are those fuel cells that use hydrogen as their fuel, and the oxygen as the oxidizing agent, as only water is produced in their reaction, but also because of the high reactivity of hydrogen when suitable catalysts are used and its high energy density when stored cryogenically [8]. Additionally, oxygen is easily available from ambient air and economically stored in a closed environment, and hydrogen can be used in its pure form (expensive to obtain) but also in other states: either as a mixture with other gases (such as $CO_2$, CO...), or as the hydrogen present in hydrocarbons such as natural gas, $CH_4$, or liquid hydrocarbons such as methanol [1]. However, in automotive applications, the FC requires hydrogen provided either directly from onboard storage or by on-board reforming of liquid hydrocarbons. The advantage of using direct hydrogen is that no harmful emissions are emitted, as water is the only product of the reaction. However, on-board hydrogen storage is challenging due to lack of infrastructure to support mass-market hydrogen dis-

tribution, as well as presenting issues related to refueling procedures and high pressurization requirements [9]. On the other hand, on-board reforming of hydrogen-bearing fuels doesn't present these issues, as fuel storage is easier and handling procedures and distribution infrastructure are better established. Nevertheless, on-board reforming results in significantly lower fuel economy [9] and the by-products generated include CO, which must be reduced to levels acceptable by the fuel cell stack, and greenhouse gases as CO2, which is undesirable in the search of a ZEV.

The basic physical structure of a fuel cell consists of an electrolyte layer in contact with a porous anode and cathode on either side [8]. In hydrogen FCs, the fuel (hydrogen) undergoes oxidation at the anode and splits between positive ions and electrons through the use of a catalyst. Through an external circuit, the electrons travel from the anode to the cathode, producing direct current electricity. These electrons are used to reduce oxygen at the cathode, forming negative oxygen ions. The electrolyte layer allows ions (depending on the type of fuel cell either positively or negatively charged) to move between the two sides of the cell. For example, in a proton-exchange membrane fuel cell (PEMFC), positively charged ions (protons) are allowed to travel from the anode to the cathode, while in a solid oxide fuel cell, negatively charged oxygen ions do the opposite way. In both cases, positive hydrogen and negative oxygen ions react, forming water and heat. A schematic representation of a hydrogen FC with the reactants, products and ion conduction flow directions is shown in Figure 3.1.

It is interesting to analyze the role of the fuel in the generation of electricity in fuel cells in comparison to other electrochemical conversion processes. Typically, in order to generate electricity from the chemical energy of a fuel, several energy conversion steps are needed. For example, and in most conventional power generation methods:

1. The fuel is combusted, thus converting its chemical energy into heat.
2. The heat is used to boil water and generate steam.
3. Steam is used to run a turbine, thus converting its thermal energy into mechanical one.

4. Mechanical energy is used to run a generator that converts mechanical energy into electricity.

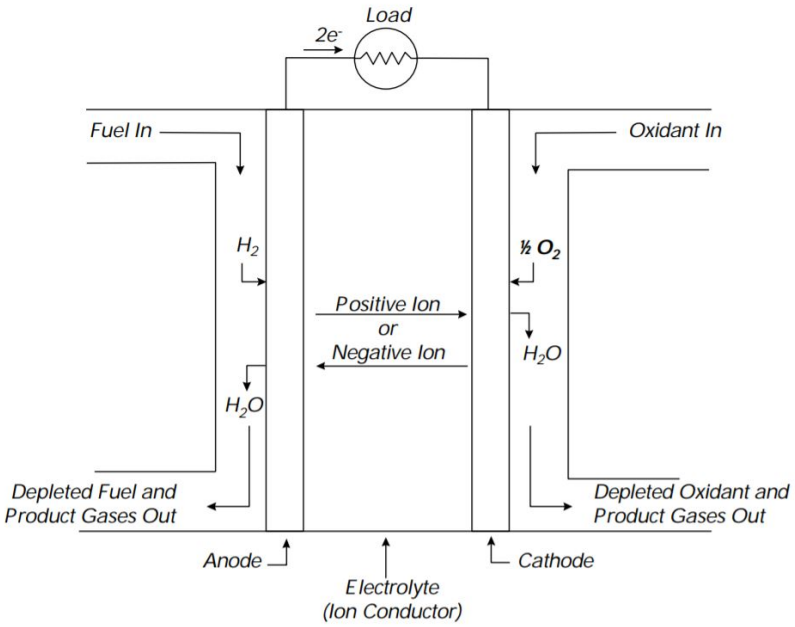


**Figure 3.1:** *Schematic representation of a hydrogen fuel cell [8]*

On the other hand, a fuel cell eludes all these processes and generates electricity in a single step [1]. As the intermediate steps of producing heat and mechanical work are circumvented, fuel cells are not limited by thermodynamic limitations of heat engines such as the Carnot efficiency [7]. In addition to that, no moving parts are involved, avoiding a possible source of low efficiency transmission and allowing the fuel cell to achieve high levels of efficiency. Finally, as combustion is not necessary, the power is produced with minimal pollutants.

Once the differences in operation between a FC and conventional power generation methods have been seen, a comparison with another electrochemical device that shares a level of resemblance with the FC can be of interest: an electric battery. Although the FC has components and characteristics similar to those of the battery, it differs in several aspects. They both follow the same principle of operation, where the electricity is generated from the mobility of electrons going from the anode to the cathode, and use

a substance that is oxidized and another one that is reduced. However, unlike batteries, the fuel cell theoretically has the capability of producing energy for as long as the fuel and the oxidizing agent are supplied to the electrode compartments, whereas the battery is an energy storage device that generates electrical energy by electrochemical reactions with reactants that are already in the battery, and will cease to produce it when the chemical materials that participate in the reaction are depleted [1]. Because of this, a battery presents a discharged state, and can be recharged (secondary batteries) by applying electricity from an external source, which reverses the electrochemical reactions and allows to repeat the process once recharged. On the other hand, in a hydrogen FC, hydrogen is required to continuously feed the anode compartment, as oxygen also continuously replenished (from ambient air) in the cathode one, allowing the chemical reaction to sustain. Though it has been said that the FC can't be discharged and has the capability of theoretically producing energy for as long as the electrodes are supplied with reactants, in reality, degradation, primarily corrosion, or malfunction of components limits its practical operating life [8].

Other notable differences between the battery and the fuel cell exist. For example, unlike in a battery, fuel cell's electrodes don't undergo chemical changes. Finally, another difference between the fuel cell and the battery is that the first one generates waste products: the reaction produces water and much higher levels of heat than the ones produces in a battery, and its system is required to manage those and drive them out.

## 3.2 PEM fuel cells

### 3.2.1 Principle of operation and basic considerations

Of the multiple types of fuel cells, the literature seems to agree that proton-exchange membrane (PEM) fuel cells are the most suitable choice for automotive applications, due to its fast start-up and high power density, which offers low weight, cost and volume [10]. Moreover, PEM fuel cells operate in low temperatures (generally between

60–80 ºC, up to 100ºC), which allows good performance in discontinuous operations and immediate response to changes in power demands [8]. The proton-exchange membrane fuel cell is also known as polymer electrolyte membrane fuel cell, the acronym of which remains intact: PEMFC. The differential component of this cell is its polymer membrane acting as the electrolyte layer. It is impermeable to gases, creating a physical barrier between the anode and cathode compartments to prevent the fuel and the oxidizing agent streams from directly mixing, but as the name implies, it conducts protons. As the positively charged ions are the ones allowed to travel from one side to the other of the electrolyte, the movement that appears in the PEM fuel cell is from the anode to the cathode. Having seen that, and although several intermediate steps and side reactions can take place, the main reactions happening in a fuel cell can be described:

- *Anode*: the hydrogen fed in the anode splits between its primary constituents. A hydrogen gas molecule consists of two protons and two electrons, giving:

$$H_2 \rightarrow 2H^+ + 2e^- \tag{3.1}$$

Consequently, when hydrogen splits between protons and electrons, the first ones travel through the membrane, whereas the electrons will travel through the electrically conductive anode and current collectors to an external circuit where they will perform useful work and come back to the cathode [1].

- *Cathode*: the oxygen fed on that side of the cell meets with the protons that went through the membrane and the electrons that came through the electrode:

$$1/2O_2 + 2H^+ + 2e^- \rightarrow H_2O \tag{3.2}$$

- *Overall*:

$$H_2 + 1/2O_2 \rightarrow H_2O \tag{3.3}$$

Moving now into a thermodynamic analysis of the chemical reaction, the energy balance of the reaction can be calculated. In order to know how much energy may be

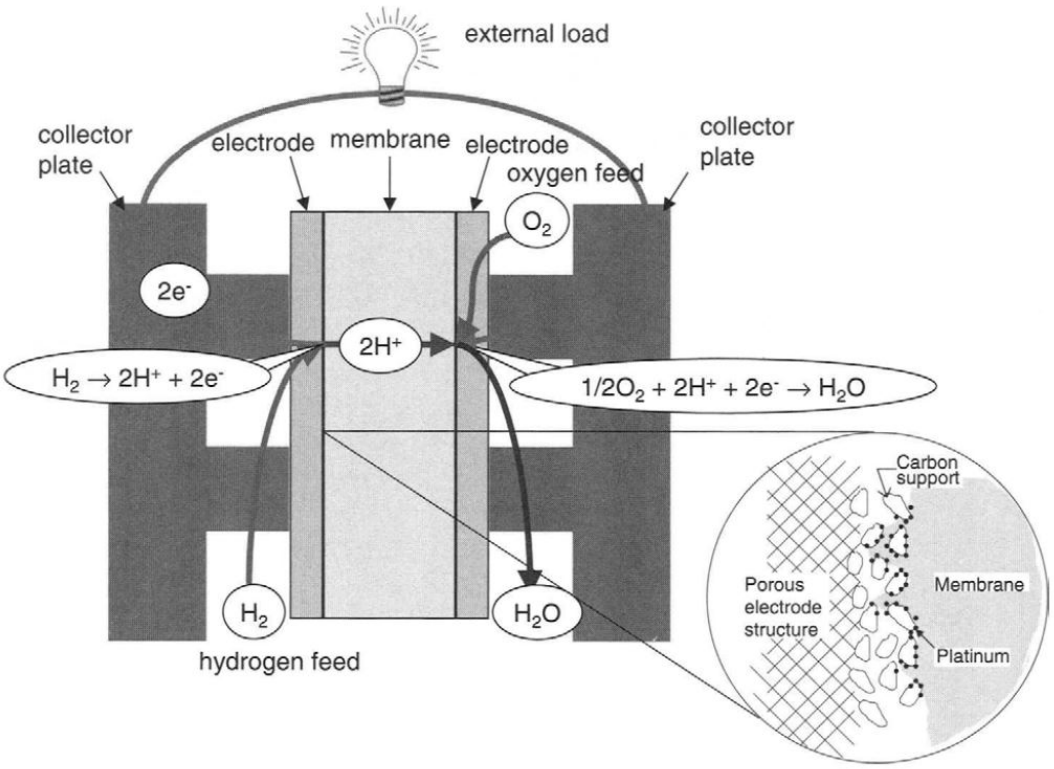


**Figure 3.2:** *Principle of operation of a PEM fuel cell [1]*

extracted from this process, the enthalpy of the reaction must be calculated by doing the difference between the enthalpy of formation of the products and reactants. As the enthalpy of formation of pure substances is 0 by definition, and using the values provided in table 3.1 for standard conditions (25ºC and 1 atm):

| Substance | h$^o{}_f$[kJ/mol] | s$^o$ [$kJ/mol$·K] |
|---|---|---|
| $H_2$ | 0 | 0.13068 |
| $O_2$ | 0 | 0.20515 |
| $H_2O$ | -285,82 | 0.06996 |

**Table 3.1:** *Enthalpies and entropies of formation for FC reactants and products at standard conditions*

This calculation indicates that by every mol of water formed 285,82 kJ of energy will be produced (by convention, a negative sign means that energy is released in the reaction). Nevertheless, not all the energy input can be converted into electricity, as

there will be some waste heat. The portion of the enthalpy of the reaction that can be converted to useful electricity corresponds to Gibbs free energy. It can be calculated using its equation, alongside with the values provided in table 3.1:

$$\Delta G^o = \Delta h^o - T \cdot \Delta s^o = -237,13 kJ/mol \tag{3.4}$$

The theoretical FC efficiency and the waste heat can be then calculated:

$$\eta_{theoretical} = \frac{\Delta G^o}{\Delta h^o} = 0.830 \tag{3.5}$$

$$heat = \Delta h^o - \Delta G^o = -48.69 kJ/mol \tag{3.6}$$

Also, the theoretical potential of the fuel cell at these conditions $E$ can be calculated, as the electric work is equivalent to the calculated $\Delta G$, and where $n$ is the number of electrons associated to the reaction ($n = 2$), and $F$ is Faraday's constant:

$$W_{el} = n \cdot F \cdot E \rightarrow E^o_{theoretical} = \frac{-\Delta G^o}{n \cdot F} = 1.229V \tag{3.7}$$

Although it is usually calculated in standard conditions, it is more useful to obtain these values in the range of operating temperatures of the FC (60-80ºC, and up to 100ºC):

| T $[K]$ | $\Delta h$[kJ/mol] | $\Delta s$[kJ/mol·K] | $\Delta G$[kJ/mol] | heat $[kJ/mol]$ | $\eta_{th}$ | $E_{th}[V]$ |
|---|---|---|---|---|---|---|
| 333,15 | -284,85 | -0,15975 | -231,63 | -53,22 | 0,813 | 1,200 |
| 353,15 | -284,18 | -0,15791 | -228,41 | -55,77 | 0,804 | 1,184 |
| 373,15 | -283,52 | -0,15617 | -225,25 | -58,27 | 0,794 | 1,167 |

**Table 3.2:** *Electrochemical theoretical magnitudes of the FC in its range of operating temperatures*

It's important to remember that the values for useful energy, efficiencies and cell potential are theoretical, and in real operating conditions different losses will appear, resulting in lower values for these variables. Further calculations will be done in future sections, and using polarization curves more accurate estimations will be conducted.

Returning to waste heat management, the power of this waste heat is theoretically around 20% of the consumed fuel power, but can achieve up to 40% of it in real use, so different waste heat recovery systems exist that use thermochemical heat storages of metal hydrides to recover this thermal energy and re-use it for cabin and battery heating [11].

On the other hand, the product of the reaction, water, also needs to be managed. The low-operating temperature of the PEM fuel cells makes that the water produced is liquid. A proper water balance during cell operation has an important impact on cell performance. The electrolyte layer needs to maintain a high water content to stay hydrated, as it is an important factor to ensure high ionic conductivity. If the rate of removal of water is higher than the one of production through the reaction, the membrane may become dehydrated, which would cause it to dry out. As a consequence, a drop of the voltage in the fuel cell and a higher resistance to ionic flow would appear, affecting its overall efficiency [12]. Additionally, dehydration would also negatively affect the adherence of the membrane to the electrode [8]. On the other hand, if the rate of water generation is higher than the one of removal, there will be accumulation of water, which could lead to cell flooding. If the electrodes' porous surface is filled with water, the transportation of reactants to the catalyst layer is impeded. Moreover, excess of water can cause water bands and columns forming inside the flow channels, blocking the flow of gas and severely reducing the FC's performance [12].

In order to have reliable water management systems, precise control of the water levels is needed. However, due to the construction characteristics of fuel cells, their internal parts are not accessible. As a consequence, a sensor that measures the content of water can't be installed [13]. The liquid water fraction can be estimated by multiple methods, for example: by pressure drops, comparing the relative humidity between input and output gases or through model-based methodology that estimates the water fraction from measurable variables [13].

### 3.2.2 Main components

The PEM fuel cell consists on several elements. Between them, the main one is the proton-exchange membrane acting as the electrolyte layer and conducting ions from the anode to the cathode. It is squeezed between two porous and electrically conductive electrodes. The electrodes consist of a gas diffusion layer and a catalytic layer in contact with the membrane. This multilayer assembly is known as the membrane electrode assembly (MEA), which is then sandwiched between the flow plates. A schematic of the different layers found in a PEM fuel cell is found in Figure 3.3. The functions of all elements are exposed in the following section, starting from the membrane and then studying the elements that surround it:

- *Polymer-electrolyte membrane*: it's the central element of a PEM fuel cell. Impermeable to gases, it conducts protons, hence its other name: proton-exchange membrane. The most common membrane is made of perfluorosulfonic acid, a polymer known as Nafion [10], due to its excellent chemical and thermal stability, mechanical strength and proton conductivity [14]. The function of the membrane is to provide a conductive path for protons while separating the reactants. As it has been said, in order to achieve an efficient performance of the membrane, a correct hydration of the membrane is necessary.

- *Catalytic layer (CL)*: in contact with the membrane, it is where the hydrogen splits into protons and electrons, in the anode's CL, and where the oxygen reduction occurs, in the cathode's CL. The catalyst particles are usually platinum supported on carbon, both for the reduction and oxidation reactions. Platinum is an expensive material, and its utilization makes the price of the FC significantly higher. To minimize potential losses, the layer must be as thin as possible, but as it's also desirable to have the maximum contact area possible, thin and small Pt particles with large surface area are used.

- *Gas diffusion layer (GDL)*: located between the catalytic layer and the flow plate, it's found either in the anode and cathode, and it's usually made of porous con-

ductive fiber materials, such as carbon paper and carbon cloth [15]. Thanks to its porosity, it ensures that the reactants effectively diffuse to the catalyst layer, and as it is made of conductive materials, it also transports electrons to and from the catalyst layer [16]. Usually alongside a micro-porous layer (MPL), it also assists in water management by allowing an appropriate amount of water to reach and remain at the membrane for hydration. Nevertheless, excessive amounts of water can flood its pores. Because of that, GDLs are typically wet-proofed with a coating of Teflon.

- *Flow plates*: they provide the pathways for flow of reactant gases and by-products evacuation and give the cell structural rigidity. In a multi-cell configuration, they are called bipolar plates, because they physically and electrically connect the cathode of one cell to the anode of the adjacent one. In the stacking of fuel cells, as it will be explained, the cells are electrically connected in series in order to achieve higher levels of power. For this reason, the bipolar plates must be electrically conductive [1]. Nevertheless, they also have to separate the gases in adjacent cells, so they have to be made of impermeable material.

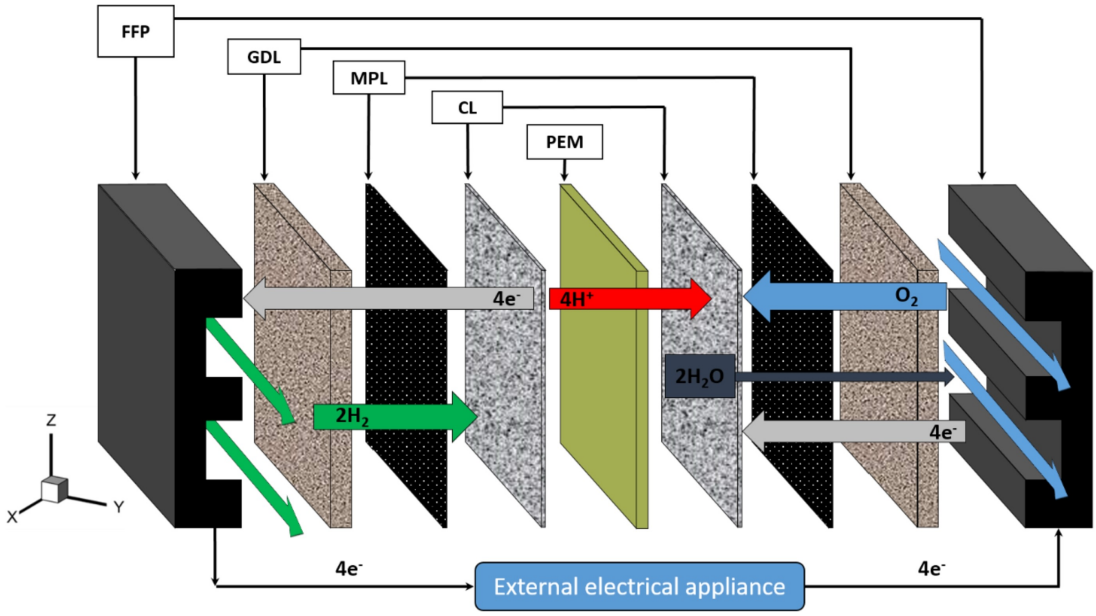


**Figure 3.3:** *Layers of a PEM fuel cell [17]*

## 3.3 FC Stacking

As seen in previous sections, the theoretical potential of a PEM fuel cell is around 1.2V when working in its normal range of operating temperatures. This value is smaller in real situations, where the voltage is lower than 1 V due to different sources of voltage loss, such as activation polarization, internal currents and crossover losses, ohmic losses and concentration polarization [18].

Considering a case where a 1 kW FC is needed; power is the product of voltage and electric current, meaning that if the voltage is lower than 1 V, the current should be higher than 1000 A. To avoid this situation, multiple fuel cells are connected electrically in series and stacked together. The connection between cells is done through the bipolar plates, as they electrically connect the cathode of one cell with the anode of the adjacent one. A representation of this fact can be seen in Figure 3.4.

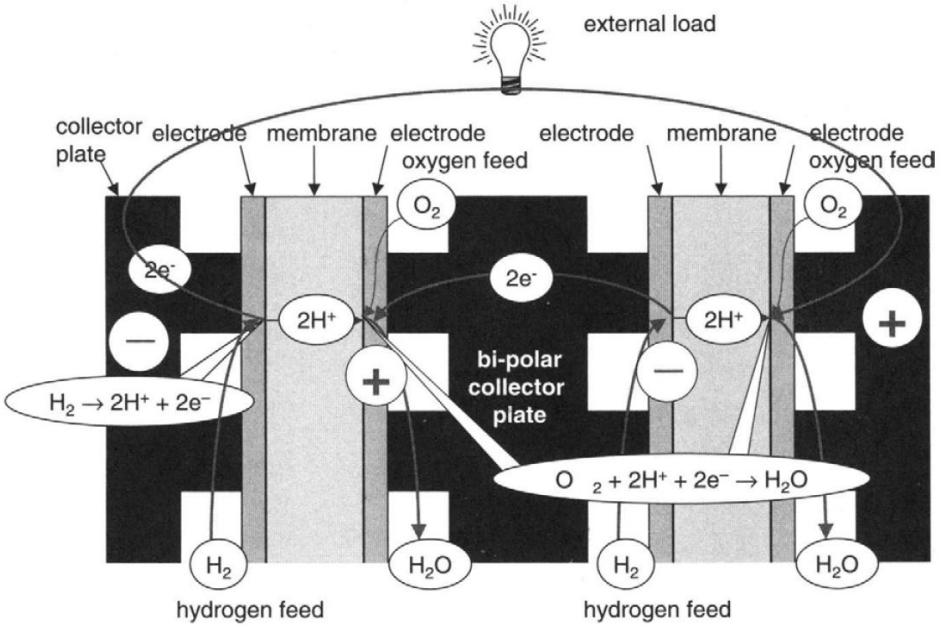


**Figure 3.4:** *Connection of adjacent cells through the bipolar plate [1]*

Increasing the number of cells increases linearly the voltage, thus reducing the current needed to achieve power output requirements. Although the current generated depends on the cell's active area, it also depends on cell voltage: higher cell voltages

lead to smaller current densities. For this reason, in the sizing process of the FC stack, an equilibrium between the cell voltage, number of cells, active FC area and current needs to be found. For this purpose, polarization curves are used, as the one depicted in figure 3.5, where cell potential is plotted against current density (current by unit of area).

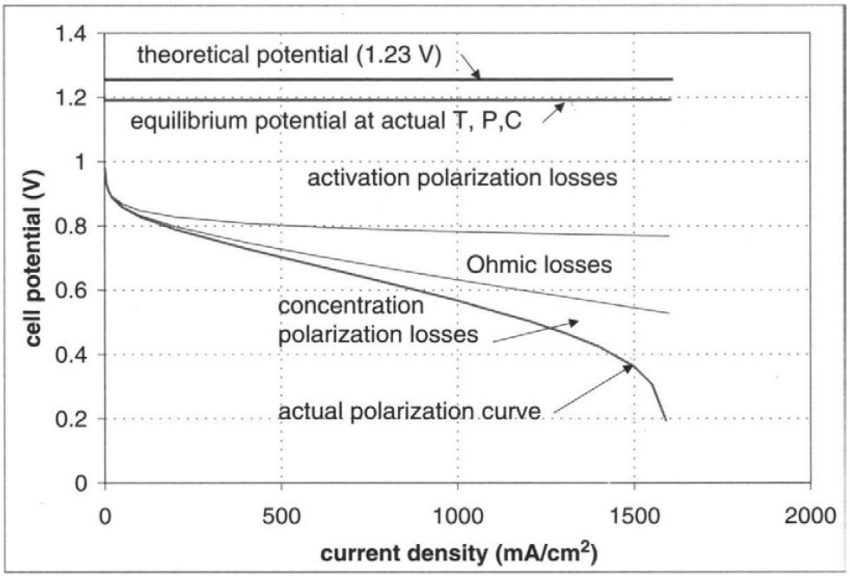


**Figure 3.5:** *Voltage losses in a FC and resulting polarization curve [1]*

In the polarization curve it can be seen the contribution of the different sources of voltage loss commented before. Generally, most FC's manufacturers select a nominal cell voltage in the range of 0,6-0,7 V, but in order to reach some efficiency goals and lower consumption ratios it would be preferable to work around the 0,8 V per cell or even higher [1].

Once fuel cell active area and the number of cells is decided, the fuel cell stack is defined. In commercial fuel cells, the information given by the manufacturer is not from a single fuel cell but from the whole stack. For this reason, the polarization curves that will be treated in future sections will already be a representation of the total stack voltage with respect to total current.

# Chapter 4

# The FC Hybrid

## 4.1 Benefits of the FC hybrid implementation

As it has been said before, fuel cells represent a solution of increasing interest for the propulsion of vehicles, as they offer two main advantages with respect to conventional ICE engines: higher efficiency and zero emissions from the on-board source of power. Nevertheless, in addition to the difficulty of hydrogen production, distribution and storage, they still present some issues related to their performance and lifetime. The main limitation to take into consideration is the slow transient response of the fuel cell which leads to underperforming with fast changing power profiles [19]. Additionally, these fast power variations cause significant drops in the stack hydrogen partial pressure, known as starvation, which rapidly decreases the voltage of the cell, promoting the damage of the fuel cell and leading to premature degradation [4]. To withstand this situation, a hybridization of the powertrain, incorporating an energy storage system, is common. Usually this energy storage device is an electric battery, but it is also usual the use of a supercapacitor (SC) or the combination of both, as the SC offers longer lifetime and higher specific power. Nevertheless, the battery has lower cost per unit of energy stored and offers higher specific energy [20], which can provide extra power for a longer period of time [21]. The use of an energy storage system presents multiple advantages [22]:

1. It can handle the recovery of kinetic energy with regenerative braking
2. It can provide big pulses of power for acceleration or fast changing power profiles
3. It provides back-up if the FC fails, and if it is large enough it can be the sole source of propulsion during a large period of time
4. Makes possible a smaller size of the expensive FC stack, decreasing the overall price
5. Allows to reach higher power levels, when both sources of power are combined

Many times, the battery can be recharged from an external power source and is the main source of power of the vehicle. In that case, the FC is used to extend the vehicle's autonomy and is known as a range extender hybridization, avoiding one of the main drawbacks of electric vehicles thanks to the adoption of the fuel cell.

## 4.2 Hybrid architectures

Generally, hybrid configurations are classified in two different architectures: active, where control elements (typically DC/DC converters) are used, and passive, where the fuel cell and the battery are coupled directly. The choice of the most adequate architecture for a given application depends on the vehicles power and energy requirements, the possible constraints in weight and volume, as well as the characteristics of the fuel cell system and batteries [23].

### 4.2.1 Passive hybrid configurations

In passive configurations, a direct connection to the DC bus by both the battery and the fuel cell is found. Its immediate consequence is the need to carefully design and size its components in order to ensure a similar voltage range operation between the batteries and the FC [23]. The direct coupling of components makes that the voltage in the DC bus is set by the battery's voltage. For this reason, a prior design of the battery

is needed, as its nominal voltage has to be around the voltage of operation of the load. Moreover, the voltage of the battery depends on its SOC, and will decrease as the battery discharges. On the other hand, the fuel cell doesn't have an independent voltage, and its operating voltage only depends on the voltage set by the battery, as it is the one found in the DC bus where it is connected, and their relative impedance. Following its polarization curve, the FC will provide electric current for the given voltage. Thus, one of the main drawbacks of this architecture is that, without an external control of the sharing of power, the fuel cells and batteries don't necessarily work at its maximum efficiency, and dangerous operating conditions can occur [24]. Additionally, the lack of control can cause a degradation in the performance of the FC, because during the dynamic operation the water, heat and streams management can be difficult, leading to problems such as flooding, drying, gas starvation or membrane damage [24]. On the other hand, the advantages of passive configurations with respect to active ones are various. The simpler architecture leads to a lower risk of failure, as well as a lower weight and volume, and a reduced cost in general. Moreover, the absence of the controllers lowers the system's losses, leading to a higher overall efficiency. For these reasons, passive configurations can be a better option for lightweight vehicles, where the energy demand is lower and the hydrogen can be stored in low-pressure on-board storages of metal hydrides.

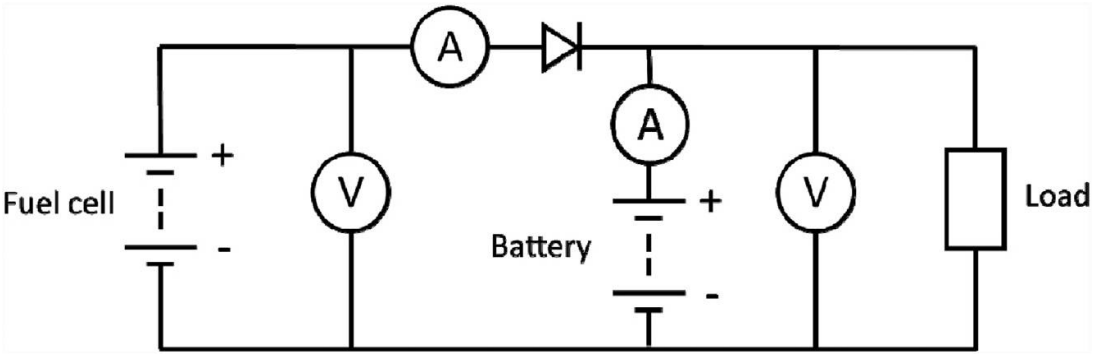


**Figure 4.1:** *Electric circuit schematic of a passive hybrid power system [23]*

In figure 4.1 the electric circuit of a passive hybrid power system can be seen. A diode is used to ensure a safe operation of the FC, as it avoids negative currents that would

be harmful. Also, an inductor can be used to prevent rapid changes in the FC's current that would be harmful for its performance. The power demands of the load are handled by the battery and the fuel cell jointly. If the power required by the load is higher than the one provided by the FC, the battery will provide the extra power to meet the power demands, and if the power provided by the FC is higher than the required by the load, it will serve for both meeting the power requirements of the load and charging the batteries with the extra power. As the battery takes care of the fast variations of power demand, the FC can provide almost constant power, with little variations in its profiles depending on the voltage of the battery and its SOC. This ensures a safe operation of the FC and premature degradation will be avoided. The equations that model this system are:

$$V_{load} = V_{bat} = V_{FC} - V_{diode} - V_L \tag{4.1}$$

$$P_{load} = \begin{cases} P_{FC} - P_{bat}, & \text{if } P_{load} < P_{FC} \\ P_{FC} + P_{bat}, & \text{if } P_{load} > P_{FC} \end{cases} \tag{4.2}$$

There are also several ways to implement a passive hybridization. For instance, several possible architectures can be found depending on whether the FC can recharge the batteries or not. In this work, only the case where the FC is able to recharge the batteries with its extra power will be studied, as the vehicle will have larger autonomy if the batteries can be recharged. Also, different systems can be found regarding the possibility of having periods where the batteries or the fuel cells act as the only source of power or acting as only a hybrid. On the one hand, the system can work as a hybrid system in all situations, and the batteries and fuel cells provide power at all running times. On the other hand, with the action of a switch in the connection of the FC and the DC bus, the battery acts as the main source of power, and the FC supplements the power supplied by the batteries when the SOC of the battery reaches a predefined minimum, detected by its corresponding voltage. Once this value is reached, the switch closes and the FC acts as a range extender, providing power to supply the demands of

the load and to charge the batteries when possible.

### 4.2.2 Active hybrid configurations

The main difference between active and passive hybrid configurations is the appearance of control elements (typically DC/DC boost converters). The battery and the FC are no longer coupled directly and can work on different voltages, meaning that the sizing and operating conditions of them both can be designed independently. This allows a more precise control of the power system, thanks to the control and management of the converters. On the other hand, their main disadvantages are the opposite of the advantages of the passive configuration: a more complex system topology, a higher system weight, volume and cost and a reduced efficiency due to voltage losses [23].

Two different cases will be studied, a first one where a DC/DC boost converter connects the fuel cells with the DC bus (it will be referred to onwards as “Semi-active” configuration), and a second case where in addition to the first DC/DC converter, a second one, bidirectional in current, connects the batteries with the DC bus. It will be referred to as “Full-active” configuration.

#### 4.2.2.1 Semi-active hybrid configuration

As it can be seen in Figure 4.2, in the semi-active hybrid configuration the battery is directly connected to the DC bus, while the FC is connected to it through the DC-DC boost converter. The voltage in the bus bar is fixed by the battery, as in the passive configuration. Nevertheless, this voltage is not the same voltage as the working one of the FC anymore, as the DC-DC booster acts as a step-up voltage converter, allowing the FC to work at lower voltage levels.

As the voltage in the FC is no longer fixed by the battery, an Energy Management Strategy (EMS) for the operating conditions of the fuel cells is needed. Different strategies to model the contribution of each power source in covering the power needs exist, depending on the objective followed. As the operating costs associated with hydrogen consumption represent a high percentage of the total cost, minimization of fuel con-

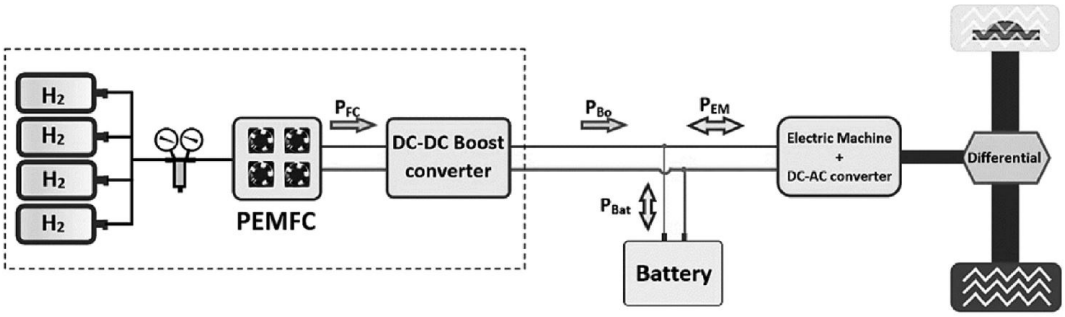


**Figure 4.2:** *Semi-active configuration schematic [4]*

sumption is one of the most common elections. Nevertheless, other criteria exist that also take into account the maximization of the vehicle's autonomy or the lifetime of some of its components, as the battery or the fuel cell, that also represent a high percentage of the total costs when its life is relatively short [19]. One of the most widely used strategies is the Equivalent Consumption Minimization Strategy (ECMS) that takes into consideration both the currents of the FC and the batteries. In general terms, the EMS selected should ensure the following [25]:

- Low hydrogen consumption
- High overall efficiency
- Long lifetime of components

In future sections the EMS selected for this work will be presented. Once the operating point of the FC is set, the contribution of each power source is determined by equations 4.3-4.5 [19]. As in the passive case, the fuel cell acts as the main power source and the battery complements it when needed. Like this the FC can work with smooth profiles in order to avoid fast changing voltages that would be detrimental as it would cause starvation. If the power required by the load is higher than the one provided by the FC, the battery will provide the extra power to meet the power demands, and if the power provided by the FC is higher than the required by the load, it will serve for both meeting the power requirements of the load and charging the batteries with the extra power.

$$P_{load} = \begin{cases} P_{booster} - P_{bat}, & \text{if } P_{load} < P_{booster} \\ P_{booster} + P_{bat}, & \text{if } P_{load} > P_{booster} \end{cases} \tag{4.3}$$

where:

$$P_{booster} = \eta_{booster} \cdot P_{FC} \tag{4.4}$$

The introduction of the DC-DC converter allows the FC to work at more optimal voltage levels even if they are lower than the voltage of the batteries, as the converter will step its input voltage (FC's voltage) up until the output voltage (DC bus' voltage). Nevertheless, as output power is smaller than the input one due to the converter efficiency, a higher output voltage leads to lower output current [26]. Equation 4.4 can be rewritten as:

$$V_{DCbus} \cdot I_{booster} = \eta_{booster} \cdot (V_{FC} \cdot I_{FC}) \tag{4.5}$$

In opposition to the passive configuration, where the operation of the FC was voltage-controlled (the voltage of the batteries fixed the voltage of the FC, and this one set its current through the polarization curves), in this configuration the FC can be current-controlled, as the FC can work at the desired current, fixing its voltage through the polarization curves.

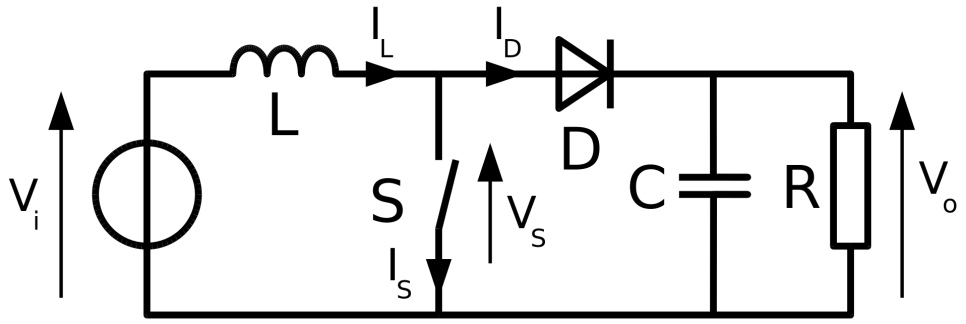


**Figure 4.3:** *DC-DC Boost Converter schematic*

In Figure 3.3 a schematic of a DC-DC Boost Converter can be seen. In this type of converter, an output DC voltage larger than the input voltage is obtained through the

rapid commutation of a switch that opens and closes periodically. Usually, the switch is implemented with transistors such as MOSFETs, IGBTs or BJTs, as they allow high-frequency commutation. However, high frequency switching can lead to current ripple in the FC, and although it doesn't affect much the hydrogen consumption of the FC it can lead to starvation. In [27] it is shown that the FC current ripple strongly depends on the DC bus voltage, and it is stated that low DC bus voltages are recommended to diminish their impact.

The proportion of the period where the switch is activated is known as the duty-cycle (D), and it is used to set the step-up voltage percentage of the DC-DC booster. The control of the duty-cycle through Pulse-Width Modulation (PWM) allows the control of the output voltage, as it is defined as:

$$D = 1 - \frac{V_o}{V_i} \tag{4.6}$$

In Figure 4.4 it can be seen the two working states of a Boost converter:

- In ON-state, the switch is closed. Current flows through the low-impedance path and the energy stored in the inductor increases.
- When the switch opens (OFF-state), the only possible path is through the diode, where the impedance is much higher than the case before, leading to a decrease in current. This decrease in current leads to a collapse of the magnetic field of the inductor and the release of its energy stored. The polarization of the inductor changes and the inductor is in series with the fuel cell. Their voltages are added, leading to a large voltage to which the capacitor is charged.

Switching between these two states at a high speed makes the voltage of the capacitor increase until it reaches an equilibrium point, where the rate at which the inductor transfers energy to the capacitor (in OFF-state) equals the rate at which the capacitor discharges energy to the output load (ON-state). The resulting output voltage, in equilibrium in less than 1 second, can be far greater than the input voltage, as it only sees the capacitor's high voltage when the switch is closed (the diode prevents the capacitor

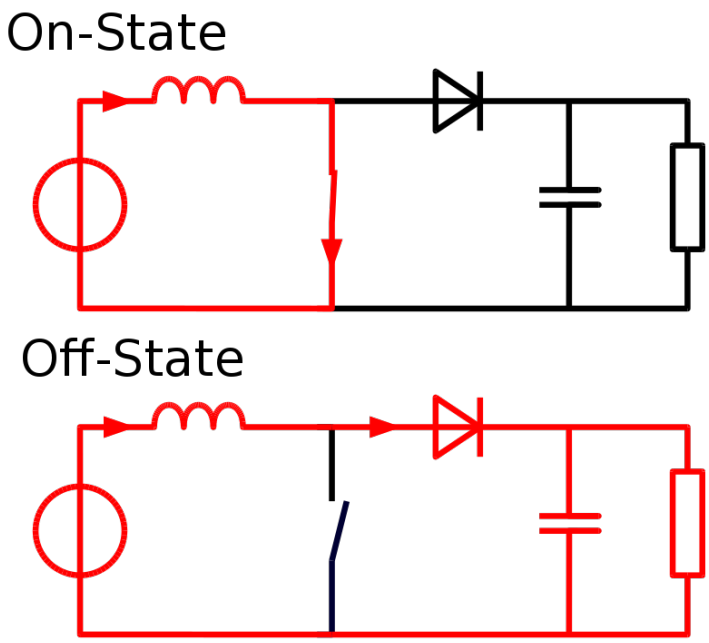


**Figure 4.4:** *DC-DC Boost Converter working states*

to discharge in the load's opposite direction), or a high voltage thanks to the inductor when the switch is closed.

#### 4.2.2.2 Full-active hybrid configuration

As it can be seen in Figure 4.5, where ESS stands for Energy Storage System, in the full-active hybrid configuration neither the battery nor the fuel cells are connected directly to the DC bus. The fuel cell, as in the case before, is connected through a unidirectional DC-DC boost converter that has the objective of stepping up the voltage of the FC to the DC bus voltage. In this case, in opposition to the semi-active architecture, the voltage of the DC bus can be controlled and is not dependent on the voltage of the batteries, as a bidirectional DC-DC converter is placed between them. This converter differs from the one that connects the fuel cells to the DC bus in several aspects. Firstly, it is bidirectional in current, as it has to ensure current flowing from the battery to the load when the FC can't cover the whole power of the load by itself, but also current from the DC bus to

the battery, when the power provided by the FC is higher than the one required by the load and the batteries can recharge with the extra energy. In second place, the DC-DC converter is not of boost type, but of buck/boost, as it has either to step the voltage of the batteries up to the voltage of the DC bus when the batteries give power to the load or step the voltage of the DC bus down in the opposite case.

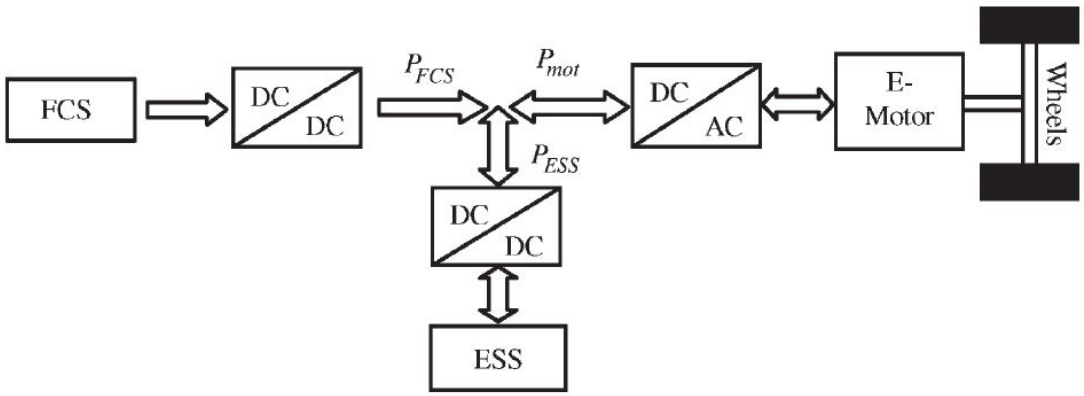


**Figure 4.5:** *Full-active hybrid configuration schematic [28]*

The introduction of the DC-DC bidirectional converter allows a total control of the system and a total decoupling of its power elements with respect to the load. The control of the system is total because in addition to the variables controlled in the semi-active configuration, the voltage of the DC bus can be controlled through the current of the batteries and can be set to the desired value. Also, not only the sizing of the FC is decoupled from the battery's design, but the battery is also independent on the load, as they no longer have to work at the same voltage. Nevertheless, it is important to consider the loss of battery current when it passes through the converter as its voltage is stepped-up, as it leads to an increase in battery's consumption levels for equal load consumptions and a faster depletion of its SOC. For this reason, this type of architecture is not very common when a battery is the only ESS of the system, and is more usual when a supercapacitor acts as the main ESS of the system or as a complement to the battery [29].

A common bidirectional DC-DC converter, and the one that will be used in this work, is known as a Half-Bridge DC-DC converter, and is implemented through the connec-

tion in anti-parallel of a buck and a boost converter [30]. In Figure 4.6 a schematic of a Half-Bridge DC-DC Converter can be seen working between a low-voltage input source (VL) and a higher voltage output (VH). This type of converter also works through rapid commutation of switches, but in opposition to the unidirectional boost converter, in a half-bridge two different switches with fly-back diodes are found that must act complementary (when one is ON-state, the other one has to be in OFF-state and vice versa). Depending on which of the switches is activated, output voltage varies between a top and a low value. Through the control of the time each switch is activated through PWM, the average output voltage value can be set for any value in between the upper and lower limits.

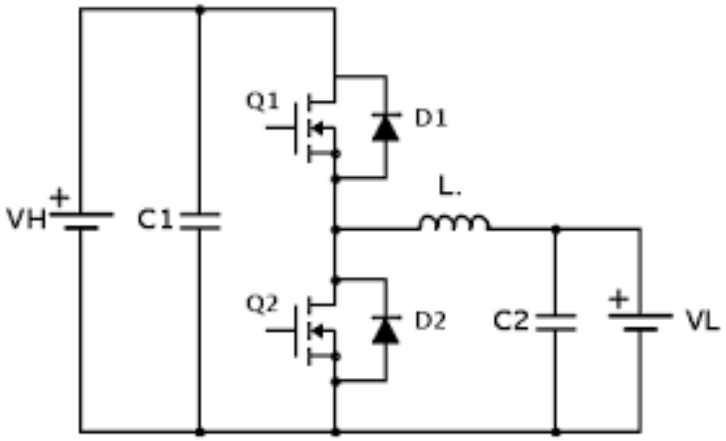


**Figure 4.6:** *Half-Bridge DC-DC converter schematic [30]*

In addition to equations 4.4 and 4.5 modeling the operating principles of the FC and the DC-DC boost converter, which don't vary with respect to the semi-active configuration, the equations that model the full-active configuration are:

$$P_{load} = \begin{cases} P_{booster} - P_{HB}, & \text{if } P_{load} < P_{booster} \\ P_{booster} + P_{HB}, & \text{if } P_{load} > P_{booster} \end{cases} \tag{4.7}$$

where:

$$P_{HB} = \eta_{HB} \cdot P_{bat} \rightarrow V_{DCbus} \cdot I_{HB} = \eta_{HB} \cdot (V_{bat} \cdot I_{bat}) \tag{4.8}$$

# Chapter 5

# The industrial mobile robot

## 5.1 Description of the robot

The industrial mobile robot can be seen in Figure 5.1. It has a low cylindrical body, with a diameter of 664 mm and a height of 324 mm, as it can be seen in the schematic of the lower part of the robot found in Figure 5.2. On top of the body, a system for carrying weights can be found.


**Figure 5.1:** *The industrial mobile robot*

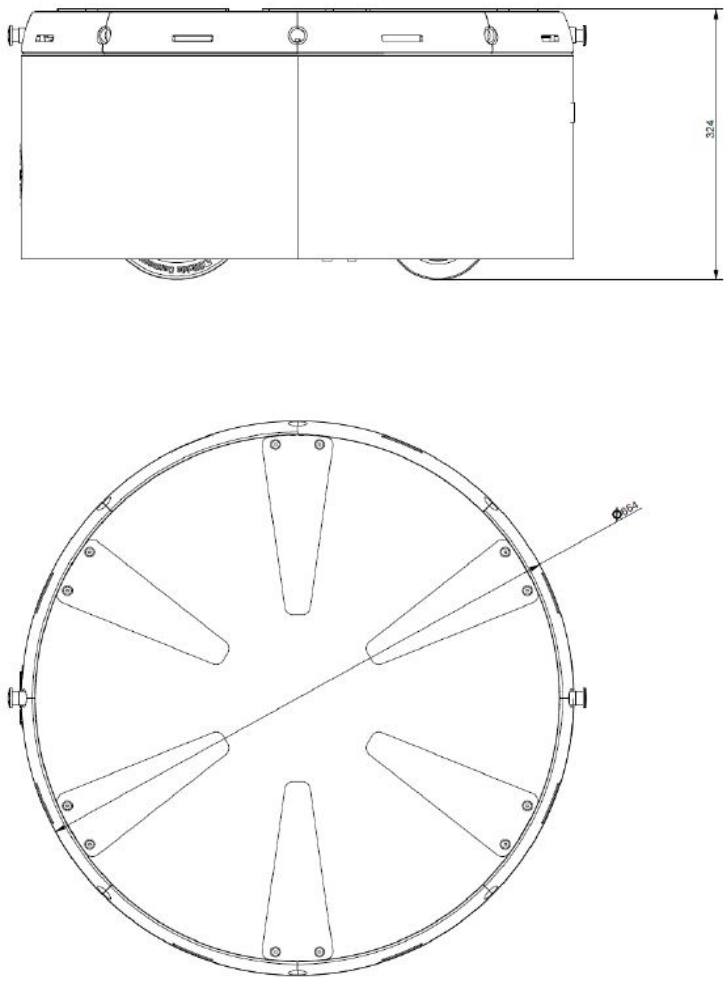

**Figure 5.2:** *Schematic of the robot's body*

The mission of the robot is to carry objects and move them across an industrial plant. It moves by the action of three wheels, in the right, left and center of the lower body. It has three motors and a driver regulating the power coming from a common power source. The driver is the model *XtrapulsEasy-ak-60/60-ST*, with an operating voltage range between 24-60 V. However, in this robot it works around 40-45 V. On the other hand, the actual power source is a Li-ion battery of 2200 mAh, working at the voltage set by the driver. As the capacity of the battery is not large, the robot offers a low autonomy, as the battery gets depleted fast. For this reason, a modified powertrain consisting in the addition of a fuel cell to the actual battery to obtain a hybrid powertrain will be studied in the following sections.

## 5.2 Test cycles

In order to correctly size and model the new hybrid powertrain for the robot, different tests have been carried out to obtain the consumption of the robot's motors in real working-like situations. In these tests, the robot is loaded with a 200 kg load and is made to follow a flat trajectory with the form of an "8" of 2 m of width. There are four different cycles of approximately 2 to 6 minutes, depending on the speed of the robot.

The data extracted from these tests is collected in four different data sheets with samples every 0.004 s, where information of the operating voltage of driver and the instantaneous consumptions of the three motors linked to each wheel (RW, LW and CW stand for the right, left and central wheel respectively), in addition to information of the kinematics of the robot: vertical and horizontal speeds and angular velocity. Of all these, only the data related to electricity with respect to time is of interest. These columns can be seen in the example of 5 data extracted from cycle 1 in Table 5.1.

| Time | Voltage [V] | $I_{RW}[A]$ | $I_{LW}[A]$ | $I_{CW}[A]$ |
|---|---|---|---|---|
| 0.084 | 44 | -0.234 | 0.096 | 1.236 |
| 0.088 | 44 | -0.258 | 0.070 | 1.234 |
| 0.092 | 44 | -0.352 | 0.128 | 1.238 |
| 0.096 | 44 | -0.322 | 0.284 | 1.240 |
| 0.100 | 44 | -0.342 | 0.240 | 1.234 |

**Table 5.1:** *Example of 5 columns of raw electric data (cycle 1)*

With the use of the data processing tool *Pandas*, of the program *Python*, the data has been processed in order to plot the consumption profiles, as well as to obtain the total consumption profile for each cycle. Moreover, it has been necessary to reduce the quantity of data in order to ease the computational burden of the simulations. For this reason, it has been decided to only store the data every 0.1 seconds, reducing the data's size by 25 times. The new data has been tested in comparison to the complete one in different simulations, achieving almost equivalent results. An example of 5 random data extracted from cycle 1 can be seen in Table 5.2.

| Time | Voltage [V] | $I_{RW}[A]$ | $I_{LW}[A]$ | $I_{CW}[A]$ | $I_{Total}$ |
|---|---|---|---|---|---|
| 149,0 | 44 | -0,259 | 0,214 | 1,414 | 1,369 |
| 149,1 | 44 | -0,134 | 0,384 | 1,435 | 1,685 |
| 149,2 | 44 | -0,345 | 0,286 | 1,444 | 1,385 |
| 149,3 | 44 | -0,298 | 0,238 | 1,442 | 1,382 |
| 149,4 | 44 | -0,326 | 0,322 | 1,444 | 1,440 |

**Table 5.2:** *Example of 5 columns of the reduced data (cycle 1)*

In the annex the current profiles for the 4 different test cycles can be seen, as well as a comparison between the profiles obtained before or after the reduction of data.

Joining the total consumption data of these 4 cycles a combined cycle can be achieved. This combined cycle can be used to test the different powertrain configurations in a longer and more complete cycle. The resultant consumption profile can be seen in Figure 5.3.

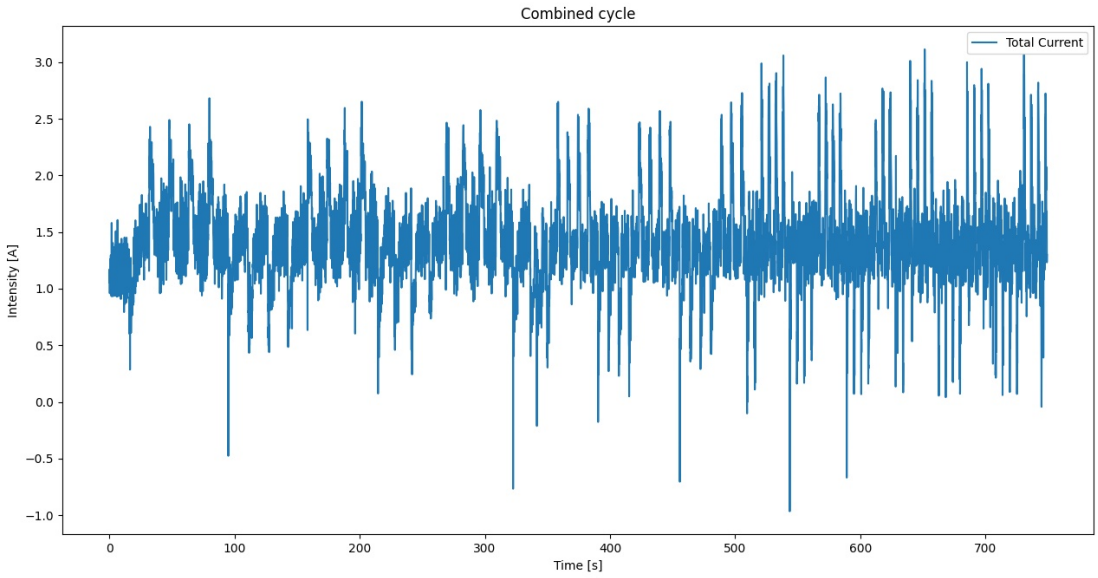


**Figure 5.3:** *Consumption profile of the combined cycle*

Furthermore, it is necessary to test the powertrain to harder conditions to correctly size it in case the real operating conditions are more demanding than the data collected. For these reason, a final consumption profile is built putting together two combined cycles, the one obtained in 5.3 and one multiplied by a security factor of 1.2, obtaining the profile shown in figure 5.4. This last profile will be the one used to test the powertrains.

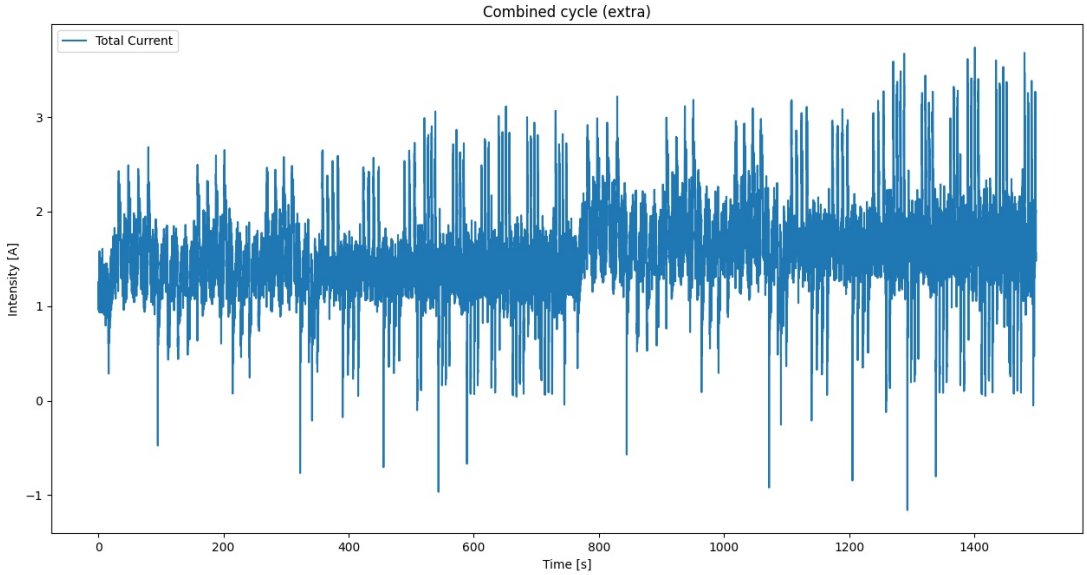


**Figure 5.4:** *Consumption profile of the test cycle*

# Chapter 6

# Testing of hybrid powertrains for the mobile robot

## 6.1 Optimization criteria

In order to find the optimal powertrain configuration and sizing for the mobile robot, different simulations will be carried out using *Matlab*'s simulation module *Simulink*. To do so, the generic battery and fuel cell models of *Simulink* will be used, with its parameters adjusted to each simulation.

These simulations are done in order to obtain the response of the battery and fuel cell in each case and compare them to find the optimal configuration. This comparison will take into consideration different aspects for each model:

- Constructive aspects
  - Simplicity of the design
  - Market considerations: price and availability
- Performance
  - Hydrogen consumption
  - $\Delta$SOC and autonomy

- Component degradation
  - FC degradation
  - Battery aging

Some of these criteria are qualitative and others are quantitative. Of the ones commented, qualitative aspects will be the ones regarding the constructive analysis and the FC degradation, the latter being considered in this group due to a lack of possible numerical analysis. The other parameters are quantitative and will be controlled using information provided by the output variables of the *Simulink* model. The $\Delta$SOC can be directly measured in the output graphs of the battery model, but the other two parameters are not directly achieved and have to be calculated. Further information on how to calculate these parameters is given below.

- Hydrogen consumption

In [1] the method to calculate reactants' flow rates is given. The rate at which hydrogen is consumed (in mol/s) is given by Faraday's Law:

$$\dot{N}_{H_2} = \frac{I_{FC}}{2F} \tag{6.1}$$

Transforming it to g/s:

$$\dot{m}_{H_2} = \frac{I_{FC}}{2F} \cdot M_{H_2} \tag{6.2}$$

On the other hand, it is common to give flow rates of gases in liters per minute (lpm) and especially in standard liters per minute (std lpm), where the standard liter is the quantity of gas that would occupy 1 liter in standard conditions - atmospheric pressure, 101.3 kPa and 15 ºC (in technical fluid mechanics standard temperature is 15 ºC, not 25 ºC as in chemistry) [1]. Thus, at standard conditions, molar volume is:

$$v = \frac{RT}{P} = \frac{8.31 \cdot 288.15}{1.013 \cdot 10^5} \cdot 1000 = 23.65\ l/mol \tag{6.3}$$

The volumetric hydrogen consumption rate in std lpm is given, then, by:

$$\dot{V}_{H_2} = \frac{I_{FC}}{2F} \cdot 23.65 \cdot 60 \tag{6.4}$$

Joining equations 6.2 and 6.4, we have the relationship between the flow rates at std lpm and the hydrogen consumed:

$$\dot{m}_{H_2} = \frac{\dot{V}_{H_2}}{23.65 \cdot 60} \cdot M_{H_2} \tag{6.5}$$

As fuel flow rate is one of the output variables the *Simulink*'s FC model gives, the total mass of hydrogen consumed can be calculated by using equation 6.5 and then integrating. The *Simulink* block distribution can be seen in Figure 6.1, where *Cons* is the fuel flow rate coming from the output signals of the FC and in the function block equation 6.5 is implemented.

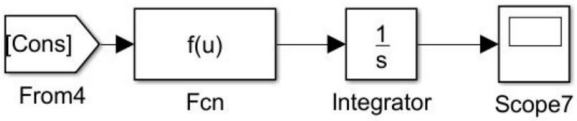


**Figure 6.1:** *Block distribution for the calculation of hydrogen consumption*

- Battery aging

In order to estimate the battery degradation in every case, a method to quantify the damage produced in the battery by a given current profile is needed. Factors such as current severity (known as C-rate), elevate temperature, discharge rate or depth of discharge (DOD), in addition to irregular patterns of charge and discharge cycles can accelerate battery degradation [31]. C-rate (defined for a given battery current) and DOD (complementary to the battery SOC) are defined as:

$$C_{rate} = \frac{|I_{Bat}|}{Q_{Bat}} \tag{6.6}$$

$$DOD = 1 - SOC \tag{6.7}$$

where $Q_{Bat}$ is the battery capacity expressed in Ah. High values of C-rate and of DOD tend to accelerate battery aging [19].

Following the strategy proposed in [19], the battery degradation will be estimated using the Ah-throughput parameter, as it takes into consideration both the current severity (either charge or discharge) and its DOD, as well as the battery working temperature. This accumulative parameter predicts the EoL of a battery when it exceeds a predetermined value, known as nominal Ah-throughput, where nominal conditions refer to a C-rate = 1, DOD = 100% and a temperature of 25 ºC. This value, and the effective Ah-throughput that a current profile produces, are calculated as follows [19]:

$$Ah_{nom} = \int_0^{EoL} |I_{nom}(t)|\, dt \tag{6.8}$$

$$Ah_{eff} = \int_0^{T_f} |I_{Bat}(t)| \cdot \sigma(t)\, dt \tag{6.9}$$

where $\sigma$(t) is a weight factor bigger than 1 named severity factor, and it depends on the DOD and the operating temperature. It can be calculated using the severity factor map found in Figure 6.2.

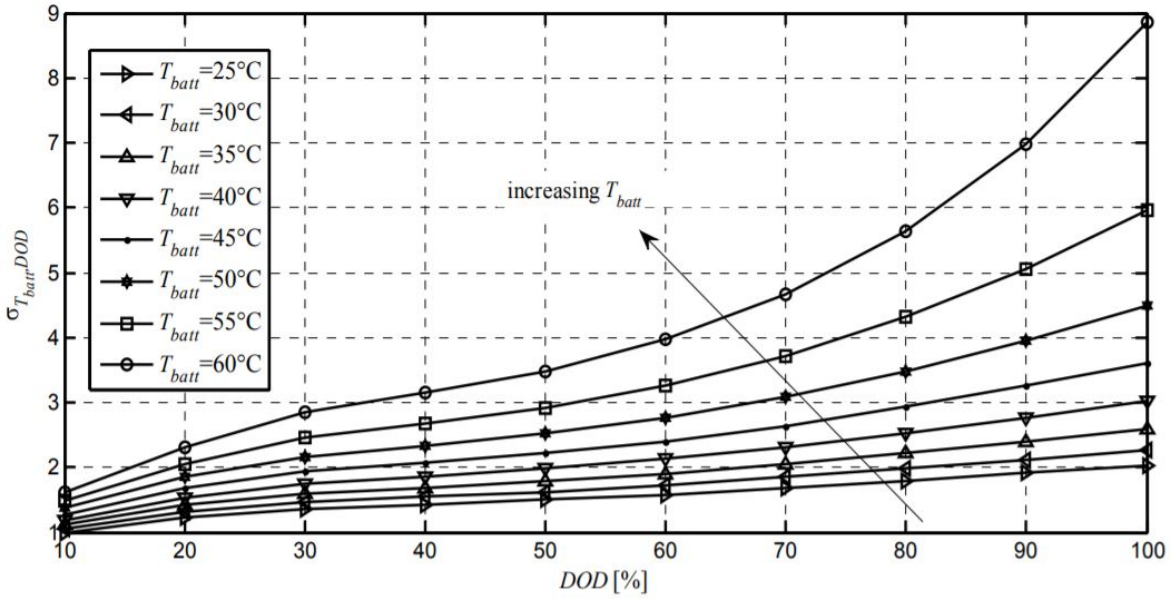


**Figure 6.2:** *Severity factor map depending on DOD and battery temperature [31]*

As battery current is expected to be kept low (the load cycles are normally between 1-3 A), following the study found at [32] the temperature of the battery can be estimated to be around 25 ºC. Looking back at the severity factor map, and considering this temperature, three different severity zones have been defined:

- DOD = 0-20% $\rightarrow \quad \sigma = 1$
- DOD = 20-60% $\rightarrow \quad \sigma = 1.2$
- DOD = 60-80% $\rightarrow \quad \sigma = 1.5$

No DOD values higher than 80% are considered, as it is considered that the battery is fully discharged when it reaches 20% SOC, as it is harmful for the battery life to operate under this limit. The *Simulink* block distribution to give the adequate severity factor to the calculation depending on the DOD can be seen in Figure 6.3, and the block distribution to calculate the effective Ah-throughput in Figure 6.4.

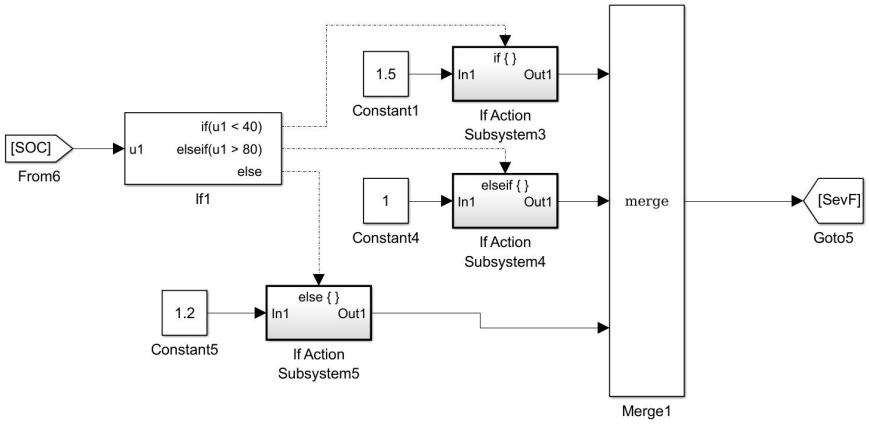


**Figure 6.3:** *Block distribution to give the adequate $\sigma$*

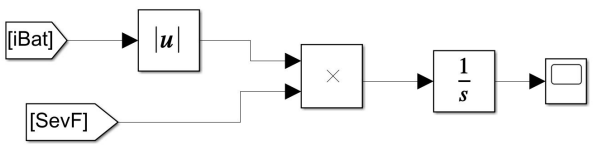


**Figure 6.4:** *Block distribution for the calculation of the effective Ah-throughput*

## 6.2 Actual state

Before entering in the analysis of the best powertrain configuration, a study of the actual state of the robot's powertrain will be conducted. To do so, a simulation of the battery will be conducted. The battery has a capacity of 2200 mAh, and works at the voltage set by the driver (44 V). To simulate it, a similar value will be given as battery's nominal voltage. The data given as the characteristic values of the battery is (will remain the same for the future sections):

| Variable | Value |
|---|---|
| Rated capacity (A· h) | 2.2 |
| Nominal voltage (V) | 40 |

**Table 6.1:** *Battery model information*

The *Simulink* circuit made to simulate the actual powertrain can be seen in Figure 6.5. It is a simple circuit where the current profile is put as input of the battery, which give as output variables its SOC, current and voltage. As the battery is the only power source of the powertrain, it is expected that the load current will be equal to the one going through the battery.

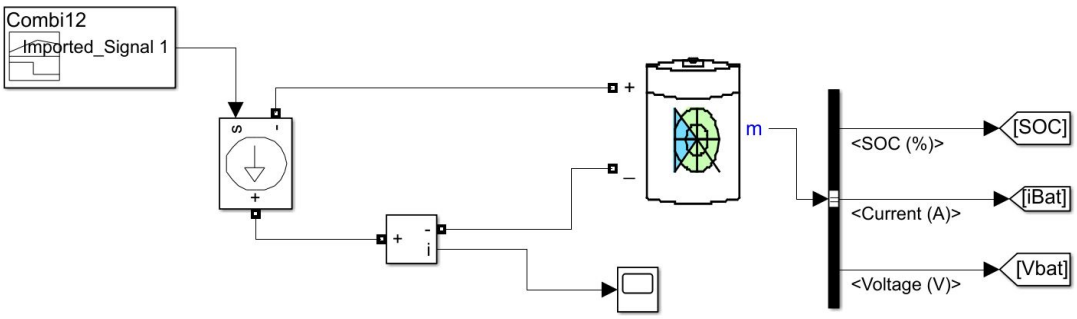


**Figure 6.5:** *Actual powertrain simulation circuit*

Two different simulations have been carried out, one at a high-SOC level and one at a medium one.

- High-SOC $\rightarrow$ $SOC_0 = 100\%$

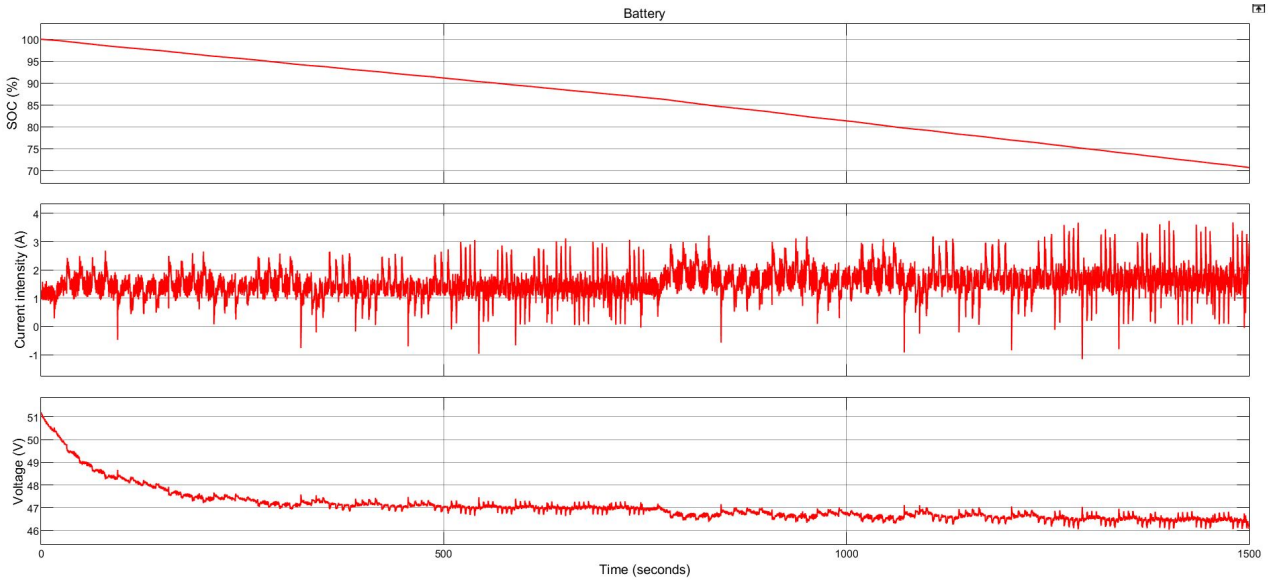


**Figure 6.6:** *High-SOC battery-only simulation*

As expected, the battery current is equal to the load current, as it is the sole power source of the vehicle. The relevant information related to this cycle can be seen in 6.2. The mean column is only of interest for the current and voltage variables, and the difference between initial and final values ($\Delta$) only is for the SOC.

| Variable | Max | Min | Mean | $\Delta$ |
|---|---|---|---|---|
| SOC (%) | 100 | 70.68 | - | -29.32 |
| Current (A) | 3.74 | -1.16 | 1.55 | - |
| Voltage (V) | 51.20 | 46.03 | 47.08 | - |

**Table 6.2:** *High-SOC battery-only simulation*

- Medium-SOC $\rightarrow$ $SOC_0 = 60\%$

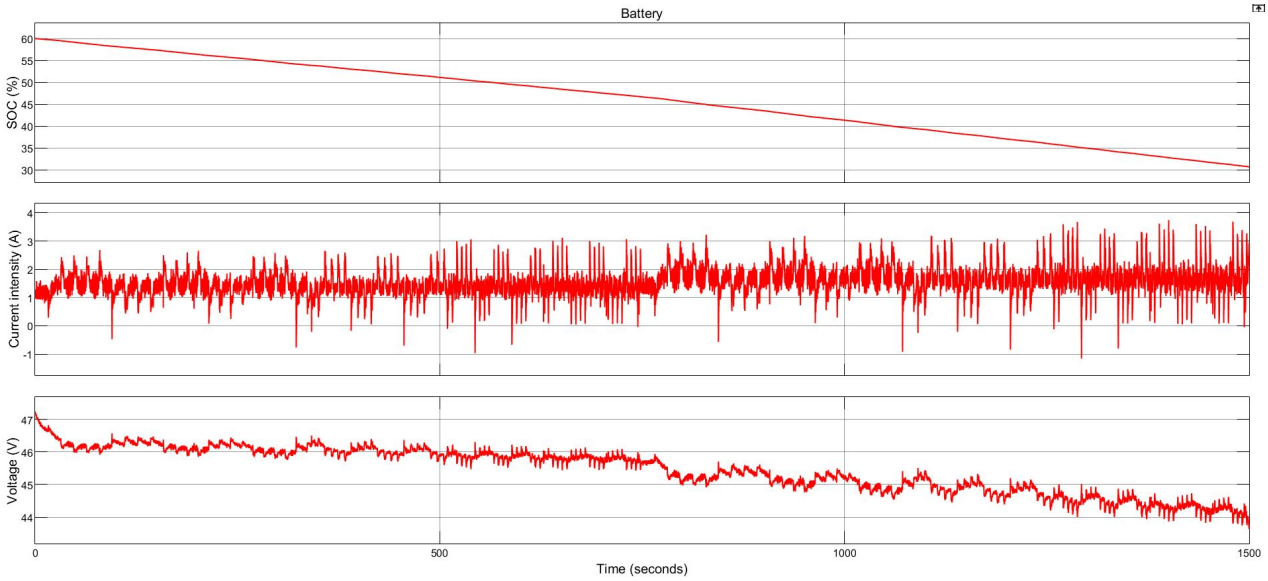


**Figure 6.7:** *Medium-SOC battery-only simulation*

The relevant information related to this cycle can be seen in 6.3

| Variable | Max | Min | Mean | $\Delta$ |
|---|---|---|---|---|
| SOC (%) | 60 | 30.68 | - | -29.32 |
| Current (A) | 3.74 | -1.16 | 1.55 | - |
| Voltage (V) | 47.23 | 43.64 | 45.45 | - |

**Table 6.3:** *Medium-SOC battery-only simulation*

It can be seen looking at tables 6.2 and 6.3 that the discharge rate, for the same current profile, is independent on the DOD of each case. With the data extracted from this simulation, an expected value of the robot's actual autonomy can be calculated, given that its viable SOC range goes from 100% to 20 %:

$$t_{autonomy} = 80\% \cdot \frac{1500\ s}{29.32\%} = 4092.8\ s \approx 1h\ 8min \tag{6.10}$$

As it can be seen, the autonomy of the robot is slightly greater than 1 h, which is insufficient for what is needed. In the following sections, different powertrains will be tested with the objective of obtaining at least 8 hours of autonomy.

## 6.3 Passive hybrid powertrain

As seen in Section 4.2.1, the battery and the FC are directly coupled in the passive architecture. Its immediate consequence is the need to carefully design the fuel cell, as it has to be able to work at the voltage set by the batteries. The relation between the FC's voltage and the one of the battery will depend on its relative impedance.

Two elements will be found between the battery and the FC: a diode to prevent negative currents entering the FC, and an inductor, as it resists fast changes in current and will ensure that the FC operates without fast current changes, which would cause starvation and will harm the cell. Nevertheless, the inductor has a high weight, so the smallest inductor that ensures the FC's safe operating conditions will be selected. After trying different inductor sizes, and selecting the default diode values, the values of the circuit's passive components are:

| | |
|---|---|
| Diode | $R_{ON}$=0.001 Ω<br>$V_{ON}$=0.8 V |
| Inductor | L = 500 mH |

**Table 6.4:** *Passive circuit passive elements*

Moving on to the sizing of the FC, it needs to be able to operate at similar voltage levels than the ones of the driver and battery, as they are the ones setting the DC bus' voltage around 40-50 V. On the other side, it should give around 2-3 A to cover for the load needs. Thus, an initial case of a 100 W 50-cell (considering a cell voltage of 0.8-1 V) fuel cell will be considered, and if it doesn't meet the requirements, more powerful systems will be considered. The following polarization curve is given to the cell:

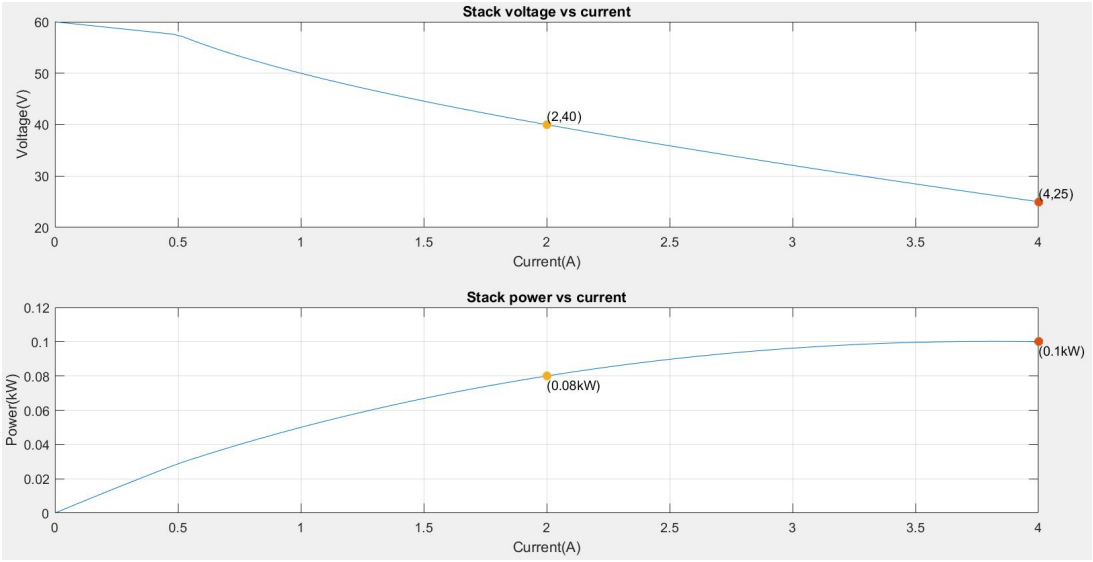


**Figure 6.8:** *Polarization curve of a 100W FC for passive configuration*

The *Simulink* circuit made to simulate the passive hybrid powertrain can be seen in Figure 6.9. It can be seen how the battery and fuel cell are directly coupled, with just an inductor and a diode between them, and together they cover the load needs as explained in section 4.2.1.

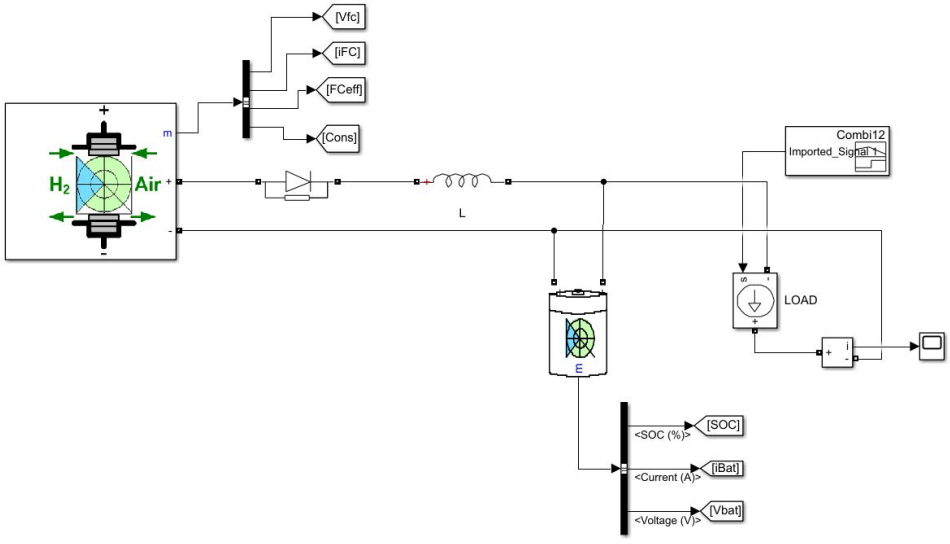


**Figure 6.9:** *Passive hybrid powertrain circuit*

The powertrain will be tested at three different SOC levels: high, medium and low.

- High-SOC → $SOC_0 = 90\%$

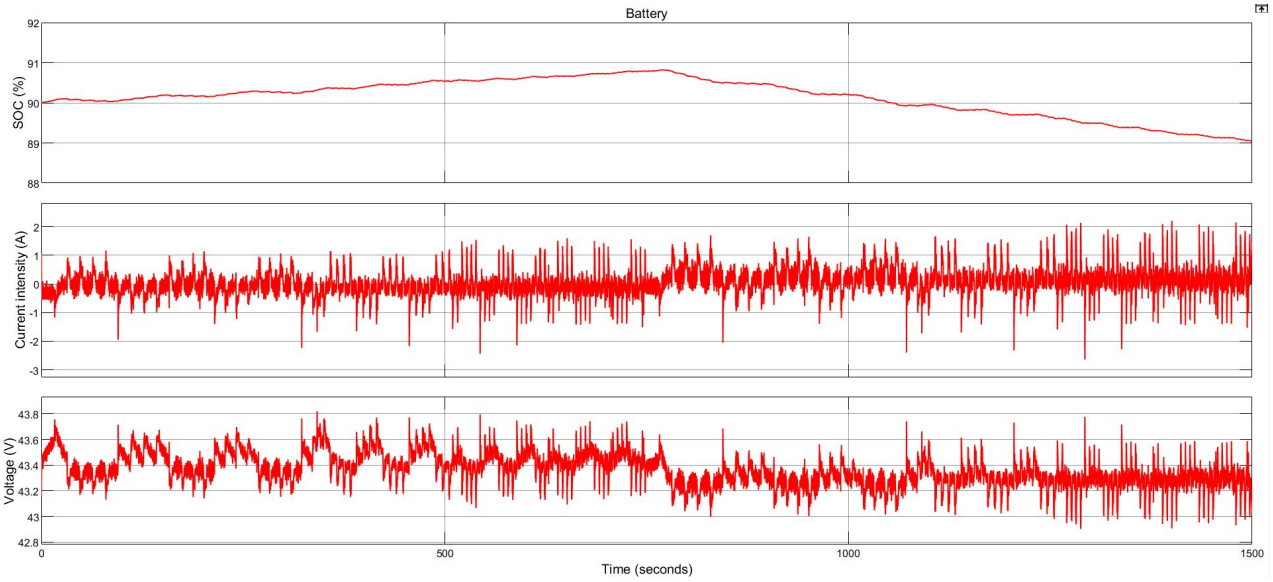


**Figure 6.10:** *Battery response in high-SOC passive hybrid simulation*

In Figure 6.10 it can be seen how the FC is able to handle the load by its own and charge the batteries with its extra power in the first half of the cycle, while in the second part of the cycle, when it is more demanding, the battery has to contribute also to cover the needs of the load. In that part, the current going through the battery is positive, thus the battery is being depleted, while in the first part the current was negative as the battery was being charged. In overall, the SOC of the battery slightly decreases. A summary of the battery's relevant information related to this cycle can be seen in Table 6.5.

| Variable | Max | Min | Mean | Δ |
|---|---|---|---|---|
| SOC (%) | 90.82 | 89.03 | - | -0.97 |
| Current (A) | 2.20 | -2.64 | 0.04 | - |
| Voltage (V) | 43.82 | 42.90 | 43.36 | - |

**Table 6.5:** *Battery response in high-SOC passive hybrid simulation*

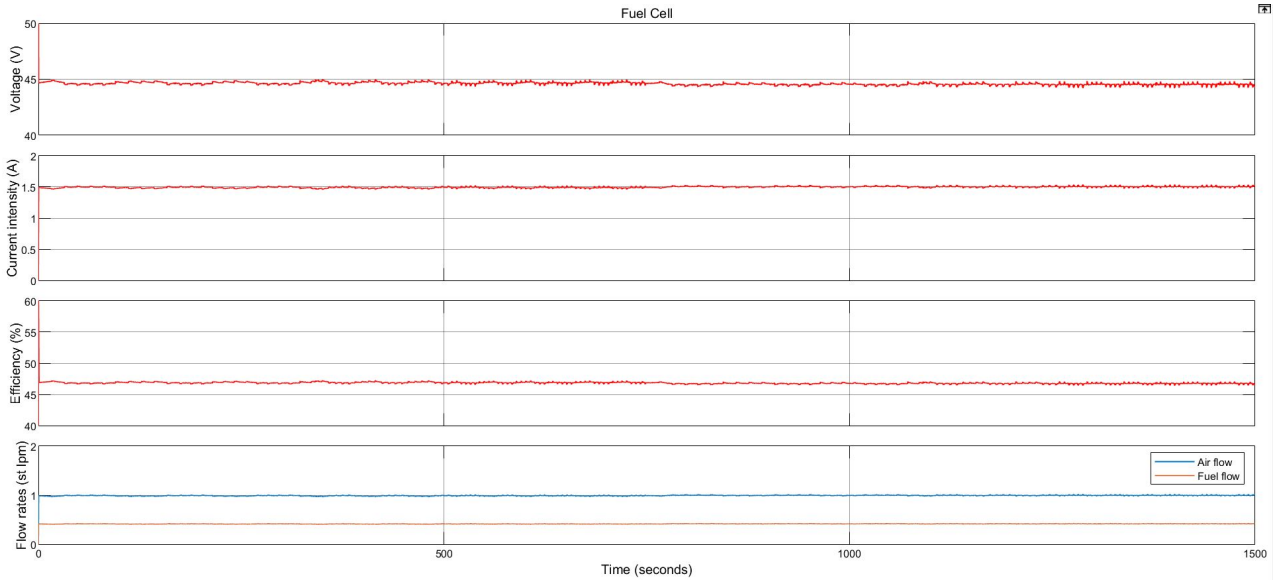


**Figure 6.11:** *FC response in high-SOC passive hybrid simulation*

In Figure 6.11 it can be seen the FC performance. Connected to the batteries, its voltage is nearly kept constant, achieving almost constant values for the current given. As the operating point is almost constant, so are the efficiency and flow rate values. A summary of the FC's relevant information related to this cycle can be seen in Table 6.6.

| Variable | Max | Min | Mean |
|---|---|---|---|
| Voltage (V) | 44.94 | 44.33 | 44.62 |
| Current (A) | 1.54 | 1.47 | 1.50 |
| Power (W) | 68.01 | 65.69 | 66.73 |
| Efficiency (%) | 47.19 | 46.54 | 46.84 |
| Air flow rate (std lpm) | 1.27 | 1.22 | 1.24 |
| Fuel flow rate (std lpm) | 0.54 | 0.51 | 0.52 |

**Table 6.6:** *FC response in high-SOC passive hybrid simulation*

- Medium-SOC $\rightarrow$ $SOC_0 = 60\%$

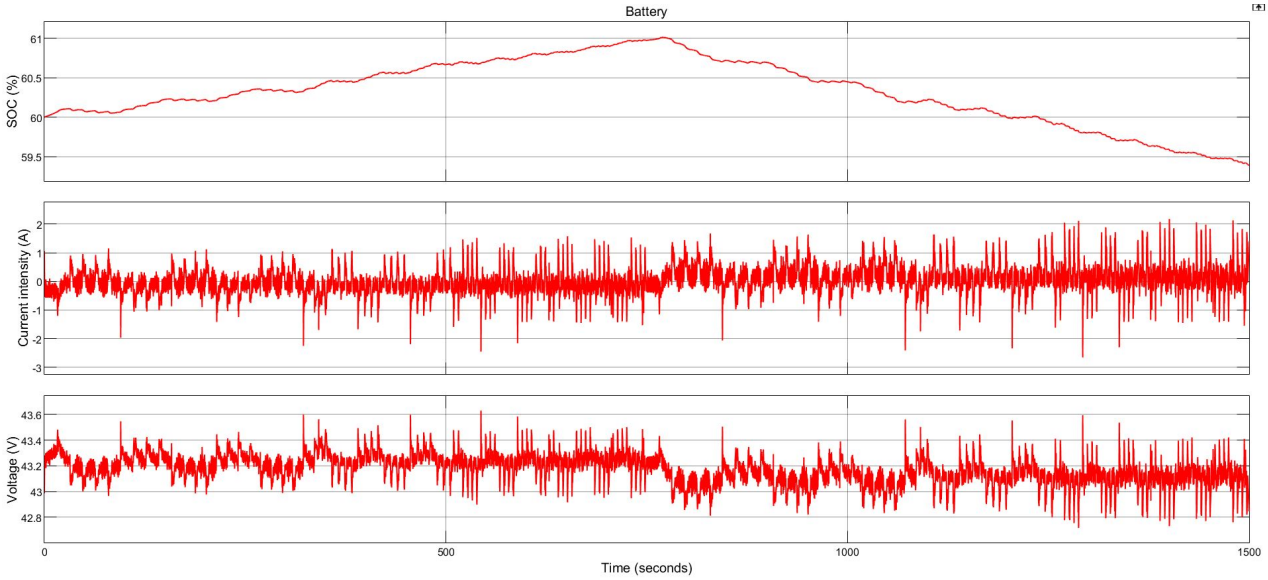


**Figure 6.12:** *Battery response in medium-SOC passive hybrid simulation*

Figure 6.12 shows very similar profiles to the ones seen in Figure 6.10: a first part of battery charging thanks to the extra power provided by the FC and a second part where the battery and FC work together to handle the load currents.A summary of the battery's relevant information related to this cycle can be seen in Table 6.7.

| Variable | Max | Min | Mean | $\Delta$ |
|---|---|---|---|---|
| SOC (%) | 61.02 | 59.38 | - | -0.42 |
| Current (A) | 2.18 | -2.66 | 0.03 | - |
| Voltage (V) | 43.63 | 42.72 | 43.17 | - |

**Table 6.7:** *Battery response in medium-SOC passive hybrid simulation*

The results, though very similar to the ones seen in Table 6.5, are slightly different, as a lower SOC leads to lower voltage, which lead to a higher current contribution from the FC.

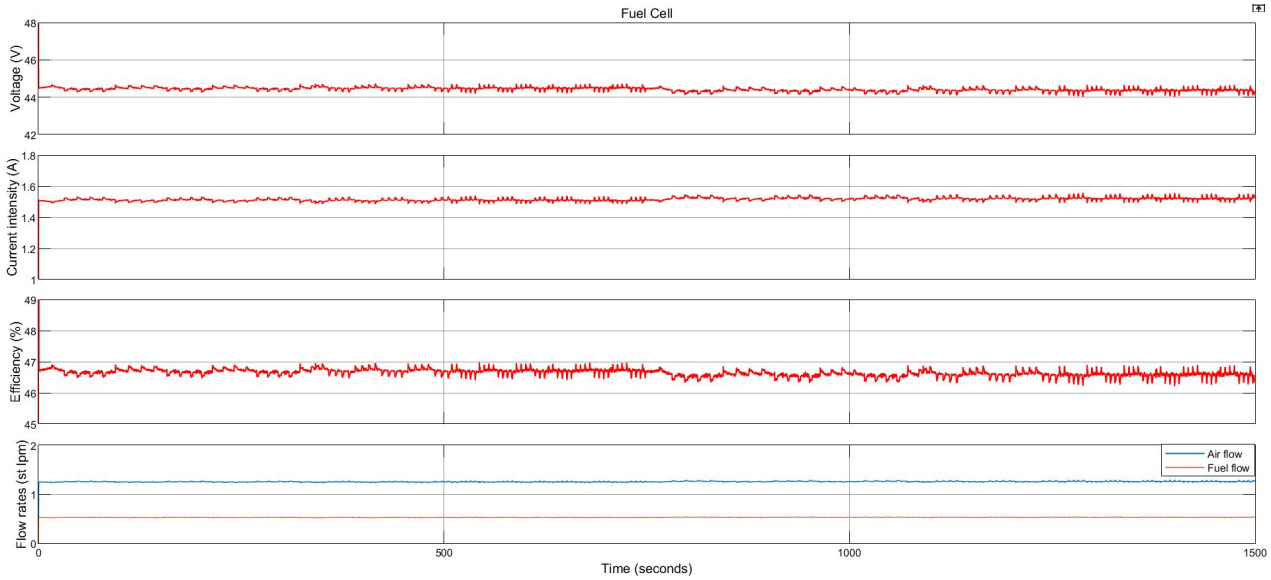


**Figure 6.13:** *FC response in medium-SOC passive hybrid simulation*

The profiles seen in Figure 6.13 show again almost constant values for the variables of the FC, as the voltage it operates doesn't nearly change.In Table 6.8 a summary of the FC's relevant information related to this cycle is found.

| Variable | Max | Min | Mean |
|---|---|---|---|
| Voltage (V) | 44.66 | 44.02 | 44.43 |
| Current (A) | 1.56 | 1.52 | 1.50 |
| Power (W) | 68.56 | 66.79 | 67.29 |
| Efficiency (%) | 46.87 | 46.35 | 46.65 |
| Air flow rate (std lpm) | 1.29 | 1.24 | 1.26 |
| Fuel flow rate (std lpm) | 0.54 | 0.51 | 0.53 |

**Table 6.8:** *FC response in medium-SOC passive hybrid simulation*

As predicted seeing the results of the battery performance, the current and power provided by the FC are slightly higher in expense of a little decrease in efficiency.

- Low-SOC → $SOC_0 = 30\%$

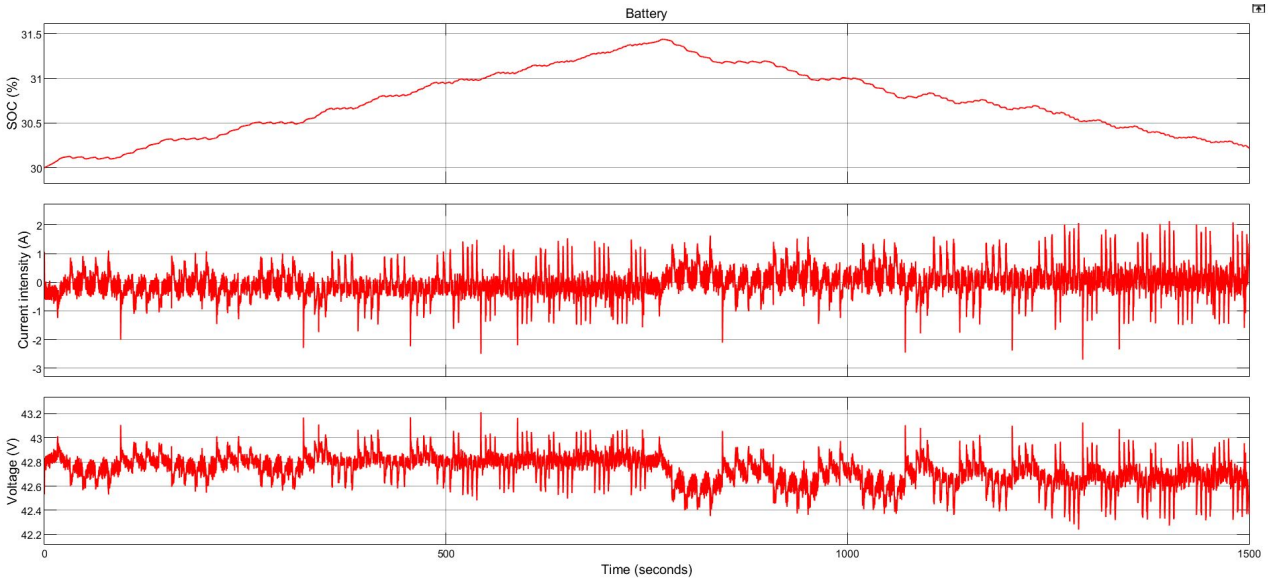


**Figure 6.14:** *Battery response in low-SOC passive hybrid simulation*

Figure 6.14 keeps up with the very similar profiles to the ones seen previously. Nevertheless, this time the battery is more charged after the cycle. A summary of the battery's relevant information related to this cycle can be seen in Table 6.9.

| Variable | Max | Min | Mean | Δ |
|---|---|---|---|---|
| SOC (%) | 31.44 | 30.00 | - | +0.22 |
| Current (A) | 2.14 | -2.70 | -0.01 | - |
| Voltage (V) | 43.21 | 42.24 | 42.73 | - |

**Table 6.9:** *Battery response in low-SOC passive hybrid simulation*

In this case, the mean current through the battery is negative, meaning that more current has been used to charge rather than discharge the battery. For this reason, the SOC increases in the overall cycle, as it can be seen in the positive value for ΔSOC. This means that with correct sizing of the hydrogen storage system, any given autonomy can be achieved.

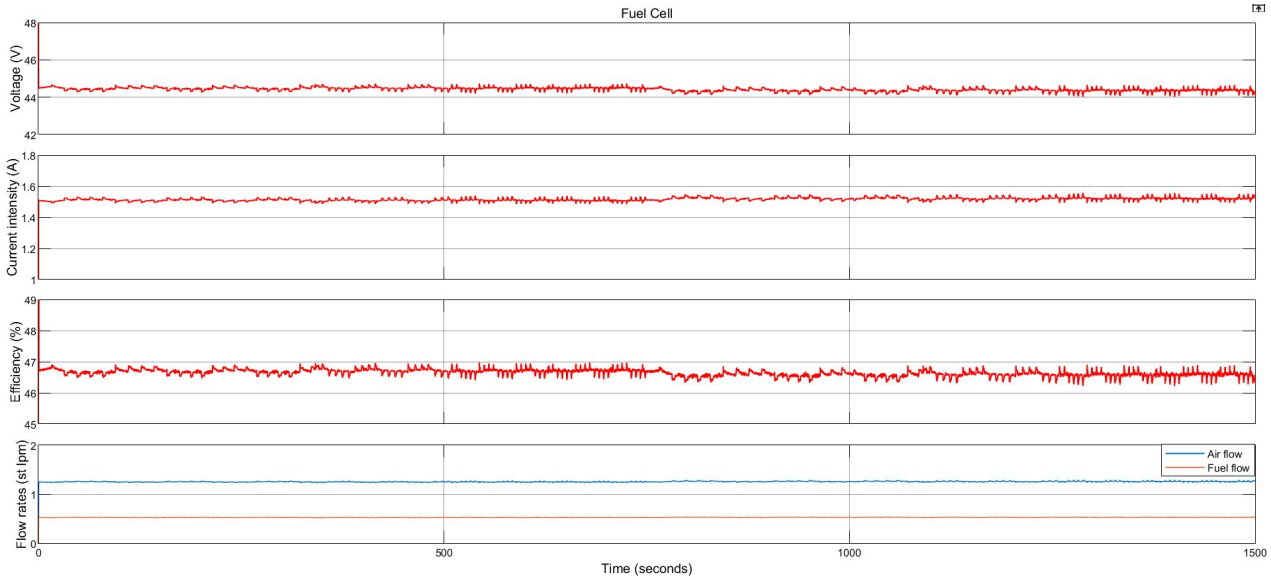


**Figure 6.15:** *FC response in low-SOC passive hybrid simulation*

The profiles seen in Figure 6.15 show again almost constant values for the variables of the FC, as the voltage it operates doesn't nearly change.In Table 6.10 a summary of the FC's relevant information related to this cycle is found.

| Variable | Max | Min | Mean |
|---|---|---|---|
| Voltage (V) | 44.26 | 43.56 | 44.01 |
| Current (A) | 1.61 | 1.55 | 1.52 |
| Power (W) | 69.94 | 68.13 | 68.57 |
| Efficiency (%) | 46.48 | 46.35 | 45.87 |
| Air flow rate (std lpm) | 1.33 | 1.27 | 1.29 |
| Fuel flow rate (std lpm) | 0.56 | 0.52 | 0.54 |

**Table 6.10:** *FC response in low-SOC passive hybrid simulation*

Again, a decrease in battery voltage leads to a slightly higher FC current and power in expense of a little decrease in efficiency.

- Overall performance

In order to compare with the other powertrains, in this section the control parameters, as hydrogen consumption or the effective Ah-throughput will be put together. They can be seen displayed in Table 6.11.

| Parameter | High-SOC | Medium-SOC | Low-SOC |
|---|---|---|---|
| $H_2$ consumption (g) | 1.11 | 1.13 | 1.16 |
| Ah-throughput (A· h) | 0.128 | 0.154 | 0.195 |

**Table 6.11:** *Performance parameters of the passive hybrid simulation*

On the qualitative performance aspects, this model has the positive aspect of making the FC work at almost constant voltage levels. Voltage decreases as the battery is being depleted, but it's done in a very slow rate, allowing the FC to operate at safe conditions as no starvation will occur.

On the negative aspect of this configuration comes the sizing of the FC. The polarization curve defined doesn't belong to any commercial FC available. The voltage levels at which the cell has to work are really high when compared to its power. Low-power FCs are designed to work at around 12-18 V, in order to give acceptable levels of current. The smallest commercial FC that works at around 40-50 V is a 500 W FC named *GreenHub2 PRO 500* [W1], but is too powerful not only for the power levels required by the load, but also for the maximum-allowed battery currents, as it would give higher currents than the ones a small-capacity battery could bear. For this reason, even though passive hybrid configurations are a must-consider case in lightweight vehicles, it's not a viable option in this case as the sizing requirements do not match with any commercial fuel cells available.

## 6.4 Semi-active hybrid configurations

The semi-active hybrid configuration overcomes the just commented FC voltage limitation of the passive one by implementing a DC-DC booster the steps the operating voltage of the FC up to the DC bus' voltage. This allows the use of low-power fuel cells with relatively high DC bus' voltages. As before, different FC sizes will be tested until achieving a point where the battery never gets depleted as long as hydrogen is supplied to the FC. In that case, any required autonomy can be achieved by correct sizing of the hydrogen storage system. In the opposite case, the autonomy of the vehicle would not only depend on the amount of hydrogen stored, as the battery could also be depleted before the hydrogen storage system empties.

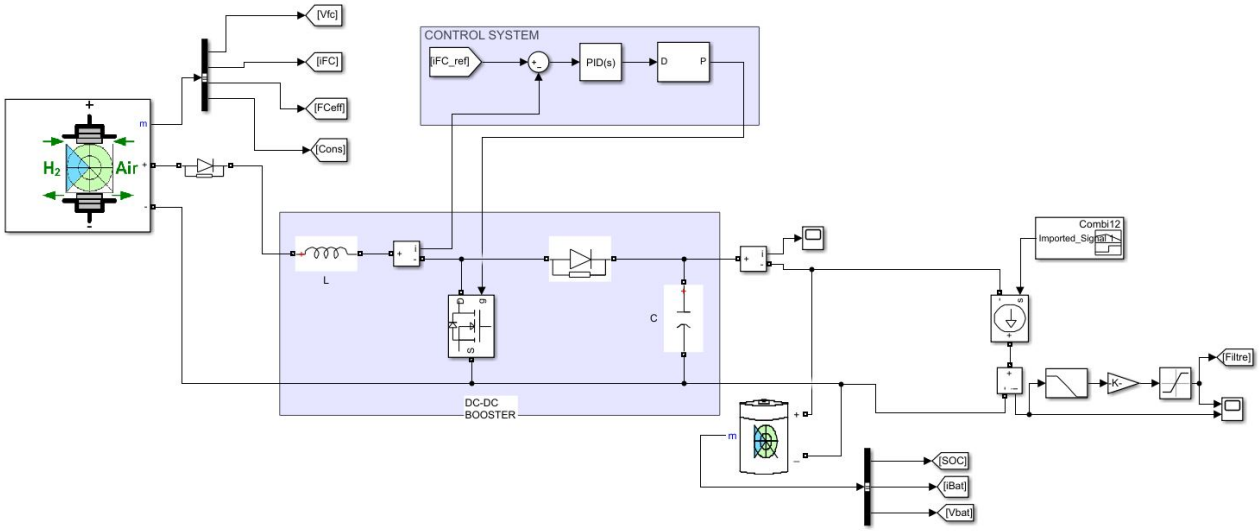


**Figure 6.16:** *Semi-active hybrid powertrain circuit*

As it can be seen in the *Simulink* circuit displayed in Figure 6.16, the circuit incorporates several elements with respect to the passive one:

- *DC-DC Booster*: consists of an inductor, a MOSFET, diode and capacitor.
- *Active-control system*: following the EMS selected, compares a reference value with the actual FC current, and through a PID controller gives a PWM signal to the MOSFET.

- *Low-pass filter*: filters the load current in order to eliminate the high-frequency ripple and give a smoother current profile as FC current reference value .

The lowpass filter, which will remain constant for following sections and adjusted until reaching the desired degree of smoothness, has the following transfer function:

$$H(s) = \frac{1}{1 + 5 \cdot s} \tag{6.11}$$

The effect of this filter can be seen with detail in the 50 s sample found in Figure 6.17. The whole 1500 s current profiles can be seen in Figure 6.20.

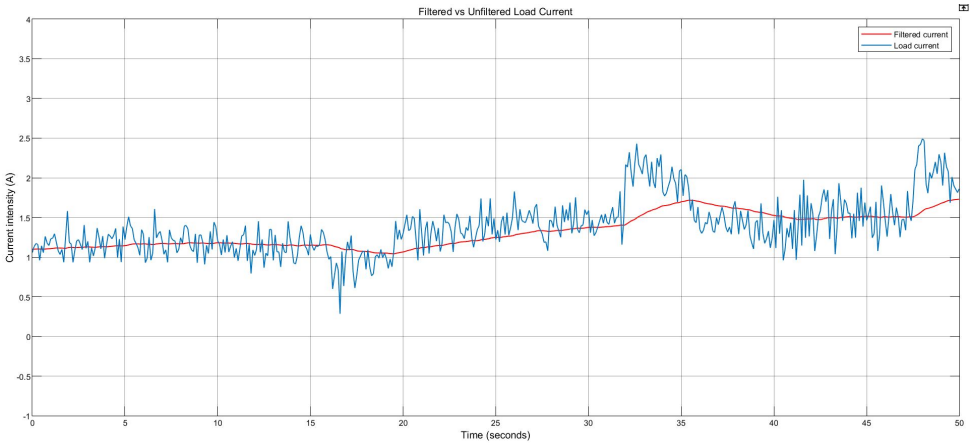


**Figure 6.17:** *50 s sample of filtered vs unfiltered load current*

Nevertheless, if this filtered current is intended to be given as reference current to the FC, an important aspect must be discussed. When the voltage of the FC is stepped-up through the boost converter, the output current is lower than the input one as power must be conserved. Thus, as the intention is that the FC acts as the main power source and the battery complements the fast-changing current profiles in order to avoid starvation, the filtered current will be multiplied by a constant, as seen in the gain block placed besides the filter, that will be set depending on the FC capabilities and load requirements, so that the FC current after the boost converter resembles the filtered current seen in Figure 6.17 as much as possible.

### 6.4.1 50W FC semi-active hybrid powertrain

Before entering in the simulation of the powertrain at different SOC levels, the different components of the circuit need to be sized, and the control system designed. In this case, commercial fuel cells can be used, so a 50W 20-cell fuel cell named *Protium-50* will be used. Its polarization curve can be seen in Figure 6.18.

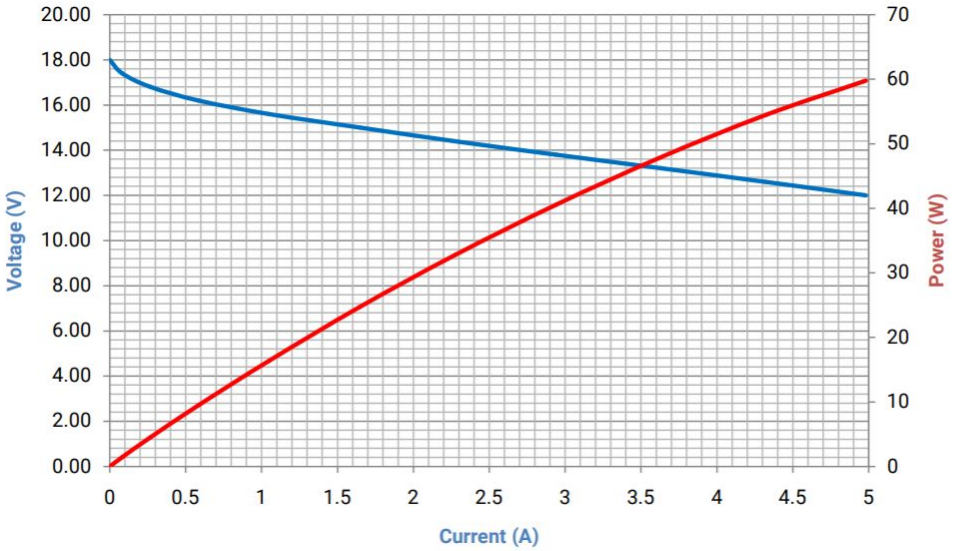


**Figure 6.18:** *Polarization curve of the Protium-50 [W2]*

Going on to the sizing of the DC-DC boost converter elements, the diode's default values are selected and the inductor's size has been chosen as the minimum possible that ensures that no high current ripples appear in the FC. Similarly for the capacitor's sizing, where a large capacitance value is needed in order to keep the voltage ripple low. For the MOSFET's period frequency of switching, it has been selected a value that ensures a good performance of the DC-DC boost converter without a great computational burden. Thus, the values for the different elements conforming the DC-DC converter are:

| | |
|---|---|
| Inductor | L = 100 mH |
| Capacitor | C = 1000 $\mu$F |
| MOSFET | f = 1000 Hz |

**Table 6.12:** *DC-DC booster element sizing*

Following the strategy found in [19] the Energy Management Strategy (EMS) followed has three different zones, depending on the battery SOC:

- SOC = 100-90% → $I_{FC}$=0 (the vehicle runs on only battery)
- SOC = 90-40% → $I_{FC}$ follows the filtered current
- SOC = 40-20% → $I_{FC}$=5 (the FC runs at maximum-power)

These three zones are achieved in the simulation through the following block distribution:

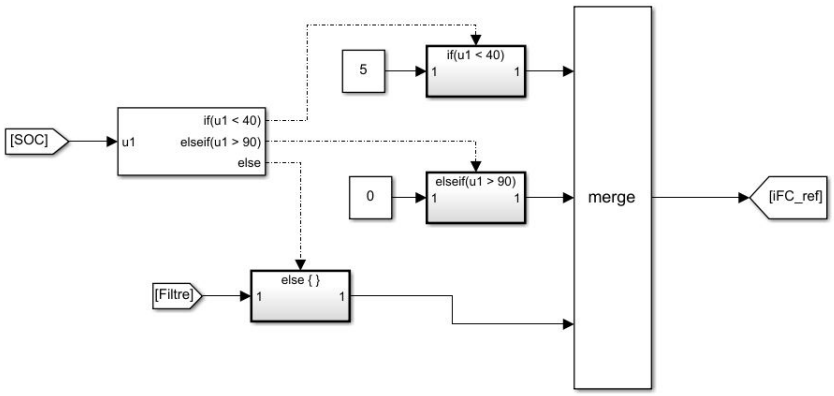


**Figure 6.19:** *Block distribution for the selection of the different EMS zones*

Between 90-40%, the FC reference current will be the filtered current. As the FC will operate between 12-14 V, and the DC bus voltage will be around 42-44 V, the boost converter will step-up the voltage around 3-3.5 times, so the current is expected to undergo a similar decrease (even bigger when considering the efficiency of the booster). Nevertheless, as it is a low-power FC and isn't able to reach currents of 6-8 A, the gain of the filtered current will be set at 2.5, with saturation at 5 A, as it is the maximum the 50W FC can provide. In Figure 6.20 the comparison between the unfiltered load current and the given FC reference current can be seen.

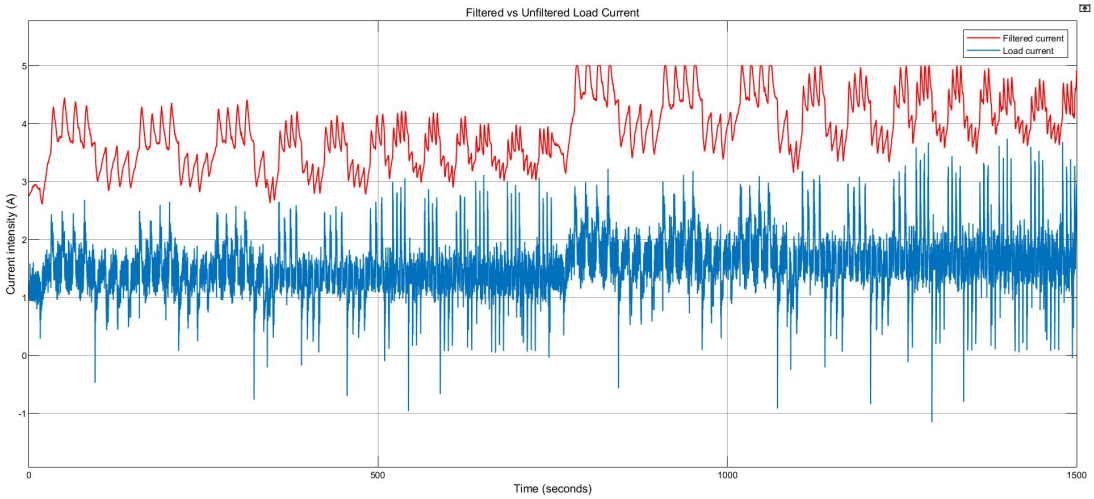


**Figure 6.20:** *Filtered vs unfiltered load current*

Another important aspect to consider is the selection of the controller. Initially an integral controller with I=2 is selected, in order to reduce the error in stationary state, which will be very effective when the reference current is constant (when the SOC of the battery is low and the FC runs at full power). Nevertheless, as it can be seen in the 50 s sample found in Figure 6.21, when the reference current is variable, the result is not optimal because lots of oscillations are found. For this reason, the proportional part of the PID controller is added, with P=1, as it can adjust more quickly to a changing profile. Its result can be seen in Figure 6.22, much better than the just-integral controller. No larger values of the PI controller are needed as they don't have noticeable effects on the the FC response. The derivative part is not included, as the stability is already good and could make noise appear in the signals. The final values, which already almost perfectly fit the desired FC current profile, can be seen in Table 6.13.

| P | I | D |
|---|---|---|
| 1 | 1 | 0 |

**Table 6.13:** *PID sizing for the 50W FC*

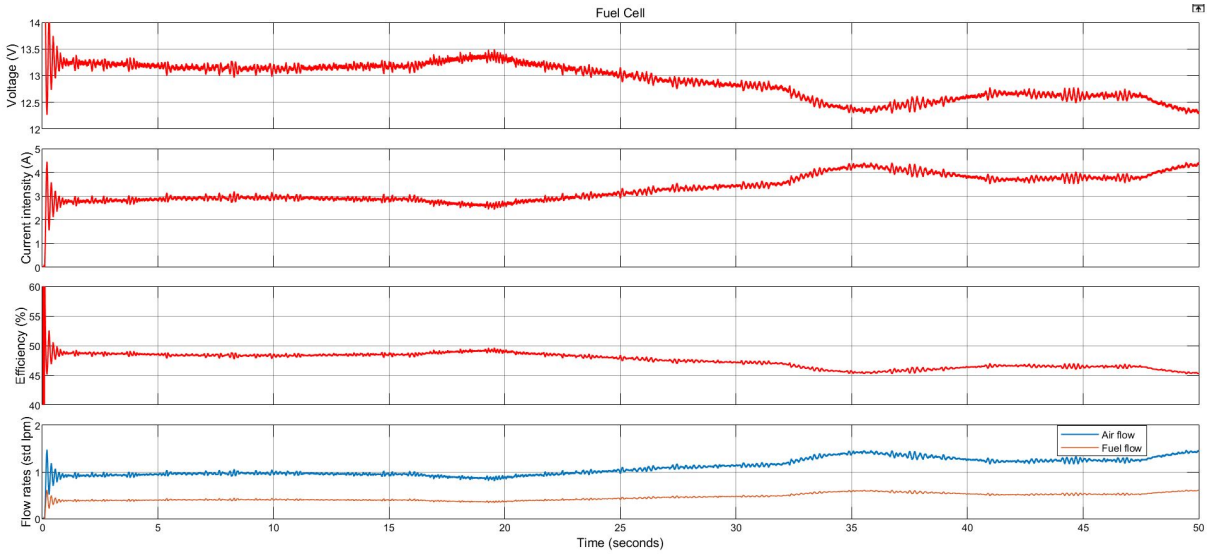


**Figure 6.21:** *FC response with an integral controller (50 s sample)*

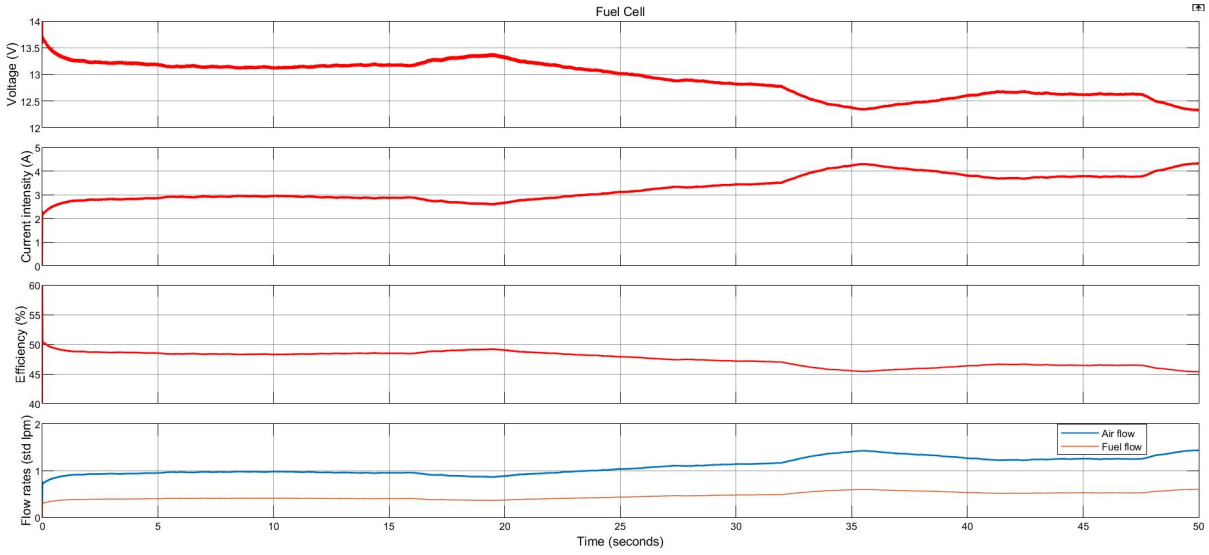


**Figure 6.22:** *FC response with a PI controller (50 s sample)*

As done before, the powertrain will be tested at three different SOC levels: high, medium and low.

- High-SOC $\rightarrow$ $SOC_0 = 90\%$

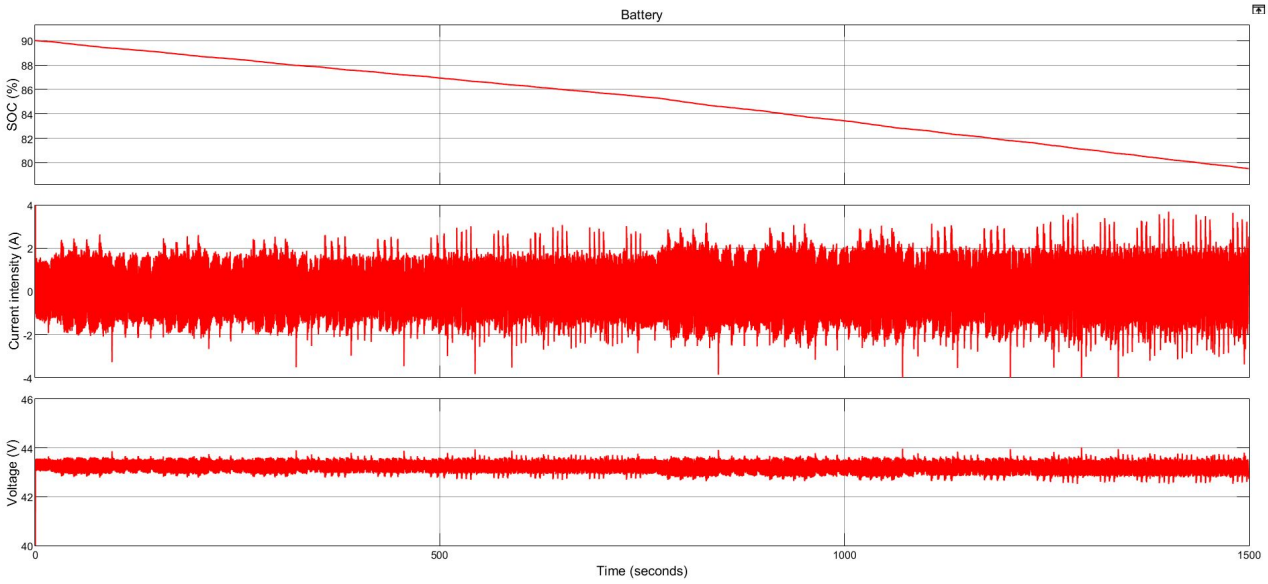


**Figure 6.23:** *Battery response in high-SOC 50W FC semi-active hybrid simulation*

Figure 6.23 shows an improvement in the battery depletion with respect to the battery-only model, which got depleted 3 times faster. Nevertheless, the high-frequency switching makes the profiles of voltage and current look very discontinuous, switching between positive and negative current values. For this reason, an approximate range of operation of current and voltage will be given without considering outliers, as it will be useful to look at the mean values of the variables to better understand the system. The battery's relevant information related to this cycle can be seen in Table 6.14.

| Variable | Range | Mean | $\Delta$ |
|---|---|---|---|
| SOC (%) | [90, 79.49] | - | -10.51 |
| Current (A) | (2.4, -2.3) | 0.20 | - |
| Voltage (V) | (43.6, 42.7) | 43.20 | - |

**Table 6.14:** *Battery response in high-SOC 50W FC semi-active hybrid simulation*

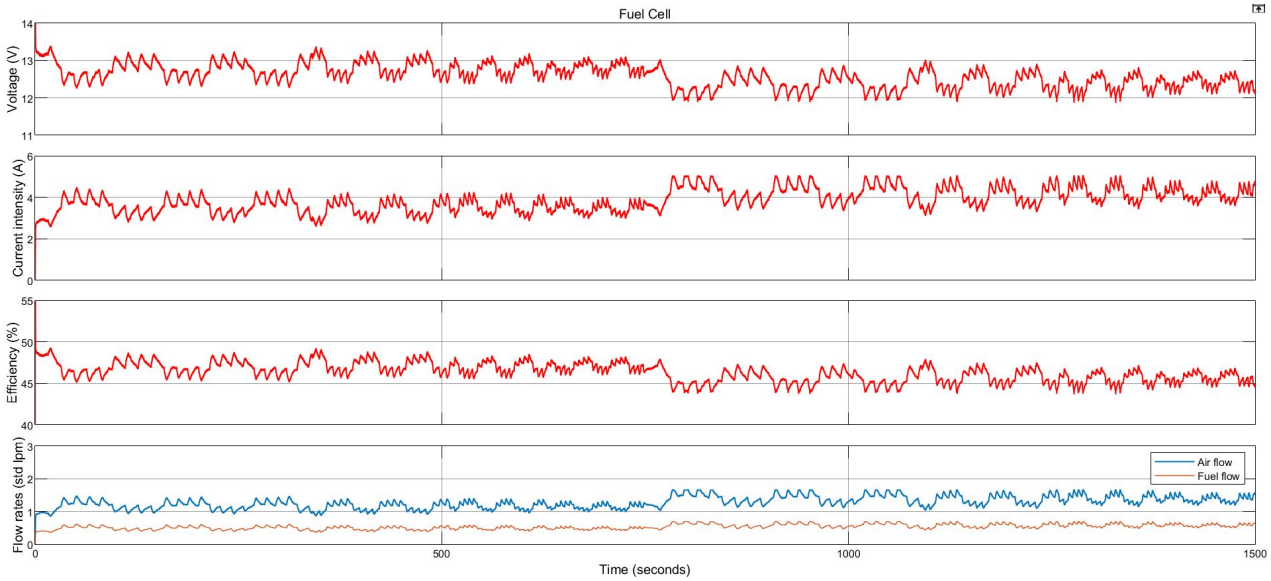


**Figure 6.24:** *FC response in high-SOC 50W FC semi-active hybrid simulation*

In Figure 6.24 it can be seen the FC performance. It has followed the load filtered current without ripple current or oscillations. The higher the current intensity, the lower the FC efficiency. A summary of the FC's relevant information related to this cycle can be seen in Table 6.15.

| Variable | Max | Min | Mean |
|---|---|---|---|
| Voltage (V) | 13.39 | 11.87 | 12.59 |
| Current (A) | 5.00 | 2.57 | 3.85 |
| Power (W) | 59.35 | 34.41 | 48.47 |
| Current after DC-DC booster (A) | - | - | 1.35 |
| Efficiency (%) | 49.27 | 44.18 | 46.34 |
| Air flow rate (std lpm) | 1.68 | 0.85 | 1.29 |
| Fuel flow rate (std lpm) | 0.71 | 0.36 | 0.54 |

**Table 6.15:** *FC response in high-SOC 50W FC semi-active hybrid simulation*

- Medium-SOC $\rightarrow$ $SOC_0 = 60\%$

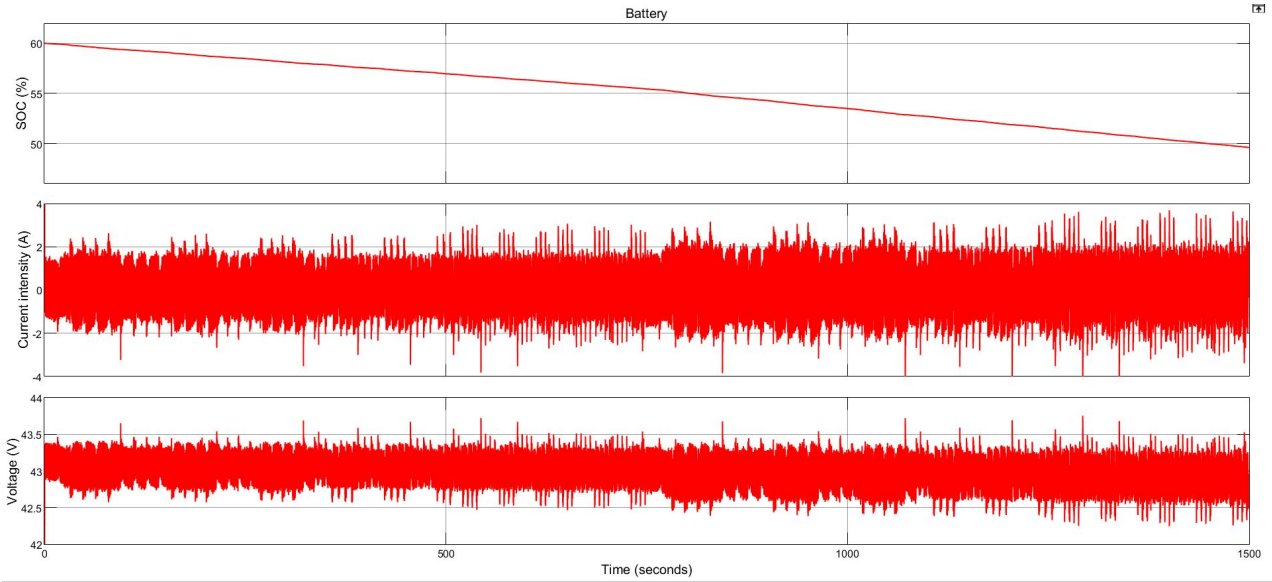


**Figure 6.25:** *Battery response in medium-SOC 50W FC semi-active hybrid simulation*

Figure 6.25 shows similar profiles than the ones seen in the high-SOC case. Lower voltage, as the SOC is lower, but the current going through the battery and its $\Delta$SOC remains almost the same.The battery's relevant information related to this cycle can be seen in Table 6.16.

| Variable | Range | Mean | $\Delta$ |
|---|---|---|---|
| SOC (%) | [60, 49.59] | - | -10.41 |
| Current (A) | (2.5, -2.4) | 0.20 | - |
| Voltage (V) | (43.4, 42.5) | 42.97 | - |

**Table 6.16:** *Battery response in medium-SOC 50W FC semi-active hybrid simulation*

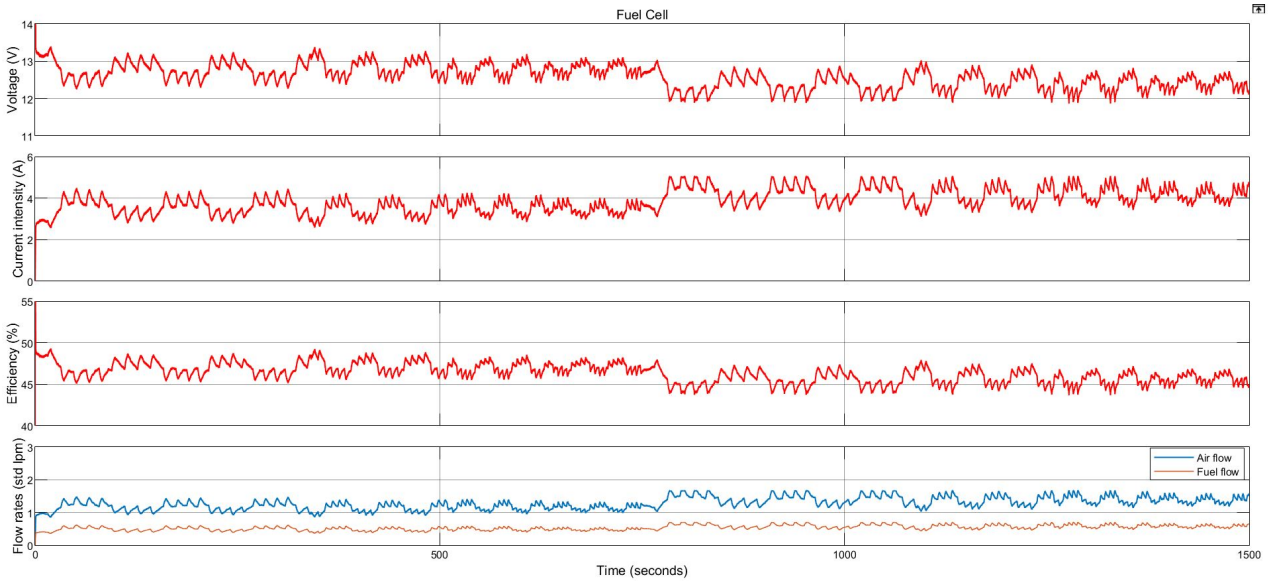


**Figure 6.26:** *FC response in medium-SOC 50W FC semi-active hybrid simulation*

In Figure 6.26 and Table 6.17 it can be seen how the FC response is completely equal to the high-SOC case, as the operating voltage of the FC no longer depends on the battery voltage, but only on the reference current given, which is the same in both cases. Nevertheless, as the voltage of the battery is slightly lower in this case than in the high-SOC one, the duty-cycle of the boost converter is smaller, which leads to a higher mean output current. However, this difference is almost negligible (1.36 A vs 1.35 A). For this reason, though the simulation of the mid-SOC case will continue to be done, in future sections no graphics or tables about the FC performance will be displayed.

| Variable | Max | Min | Mean |
|---|---|---|---|
| Voltage (V) | 13.39 | 11.87 | 12.59 |
| Current (A) | 5.00 | 2.57 | 3.85 |
| Power (W) | 59.35 | 34.41 | 48.47 |
| Current after DC-DC booster (A) | - | - | 1.36 |
| Efficiency (%) | 49.27 | 44.18 | 46.34 |
| Air flow rate (std lpm) | 1.68 | 0.85 | 1.28 |
| Fuel flow rate (std lpm) | 0.71 | 0.36 | 0.54 |

**Table 6.17:** *FC response in medium-SOC 50W FC semi-active hybrid simulation*

- Low-SOC → $SOC_0 = 30\%$

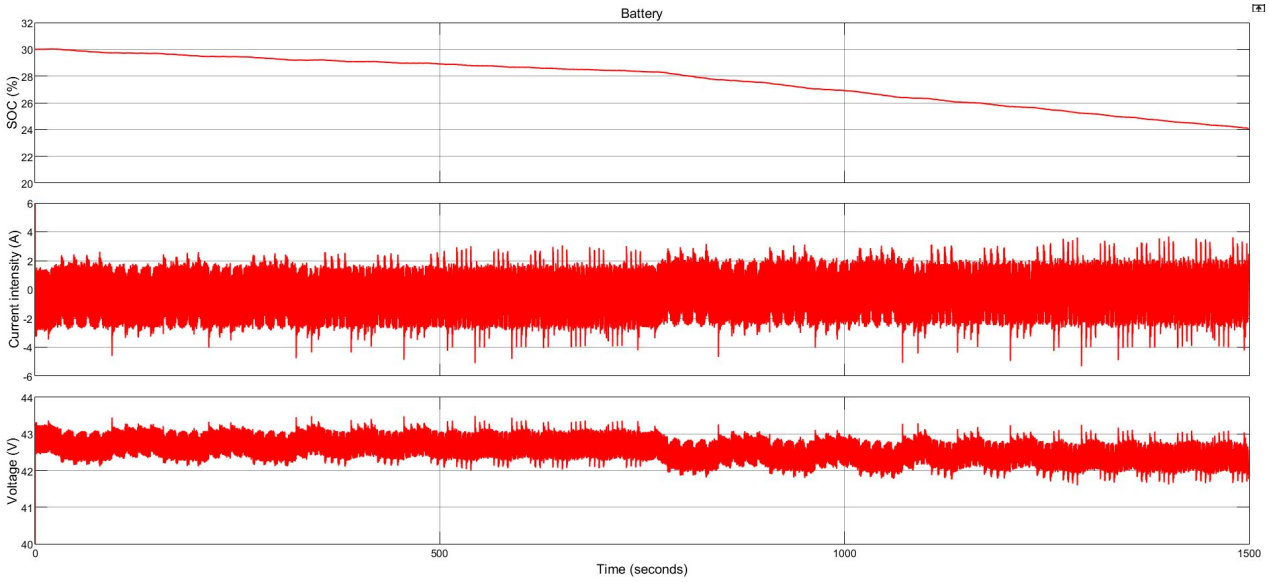


**Figure 6.27:** *Battery response in low-SOC 50W FC semi-active hybrid simulation*

Figure 6.27 shows that when the FC is running at full power it is not able to charge the batteries. However, the depletion rate of the battery is pretty low, meaning that a long autonomy can be achieved. The battery's relevant information related to this cycle can be seen in Table 6.18.

| Variable | Range | Mean | $\Delta$ |
|---|---|---|---|
| SOC (%) | [30, 24.07] | - | -5.93 |
| Current (A) | (2.2, -3.0) | -0.13 | - |
| Voltage (V) | (43.2, 42.0) | 42.53 | - |

**Table 6.18:** *Battery response in low-SOC 50W FC semi-active hybrid simulation*

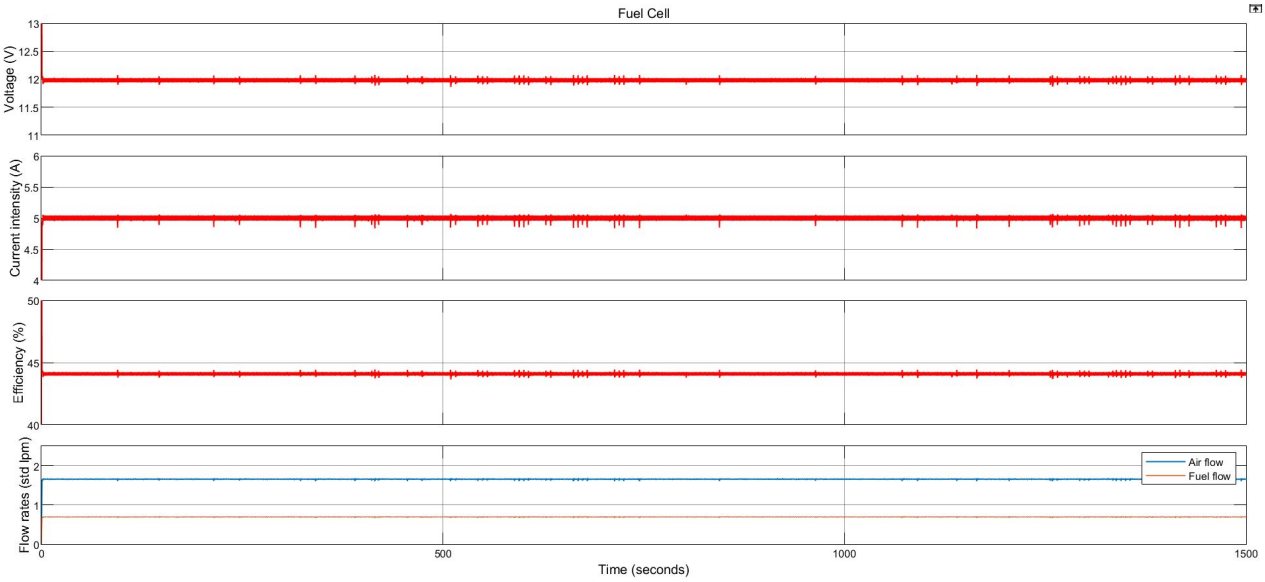


**Figure 6.28:** *FC response in low-SOC 50W FC semi-active hybrid simulation*

Figure 6.28 shows how the FC is running at full-power, adjusting almost perfectly to the given 5 A reference current. However, high-power is achieved in expense of a decrease in the efficiency of the FC. A summary of the FC's relevant information related to this cycle can be seen in Table 6.19.

| Variable | Max | Min | Mean |
|---|---|---|---|
| Voltage (V) | 12.05 | 11.86 | 12.00 |
| Current (A) | 5.07 | 4.83 | 4.99 |
| Power (W) | 60.13 | 58.21 | 59.93 |
| Current after DC-DC booster (A) | - | - | 1.66 |
| Efficiency (%) | 44.45 | 43.65 | 44.15 |
| Air flow rate (std lpm) | 1.68 | 1.60 | 1.66 |
| Fuel flow rate (std lpm) | 0.71 | 0.67 | 0.70 |

**Table 6.19:** *FC response in low-SOC 50W FC semi-active hybrid simulation*

- Overall performance

The parameters controlled can be seen displayed in Table 6.20.

| Parameter | High-SOC | Medium-SOC | Low-SOC |
|---|---|---|---|
| $H_2$ consumption (g) | 1.15 | 1.15 | 1.49 |
| Ah-throughput (A· h) | 0.421 | 0.500 | 0.695 |

**Table 6.20:** *Performance parameters of the passive hybrid simulation*

On the qualitative performance aspects, it can be said that the EMS selected and the control system adopted has allowed the FC to work following smooth profiles and within its reach, so safe operating conditions have been achieved. However, the use of the DC-DC converter has lead to discontinuous operation in battery current, although the Ah-throughput has not been affected by it and has stayed in reasonable levels.

When compared to the passive configuration, both the hydrogen consumption and the effective Ah-throughput have grown. However, it overcomes the constructional problems that the passive configuration presented, and a control of the system is possible.

Finally, as in neither of the three zones tested the final SOC value was greater than the initial one, thus meaning that the autonomy would only depend on the size of the hydrogen storage systems, the maximum autonomy possible of the vehicle in this powertrain has to be calculated. Considering the three different EMS zones:

| SOC range | $\Delta$SOC per cycle |
|---|---|
| [100, 90) | -29.32 |
| (90, 40) | -10.46 |
| (40, 20] | -5.93 |

**Table 6.21:** *Battery depletion in the three different EMS zones*

where the $\Delta$SOC per cycle in the 90-40% has been calculated as the mean between the high-SOC and medium-SOC zones, the vehicle's maximum achievable autonomy is calculated as:

$$t_{autonomy} = 10\% \cdot \frac{1500\ s}{29.32\%} + 50\% \cdot \frac{1500\ s}{10.46\%} + 20\% \cdot \frac{1500\ s}{5.93\%} = \\ = 511.6\ s + 7170.2\ s + 5059.0\ s = 12740.8\ s \approx 3h\ 32min \tag{6.12}$$

which is a great improvement when compared to the actual state, but it doesn't meet the autonomy requirements. For this reason, a more powerful fuel cell is needed.

### 6.4.2 150W FC semi-active hyrbid powertrain

As the 50W fuel cell doesn't meet with the autonomy requirements, a most powerful FC is needed. However, the 50W FC gave a good performance and was not far from covering the desired requirements. For this reason, the FC needed is not much more powerful than this last one. Initially, a 100W FC is considered, and the *GreenBox 2-100W* is found in the market [W3]. However, another fuel cell is found [W4], of 150W, the *Protium-150*, which is far cheaper than the less-powerful *GreenBox 2*: 4265$ vs 5720$. The fact that it's cheaper, combined with the fact that it is more powerful in case in the future a more powerful FC is needed, makes that the *Protium-150* is selected. It's a 20-cell FC, and its polarization curve can be seen in Figure 6.29.

Going on to the sizing of the DC-DC boost converter elements, and as before, where the diode's default values were selected, and the inductor, capacitor and MOSFET's switching frequency were selected to be the minimum that ensure no current or voltage ripples and good performance of the DC-DC booster. A larger capacitance has been selected, as the input current was higher and it was needed that the capacitor stored more energy. Thus, the values for the different elements conforming the DC-DC converter can be seen in Table 6.22.

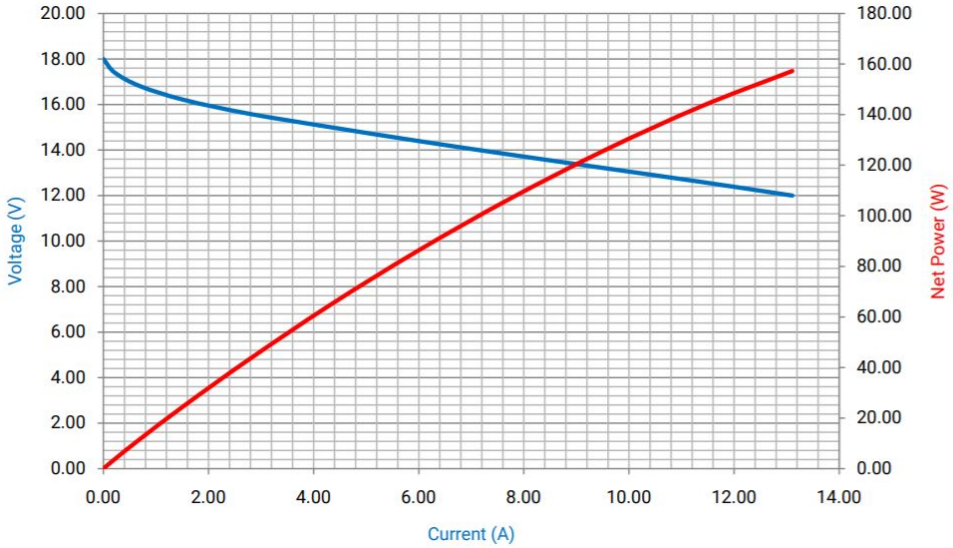


**Figure 6.29:** *Polarization curve of the Protium-150 [W4]*

| | |
|---|---|
| Inductor | L = 100 mH |
| Capacitor | C = 2000 $\mu$F |
| MOSFET | f = 1000 Hz |

**Table 6.22:** *DC-DC booster element sizing*

Although being a 150W FC, and be able to provide more than 12 A of current, it won't be made to operate at maximum power as it won't be necessary. Thus, the decided EMS followed will have, as before, three different zones, depending on the battery SOC:

- SOC = 100-90% → $I_{FC}$=0 (the vehicle runs on only battery)
- SOC = 90-40% → $I_{FC}$ follows the filtered current
- SOC = 40-20% → $I_{FC}$=6 (the FC runs at half power)

These three zones are achieved in the simulation through the following block distribution:

For low-SOC levels, the FC reference current was intially set to 8, the FC nominal operating point. However, it was seen that this current was too large for the load

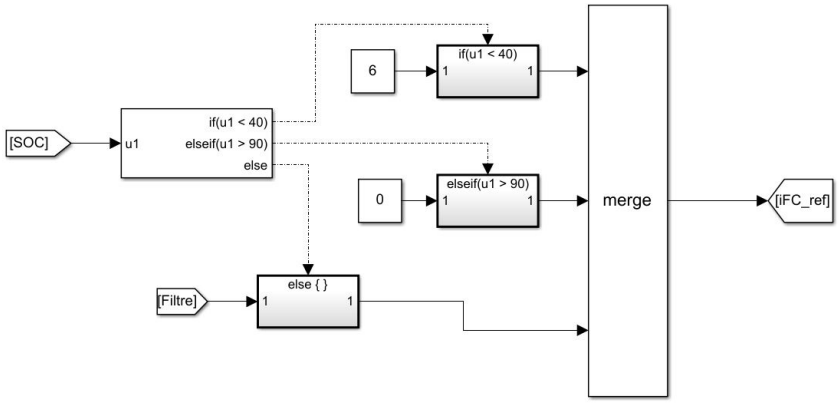


**Figure 6.30:** *Block distribution for the selection of the different EMS zones*

requirements and that the batteries were charged with large currents that could highly accelerate its degradation. For this reason, it has been decided that the FC provides 6 A of current when the SOC is low. Between 90-40%, the FC reference current will be the filtered current. As it has been oversized, the FC will operate at higher voltages when providing similar currents than in the 100W FC case, between 12-16 V, and the DC bus voltage will be around 42-44 V. Thus, the boost converter will step-up the voltage around 2.5-3.5 times, so the current is expected to undergo a similar decrease. Initially a gain of the filtered current of 3.5 is proposed, but the result is too powerful. The objective of the middle EMS zone is to share the power of the load between the FC and the battery, not that the FC provides extra power. For this reason, the gain is finally set to 3, with a saturation of 12 A, which is almost the maximum the FC can provide. In Figure 6.31 the comparison between the unfiltered load current and the given FC reference current can be seen.

The last step before starting the simulation is the control system's sizing. As before, a PI controller will be selected, as the integral part is able to reduce the error in stationary state, which will be very effective when the reference current is constant (when the SOC of the battery is low), and the proportional part makes it adapt better when the reference current is variable. Without the proportional part, lots of noise appear in the FC signals. The values for the PI controller are adjusted and the ones decided can be seen in Table 6.23, and the FC response to this controller in Figure 6.32.

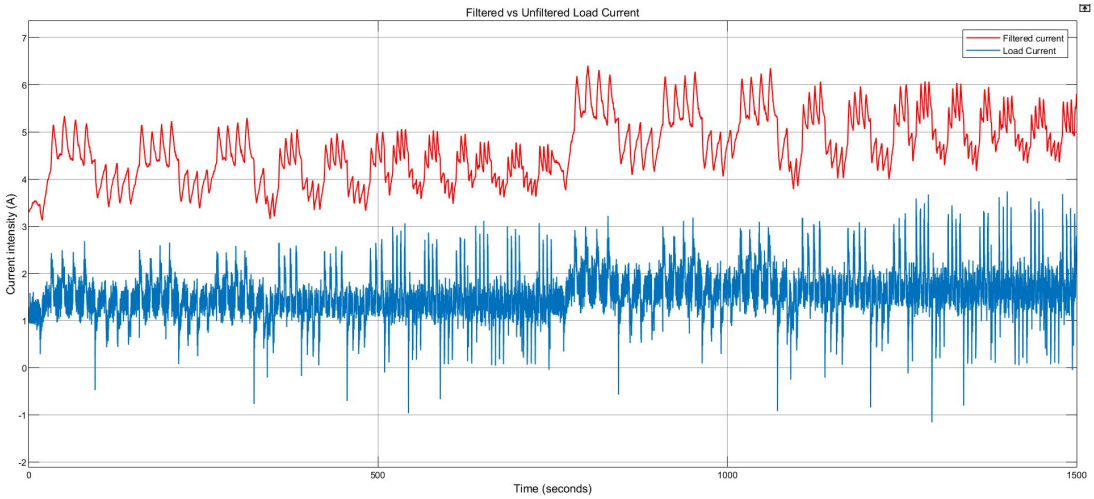


**Figure 6.31:** *Filtered vs unfiltered load current*

| P | I | D |
|---|---|---|
| 1 | 1 | 0 |

**Table 6.23:** *PID sizing for the 150W FC*

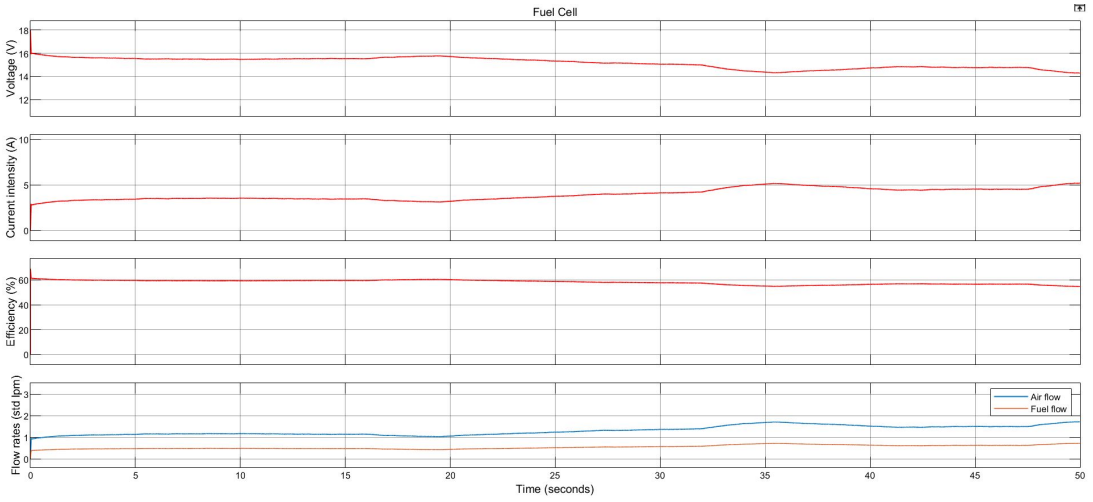


**Figure 6.32:** *FC response with a PI controller (50 s sample)*

As done before, the powertrain will be tested at three different SOC levels: high, medium and low.

- High-SOC $\rightarrow$ $SOC_0 = 90\%$

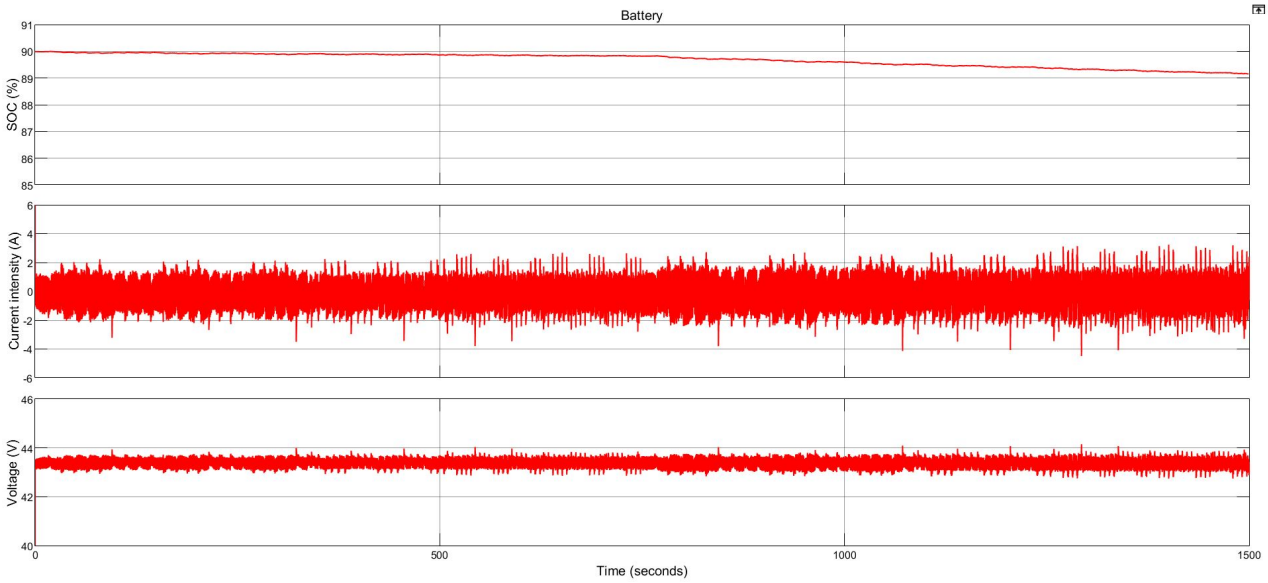


**Figure 6.33:** *Battery response in high-SOC 150W FC semi-active hybrid simulation*

Figure 6.33 shows an improvement in the battery depletion with respect to the 50W case. Moreover, the bigger capacitor allows to narrow the voltage and current range. As the current that arrives through the boost converter is higher, the battery has to contribute to the load needs in smaller quantities, and many times (seen when the battery current is negative) it can recharge with the extra power. The battery's relevant information related to this cycle can be seen in Table 6.24.

| Variable | Range | Mean | $\Delta$ |
|---|---|---|---|
| SOC (%) | [90, 89.14] | - | -0.86 |
| Current (A) | (1.8, -2.2) | -0.11 | - |
| Voltage (V) | (43.6, 43.0) | 43.37 | - |

**Table 6.24:** *Battery response in high-SOC 150W FC semi-active hybrid simulation*

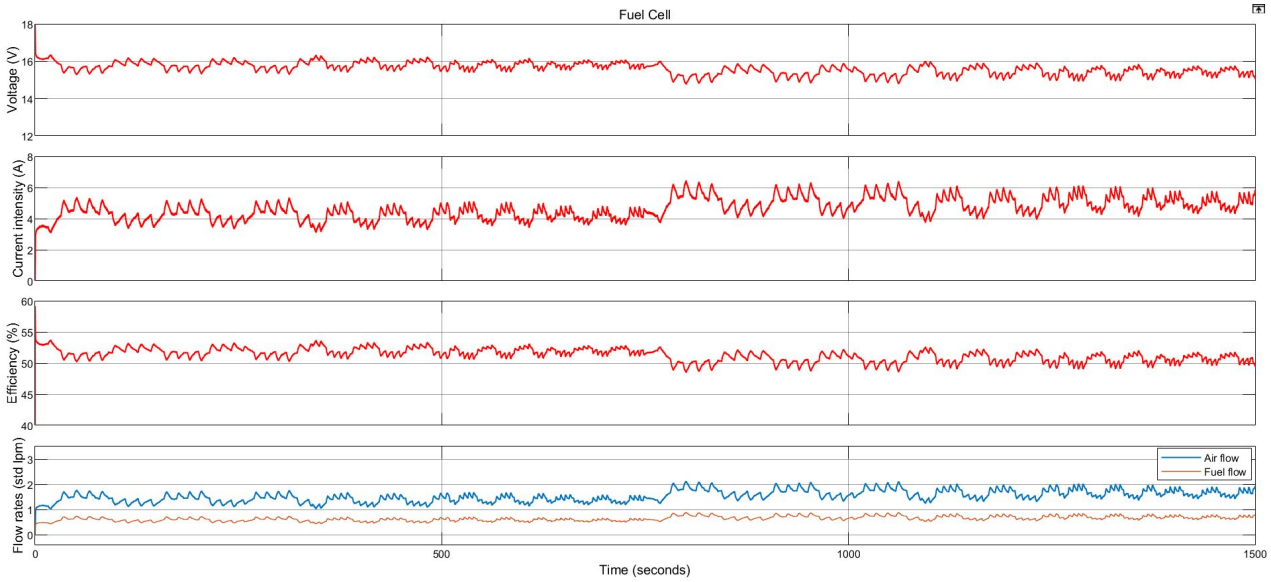


**Figure 6.34:** *FC response in high-SOC 150W FC semi-active hybrid simulation*

In Figure 6.34 it can be seen the FC performance, that has followed the reference current without ripple current or oscillations. A summary of the FC's relevant information related to this cycle can be seen in Table 6.25. Looking at the power numbers, it can be seen that the maximum power of the FC is below 100W, so it could have been achieved by the 100W FC if the price would have been favorable. Nevertheless, a positive aspect of using a 150W FC is that as the voltage range is the same as the 100W one, for the same current the FC of 150W operates at higher voltages. This is positive because when the voltage is stepped-up the increase in voltage is lower, and as a consequence the amount of output current of the boost converter is higher.

| Variable | Max | Min | Mean |
|---|---|---|---|
| Voltage (V) | 16.35 | 14.75 | 15.62 |
| Current (A) | 6.46 | 3.08 | 4.60 |
| Power (W) | 95.29 | 50.36 | 71.85 |
| Current after DC-DC booster (A) | - | - | 1.65 |
| Efficiency (%) | 53.72 | 48.60 | 51.33 |
| Air flow rate (std lpm) | 2.14 | 1.02 | 1.53 |
| Fuel flow rate (std lpm) | 0.90 | 0.43 | 0.64 |

**Table 6.25:** *FC response in high-SOC 150W FC semi-active hybrid simulation*

- Medium-SOC $\rightarrow$ $SOC_0 = 60\%$

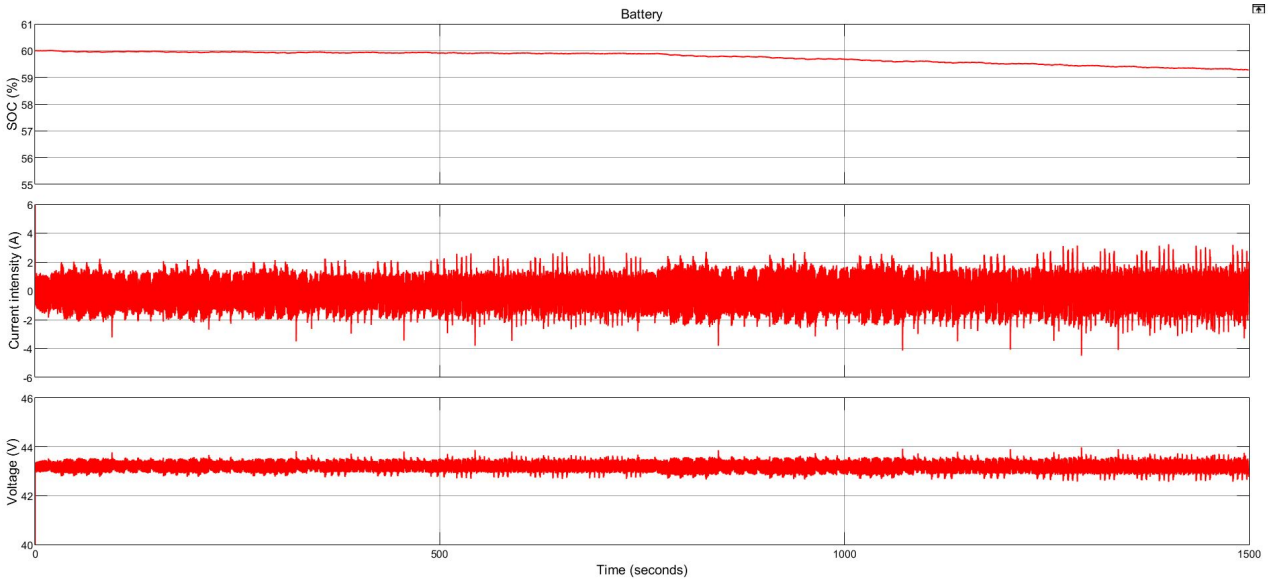


**Figure 6.35:** *Battery response in medium-SOC 150W FC semi-active hybrid simulation*

Figure 6.35 shows similar profiles than the ones seen in the high-SOC case. Slightly lower voltage, as the SOC is lower, but the current going through the battery and its $\Delta$SOC remains very similar.The battery's relevant information related to this cycle can be seen in Table 6.26.

| Variable | Range | Mean | $\Delta$ |
|---|---|---|---|
| SOC (%) | [60, 59.27] | - | -0.73 |
| Current (A) | (1.8, -2.2) | -0.11 | - |
| Voltage (V) | (43.4, 42.9) | 43.19 | - |

**Table 6.26:** *Battery response in medium-SOC 150W FC semi-active hybrid simulation*

On the other hand, as it has been said before, the FC performance is exactly equal as the high-SOC one. For this reason, its profiles can be seen in Figure 6.34 and its information in Table 6.25.

- Low-SOC → $SOC_0 = 30\%$

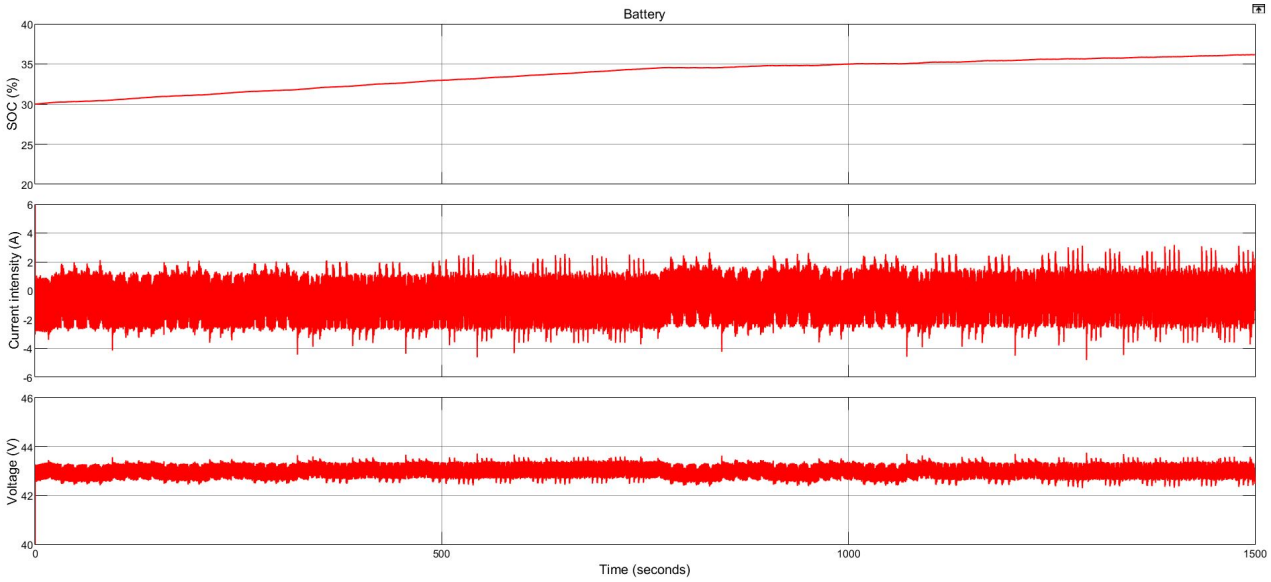


**Figure 6.36:** *Battery response in low-SOC 150W FC semi-active hybrid simulation*

Figure 6.36 shows how the FC is able to cover the load needs and charge the batteries with its extra power when providing a constant 6A of current. As in this period the FC has been able to charge the batteries, it means that the battery won't be depleted while there is hydrogen available. The battery's relevant information related to this cycle can be seen in Table 6.27.

| Variable | Range | Mean | Δ |
|---|---|---|---|
| SOC (%) | [30, 36.16] | - | +6.16 |
| Current (A) | (1.6, -2.8) | -0.53 | - |
| Voltage (V) | (43.4, 42.6) | 42.97 | - |

**Table 6.27:** *Battery response in low-SOC 150W FC semi-active hybrid simulation*

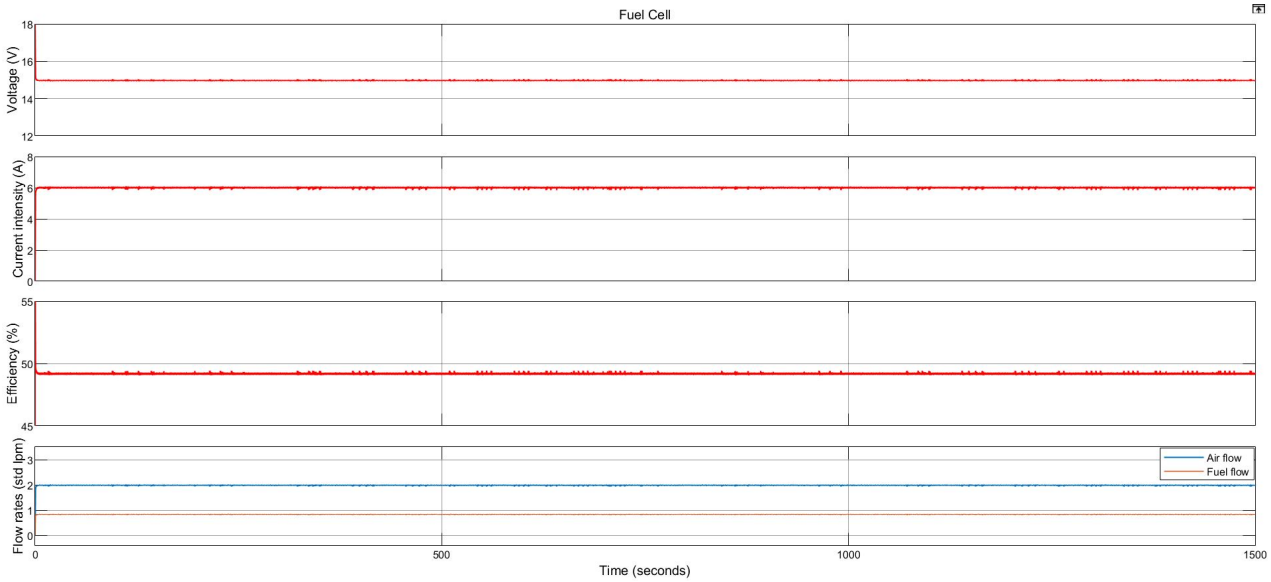


**Figure 6.37:** *FC response in low-SOC 150W FC semi-active hybrid simulation*

Figure 6.37 shows how the FC is running at constant 6A of current, adjusting perfectly to the given constant reference current. A summary of the FC's relevant information related to this cycle can be seen in Table 6.28, where all parameters are kept almost constant. Looking at the power numbers, it can be seen that it could have been achieved by a 100W FC. Nevertheless, the difference in price, and the possibility of handling heavier loads when needed in the future as the FC is oversized, makes the choosing of the 150W FC a good choice.

| Variable | Max | Min | Mean |
|---|---|---|---|
| Voltage (V) | 14.99 | 14.93 | 14.97 |
| Current (A) | 6.09 | 5.93 | 6.00 |
| Power (W) | 90.92 | 88.89 | 89.82 |
| Current after DC-DC booster (A) | - | - | 2.08 |
| Efficiency (%) | 49.26 | 49.11 | 49.19 |
| Air flow rate (std lpm) | 2.02 | 1.96 | 1.99 |
| Fuel flow rate (std lpm) | 0.85 | 0.82 | 0.84 |

**Table 6.28:** *FC response in low-SOC 150W FC semi-active hybrid simulation*

- Overall performance

The parameters controlled can be seen displayed in Table 6.29.

| Parameter | High-SOC | Medium-SOC | Low-SOC |
|---|---|---|---|
| $H_2$ consumption (g) | 1.38 | 1.38 | 1.78 |
| Ah-throughput (A· h) | 0.295 | 0.355 | 0.556 |

**Table 6.29:** *Performance parameters of the semi-active hybrid simulation*

On the qualitative performance aspects, it can be said that the EMS selected and the control system adopted has allowed the FC to work following smooth profiles and within its reach, so safe operating conditions have been achieved. However, as before, the use of the DC-DC converter has lead to discontinuous operation in battery current.

Comparing it to the 50W FC case, it can be seen that the hydrogen consumption has suffered an increase of a 20% approximately for all SOC-levels, as it could have been expected after choosing a more powerful FC. However, this increase in the FC power doesn't just affect the hydrogen consumption, but as the FC contributes with higher levels of current, the battery's contribution is lower. As a consequence, the Ah-throughput has decreased in a 40% when the vehicle is in power-shared mode (high and medium SOC levels), and a 25% for low SOC levels, when the batteries are charged with the extra power of the FC. For this reason, and for the increased autonomy of the vehicle, this option can be considered a better one than the 50W one.

## 6.5 Full-active hybrid configurations

The full-active hybrid configuration presents several advantages with respect to the semi-active configuration. On one hand, a total control is possible, as the voltage of the DC bus can be adjusted to the desired reference value. This allows a decoupling of the battery's operating conditions with respect to the DC bus' voltage. Like this, the voltage of the DC bus can be set to 44V, the nominal operating voltage of the driver, and the

battery can work at lower voltage levels. As it is a low-capacity battery, 2200 mAh, a normal operating voltage has been considered to be around 12V.

As before, different FC sizes will be tested until achieving a point where the battery never gets depleted as long as hydrogen is supplied to the FC. For this configuration, the 50W FC won't be considered as the initial case, as it has been shown in the semi-active configuration that is not powerful enough for the requirements of the load. In the full-active configuration, two DC-DC converters are found, which means that the battery will have to produce a higher current for the same load requirements, as it will get reduced in the converter. If the 50W FC wasn't enough in the semi-active case, it won't give a better performance in this powertrain configuration.

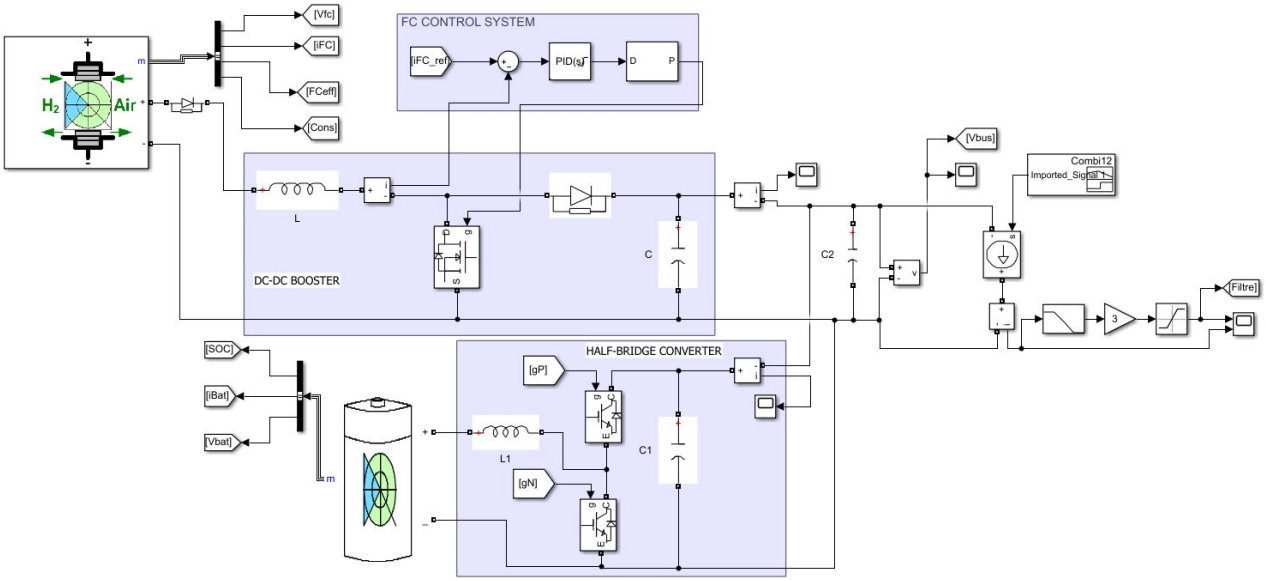


**Figure 6.38:** *Full-active hybrid powertrain circuit*

As it can be seen in the *Simulink* circuit displayed in Figure 6.38, with respect to the semi-active case the circuit incorporates a half-bridge converter between the battery and the DC bus. This converter controls the voltage of the DC bus through this control system seen in Figure 6.39. In the control system for the FC current, the actual current was compared with a reference one and through a PI controller a PWM was given to the switching device. However, in this case, it works in a different way, as the desired voltage in the DC bus is achieved by adjusting the current given by the battery. For this

reason, the desired DC bus voltage (44 V) is compared with the actual one, and through a controller the reference battery current is given, which in turn will be compared with the actual battery current, giving through another controller a PWM to the switching devices. These switches have to be complementary, so when one of them is open the other is closed and vice-versa. For this purpose, a logic NOT gate is used.

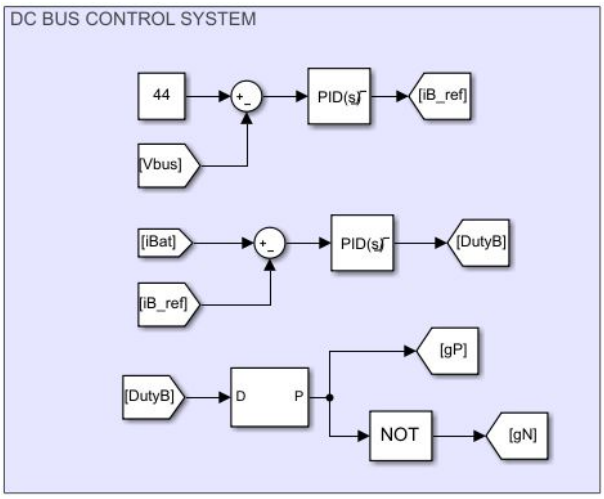


**Figure 6.39:** *DC bus control system*

### 6.5.1 150W FC full-active hyrbid powertrain

Again, the 150W FC *Protium-150* is selected, as it cheaper and more powerful, if necessary, than the 100W *GreenBox 2*. Its polarization curve can be seen in Figure 6.29. As the FC doesn't change, neither does the sizing of all its related components: the DC-DC boost converter sizing remains the same as in Table 6.22, and its control system will still be a PI controller with the same values as the ones presented in Table 6.23. Also, the EMS selected will be the same, and the reference current for the FC will still be the filtered current multiplied by a constant value of 3.

Moving on to the sizing of the battery related components, larger characteristic values for the main components have been adopted as the battery current and voltage presented severe ripples and discontinuities. Starting at the sizing of the half-bridge converter elements, the diode's default values were selected and the frequency of the

IGBTs was kept the same as for the MOSFET. However, larger inductance and capacitance values have been selected. Although optimal results are not obtained, it has been decided to not make them bigger in order to avoid an overweight in the system. Thus, the values for the different elements conforming the DC-DC half-bridge converter can be seen in Table 7.5. Additionally, a second capacitor, $C_2$, with a large capacitance value of 5000 $\mu$F has been added in the DC bus with the objective of stabilizing its voltage.

| | |
|---|---|
| Inductor | $L_1$ = 500 mH |
| Capacitor | $C_1$ = 5000 $\mu$F |
| IGBTs | f = 1000 Hz |

**Table 6.30:** *DC-DC Half-Bridge converter component sizing*

The last step before starting the simulation is the battery control system's sizing, where two different controllers are needed. As before, PI controllers will be selected, as the integral part is able to reduce the error in stationary state, and the proportional part makes it adapt quicker. Output saturation values are set in order to limit the battery reference current between [-4,4] and the PWM's duty-cycle between [0,0.95]. Initially a larger integral component of the PI controller is considered for both controllers, as it the part that makes the signal adjust better to the constant value of 44V. A combination of P=1 and I=5 is considered. Nevertheless, as it can be seen in Figure 6.40 lots of oscillations appear. It could be for a higher than optimal P value, but when making it smaller the results are even worse, as it happens with larger values for the I controller. In the end, the I value is reduced in both controllers and better adjusts are found, although the oscillations don't disappear. The mean of the signal, though, is adjusted correctly to the wanted 44V. The results can be seen in Figure 6.41, and the final values of the controllers can be seen in Table 6.31.

| Controller | P | I | D |
|---|---|---|---|
| $V_{DCBus}$ | 1 | 0.1 | 0 |
| $I_{Bat}$ | 1 | 0.1 | 0 |

**Table 6.31:** *PID sizing for the DC bus' voltage control*

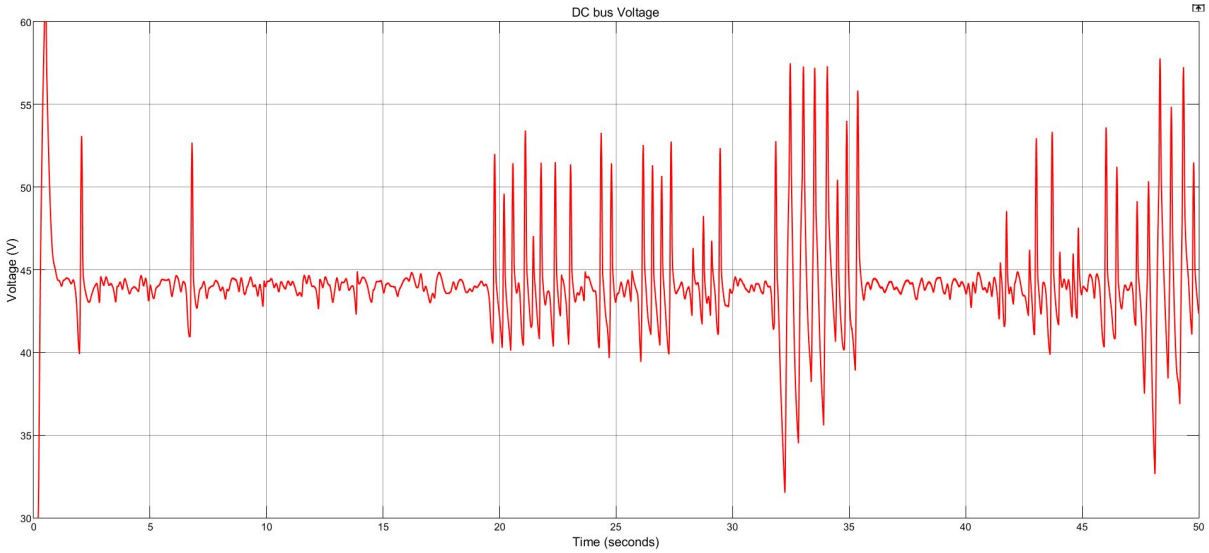


**Figure 6.40:** *DC bus' voltage when P=1 and I=5 (50 s sample)*

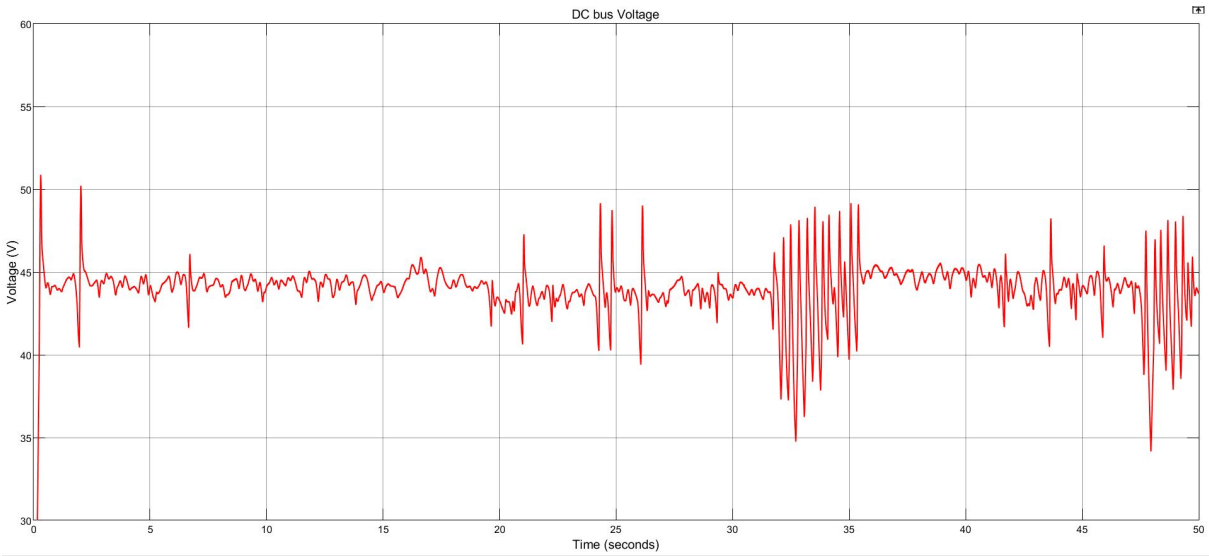


**Figure 6.41:** *DC bus' voltage when P=1 and I=0.1 (50 s sample)*

As done before, the powertrain will be tested at three different SOC levels: high, medium and low. The fuel cell information won't be displayed in this section as its profiles are exactly equal than in the semi-active case for high, medium and low-SOC.

- High-SOC $\rightarrow$ $SOC_0 = 90\%$

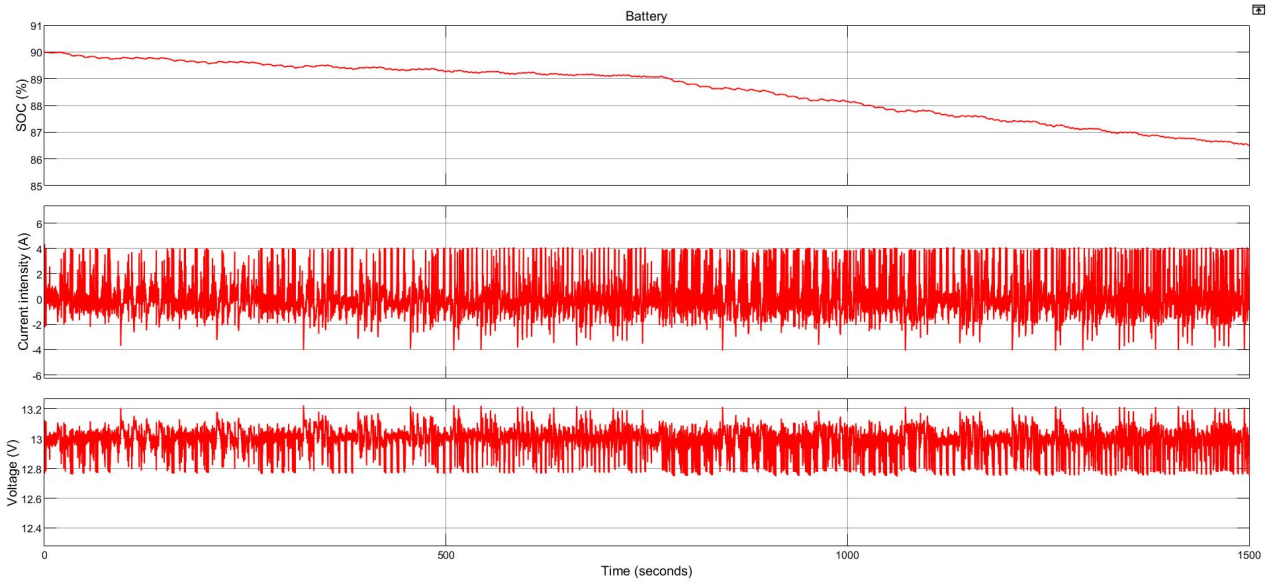


**Figure 6.42:** *Battery response in high-SOC 150W FC full-active hybrid simulation*

In Figure 6.42 it is shown that for the same FC performance, the battery gets depleted faster in the full-active configuration than in the semi-active one. This is due the appearance of the converter between the battery and DC bus. Looking back at equations 4.7 and 4.8, for a given current coming of the boost converter, if the output current of the half-bridge converter needs to cover for the remaining requirements of the load, the current that the battery needs to generate is higher, as increasing its voltage will cause a decrease in the current.

Moreover, the battery isn't operating in safe conditions, as lots of irregularities appear in its current and voltage profiles, even if the system has been provided with big inductors and capacitors. The battery's relevant information related to this cycle can be seen in Table 6.32.

| Variable | Range | Mean | Δ |
|---|---|---|---|
| SOC (%) | [90, 86.49] | - | -3.51 |
| Current (A) | (4, -2) | 0.17 | - |
| Voltage (V) | (13.2, 12.8) | 12.99 | - |
| Current after HB converter (A) | (3.5, -2) | -0.17 | - |

**Table 6.32:** *Battery response in high-SOC 150W FC full-active hybrid simulation*

On the other hand, the evolution of the voltage of the DC bus can be seen in Figure 6.43 and its main information in Table 6.33. Even though the mean voltage is 44 V, it hasn't been possible to control it in a short range of voltages, even when using high capacity capacitors and adjusting its PI controllers. However, though graphically it can appear that the voltage ripple is constant and high, the truth is not that harsh and the voltage has been kept between 43-45V for most of the time.

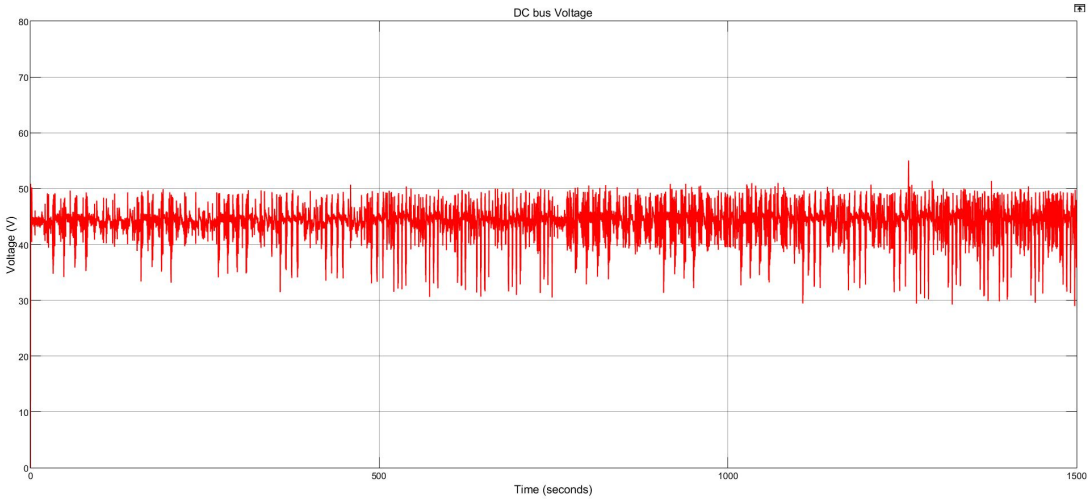


**Figure 6.43:** *Evolution of the voltage of the DC bus in high-SOC 150W FC full-active hybrid simulation*

| Normal Range (V) | Mean (V) | Max (V) | Min (V) |
|---|---|---|---|
| 48-40 | 44.03 | 55.05 | 29.37 |

**Table 6.33:** *DC bus's controlled voltage response in high-SOC 150W FC full-active hybrid simulation*

- Medium-SOC → $SOC_0 = 60\%$

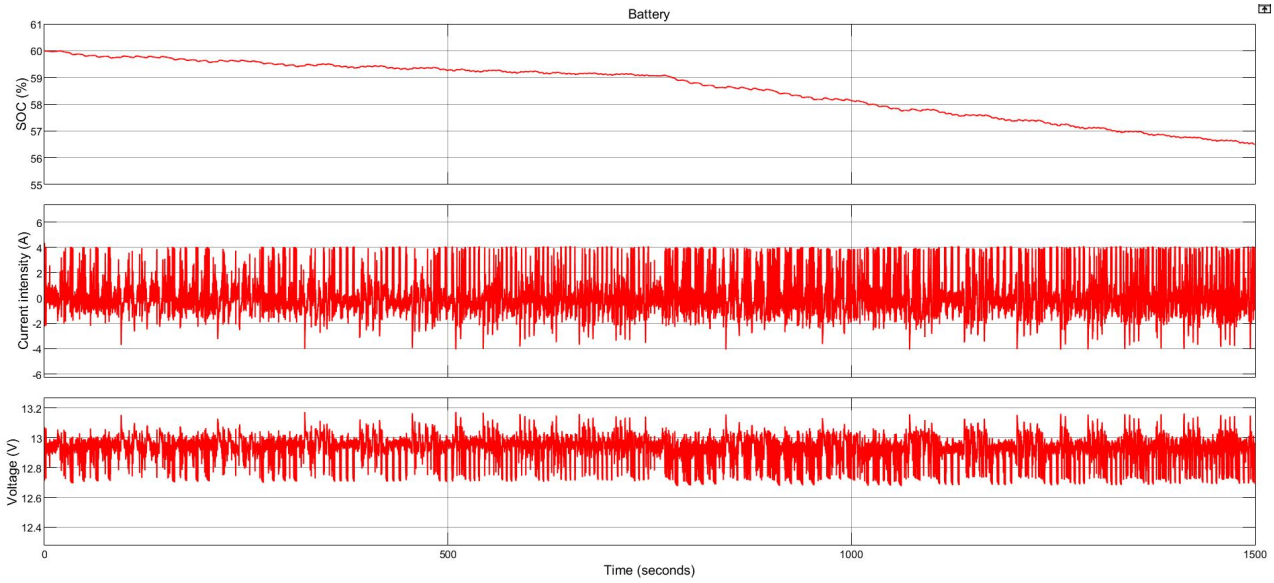


**Figure 6.44:** *Battery response in medium-SOC 150W FC full-active hybrid simulation*

The battery's performance is very similar between the medium and high-SOC case, as it can be seen in Table 6.34, with a battery depletion much quicker than in the semi-active case.

| Variable | Range | Mean | Δ |
|---|---|---|---|
| SOC (%) | [60, 56.48] | - | -3.52 |
| Current (A) | (4, -2) | 0.17 | - |
| Voltage (V) | (13.1, 12.7) | 12.93 | - |
| Current after HB converter (A) | (3.5, -2) | -0.17 | - |

**Table 6.34:** *Battery response in medium-SOC 150W FC full-active hybrid simulation*

On the other hand, the evolution of the voltage of the DC bus is, again, practically equal as the high-SOC case. This shows how the voltage in the DC bus is independent of the state of the batteries. Its profile is not included as no noticeable differences appear with respect to the one shown in Figure 6.43. In Table 6.35 the minimal differences with respect to Table 6.33 can be seen.

| Normal Range (V) | Mean (V) | Max (V) | Min (V) |
|---|---|---|---|
| 48-40 | 44.03 | 55.19 | 29.36 |

**Table 6.35:** *DC bus's controlled voltage response in medium-SOC 150W FC full-active hybrid simulation*

- Low-SOC → $SOC_0 = 20\%$

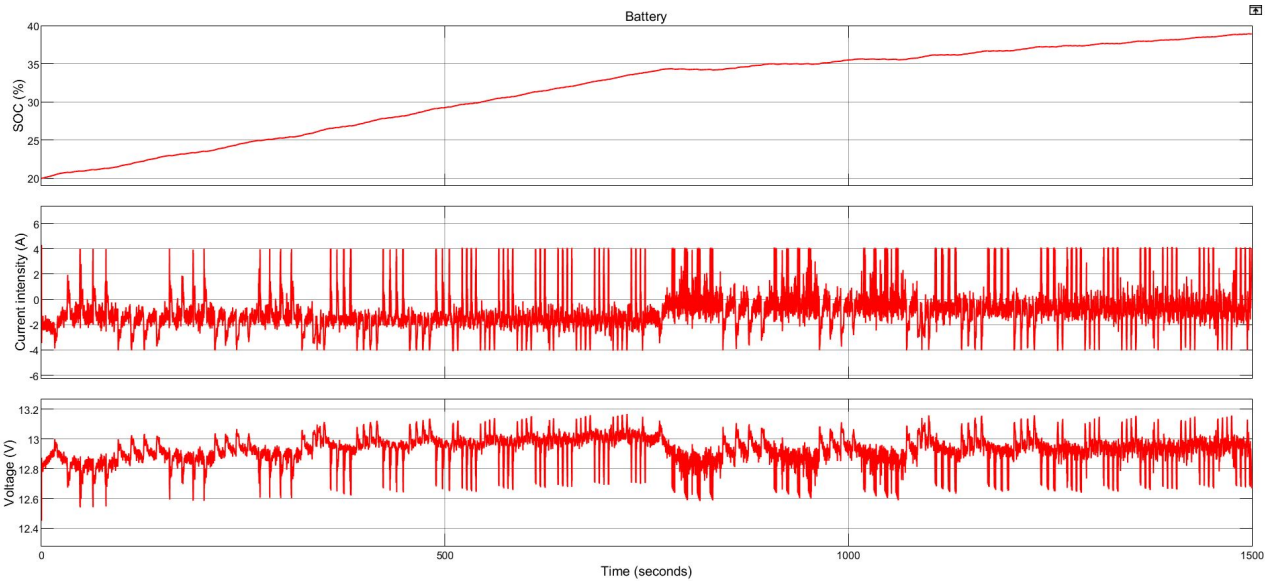


**Figure 6.45:** *Battery response in low-SOC 150W FC full-active hybrid simulation*

In the high and medium-SOC cases of the full-active configuration, it has been seen how the half-bridge converter made the battery provide higher levels of current as the current that arrived to the DC bus decreased when stepping the voltage up. However, when the FC provides more power than necessary, and the extra current is used to charge the batteries, it decreases its voltage when going through the bidirectional converter. As a consequence, the current arriving to the battery is higher, causing a much-faster charge than in the semi-active configuration, where the charge was done at lower rates, thus less damaging conditions for the battery. The battery's performance can be seen in Figure 6.45 and Table 6.36.

| Variable | Range | Mean | Δ |
|---|---|---|---|
| SOC (%) | [20, 38.92] | - | +18.92 |
| Current (A) | (2, -4) | -1.01 | - |
| Voltage (V) | (13.1, 12.6) | 12.93 | - |
| Current after HB converter (A) | (1, -2) | -0.59 | - |

**Table 6.36:** *Battery response in low-SOC 150W FC full-active hybrid simulation*

On the other hand, the evolution of the voltage of the DC bus seems to be better controlled in this case than in the ones related to higher-SOC levels. As no significant difference has been reported between the high and medium-SOC levels, it could be attributed to the fact of having a constant FC current. Its profile and main information are like the ones found in Figure 6.46 and Table 6.37.

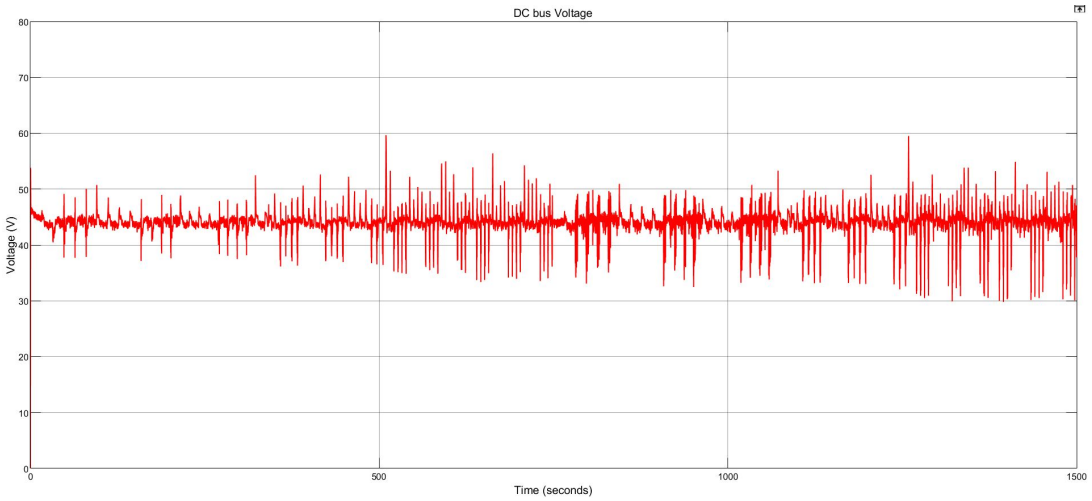


**Figure 6.46:** *Evolution of the voltage of the DC bus in low-SOC 150W FC full-active hybrid simulation*

| Normal Range (V) | Mean (V) | Max (V) | Min (V) |
|---|---|---|---|
| 46-42 | 44.02 | 59.64 | 30.22 |

**Table 6.37:** *DC bus's controlled voltage response in low-SOC 150W FC full-active hybrid simulation*

- Overall performance

The parameters controlled can be seen displayed in Table 6.38.

| Parameter | High-SOC | Medium-SOC | Low-SOC |
|---|---|---|---|
| $H_2$ consumption (g) | 1.38 | 1.38 | 1.78 |
| Ah-throughput (A· h) | 0.383 | 0.462 | 0.868 |

**Table 6.38:** *Performance parameters of the full-active hybrid simulation*

On the qualitative performance aspects, as the performance of the FC has been the same than in the semi-active case, there are no differences with respect to that case, and the FC still has operated under safe conditions. However, with the introduction of the voltage of the DC bus has been hard to stabilize, and though in general it has been kept between 48-40V, high peaks of voltage have appeared. The battery, on its turn, has also worked on discontinuous conditions both in voltage and current.

Comparing it to the results of the 150W FC semi-active configuration, it can be seen that the hydrogen consumption is the same for both configurations, but the introduction of the bidirectional converter has increased substantially battery degradation: the effective Ah-throughput has suffered an increase of a 30% approximately for high and medium-SOC levels, and an important 56% when the extra energy of the FC is used to charge the batteries, as the converter made the recharging currents very high.

# Chapter 7

# The selected powertrain

## 7.1 Selection of the powertrain

To make the selection of the most adequate powertrain different comparisons between the powertrains performances will be done. To do so, the different models will be referred as:

- Passive configuration with a 100W FC → P100
- Semi-active configuration with a 50W FC → SA50
- Semi-active configuration with a 150W FC → SA150
- Full-active configuration with a 50W FC → FA150

The selection will be done using the criteria presented in Section 6.1, regarding constructive aspects, such as availability or component degradation, and performance aspects, such as fulfillment of requirements or hydrogen consumption. Initially, a comparison of the performance parameters is made:

| Parameter | Model | High-SOC | Medium-SOC | Low-SOC |
|---|---|---|---|---|
| ΔSOC (%) | P100 | -0.97 | -0.42 | +0.22 |
| | SA50 | -10.51 | -10.41 | -5.93 |
| | SA150 | -0.86 | -0.73 | +6.16 |
| | FA150 | -3.51 | -3.52 | +18.92 |
| $H_2$ consumption (g) | P100 | 1.11 | 1.13 | 1.16 |
| | SA50 | 1.15 | 1.15 | 1.49 |
| | SA150 | 1.38 | 1.38 | 1.78 |
| | FA150 | 1.38 | 1.38 | 1.78 |
| Ah-throughput (A· h) | P100 | 0.128 | 0.154 | 0.195 |
| | SA50 | 0.421 | 0.500 | 0.695 |
| | SA150 | 0.295 | 0.355 | 0.556 |
| | FA150 | 0.383 | 0.462 | 0.868 |

**Table 7.1:** *Comparison of performance parameters hybrid configurations*

It can be seen that the best performance is given by the passive configuration, with low consumption and battery degradation rates, as well as controllable autonomy, as its battery would only fully deplete if its FC ran out of hydrogen supply. Between the semi-active configurations, the more powerful the FC is, the higher the hydrogen consumption, but at the same time there is a relief in the battery contribution: less current needed from the battery reflect in a decrease of battery degradation and larger autonomy. Lastly, the full-active configuration present the worst performance parameters of all: the hydrogen consumption is the same as the SA150 as its FC performance is equal, but the battery depletion rate increases, and when there is extra power to charge up the batteries, the current entering the battery is too high, resulting in the highest values of the battery degradation indicator, the effective Ah-throughput.

Nevertheless, the decision doesn't just rely on the performance aspects, as the chosen configuration needs to ensure that it can be build and that it fulfills the necessary requirements.

| Model | Constructability | 8 h of minimum autonomy |
|---|---|---|
| P100 | × | ✓ |
| SA50 | ✓ | × |
| SA150 | ✓ | ✓ |
| FA150 | ✓ | ✓ |

**Table 7.2:** *Constructability and requirement's fulfillment analysis*

As it has been commented in its respective sections, the passive model can't be implemented because the integration of its elements is not possible, as the FC needed has a voltage range that can only be found in powerful FCs, making it both an unnecessary higher investment, and battery's impossibility to deal with the high currents generated by the FC. On the other hand, the SA50 model doesn't meet the autonomy requirements, leaving only the SA150 and FA150 models.

The FA150 presents several disadvantages with respect to its semi-active counterpart. Its battery degradation is far worse, it presents added system complexity with more elements which lead to a higher cost, weight and volume, and additionally its control of the DC bus voltage is hard, which leads to harsh current and voltage profiles. Its main advantage is the ability to adapt a low-voltage battery to a higher-voltage environment, which could be the case as the used battery has a low capacity. However, as the actual state of the powertrain already has this low-capacity battery working around 44 V, it is considered unnecessary to now create a system to suit the battery to these operating voltages. For all these reasons, the configuration chosen for the robot's powertrain is the **semi-active hybrid configuration with a 150 W Fuel Cell**.

## 7.2 Sizing of the powertrain

Most of the powertrain's sizing has already been discussed, as it is the power sources sizing or the passive components of the circuit. It can be seen in the following table:

| Group | Component | Sizing |
|---|---|---|
| Power sources | Fuel Cell | 20-cell 150 W |
| | Battery | 2200 mAh, 40 V |
| DC-DC Booster | Diode | $R_{ON}$=0.001 $\Omega$, $V_{ON}$=0.8 V |
| | Inductor | L=100 mH |
| | Capacitor | C=2000 $\mu$F |
| | MOSFET | f=1000 Hz |
| | PI controller | P=1, I=1 |
| Other components | FC Diode | $R_{ON}$=0.001 $\Omega$, $V_{ON}$=0.8 V |
| | Filter | Lowpass G(s) |

**Table 7.3:** *Powertrain's sizing (already discussed elements)*

However, there are still some components related to the FC that need to be sized. The first one is the hydrogen storage tank. It has been discussed in previous sections that as the FC is able to recharge the batteries after one cycle at low-SOC levels, the battery won't be depleted as long as hydrogen is provided to the FC, and thus its autonomy depends only on the amount of hydrogen that can be stored. The amount of time, starting at a state of full-charge, that the robot will operate at battery-only mode and at power-shared mode can be calculated as follows:

$$t_{Bat-only} = (100\% - 90\%) \cdot \frac{1500\ s}{29.32\%} = 511.6\ s \approx 8.5min \tag{7.1}$$

$$t_{Power-Shared} = (90\% - 40\%) \cdot \frac{1500\ s}{0.80\%} = 93750\ s \approx 26h\ 2.5min \tag{7.2}$$

where 0.80% is the average between the battery depletion of the high and medium-SOC levels. It can be seen that the autonomy of the vehicle (in just the high and medium-SOC levels) is far higher than the 8 hours required. The hydrogen needed to provide a minimum autonomy of 8 h of continuous operation is calculated as follows:

$$m_{H_2}(g) = 511.6\ s \cdot 0 + (8h \cdot 3600\ s\ - 511.6\ s) \cdot \frac{1.38\ g\ H_2}{1500\ s} = 26.03\ g\ H_2 \tag{7.3}$$

$$V_{H_2}(std\ l) = 26.03\ g\ H_2 \cdot \frac{1\ mol\ H_2}{2.01588\ g\ H_2} \cdot \frac{23.65\ std\ l}{1\ mol} = 305.33\ std\ l\ H_2 \tag{7.4}$$

This amount of hydrogen represents the total used since the start of the engine at full charge until 8 hours have passed. For this reason, the battery wouldn't be totally depleted after this amount of hydrogen is consumed, as the vehicle could still run some extra time operating at battery-only mode. For this reason, it would be reasonable to adopt a 300 L hydrogen storage tank. However, when comparing commercial low-pressure tanks in *www.fuelcellstore.com*, the only 300 liter tank available, the *MyH2 300* [W5]is more expensive than the 400 liter *CL-400 Metal Hydride* [W6]. Oversizing the hydrogen storage tank can be beneficial as the hydrogen utilization rate is not of a perfect 100% and some hydrogen consumed is not used to effectively produce energy. Additionally, this extra amount of hydrogen can lead to just needing to refill the hydrogen storage tank once every two working days. As the size and weight differences are not important, as it can be seen in Table 7.4, the storage tank selected will be the *CL-400 Metal Hydride*.

| Variable | *MyH2 300* | *CL-400 Metal Hydride* |
|---|---|---|
| Storage capacity (std l) | 300 | 400 |
| Price ($) | 2568 | 1053 |
| Physical volume (l) | 1.21 | 1.36 |
| Mass (kg) | 2.4 | 2.9 |

**Table 7.4:** *Comparison of hydrogen storage tanks [W5,W6]*

On the other hand, the membrane of the fuel cell needs to be moisturized for maintaining a hydrated state, as it provides elevated proton conductivity, which enhances the fuel cell's performance. Therefore, an humidifier is implemented to maintain the mem-

brane's high hydration state [33], and the one selected is a 250 W FC Stack Humidifier [W7], as no less-powerful humidifiers are available.

Finally, one last element needs to be sized, and it's the filter. Although its transfer function G(s) has already been defined in equation 6.11, the sizing of the filter still needs to be done. As it is a first order transfer function with $\tau = 5$, it has its only pole in $s = -1/5$. The cut-off frequency is defined as the point where a fall of 3 dB is found with respect the signal maximal gain, and is approximately found in $\omega_0 = 1/\tau = 0.2\ rad/s$, as it can be seen in its Bode diagram found in Figure 7.1.

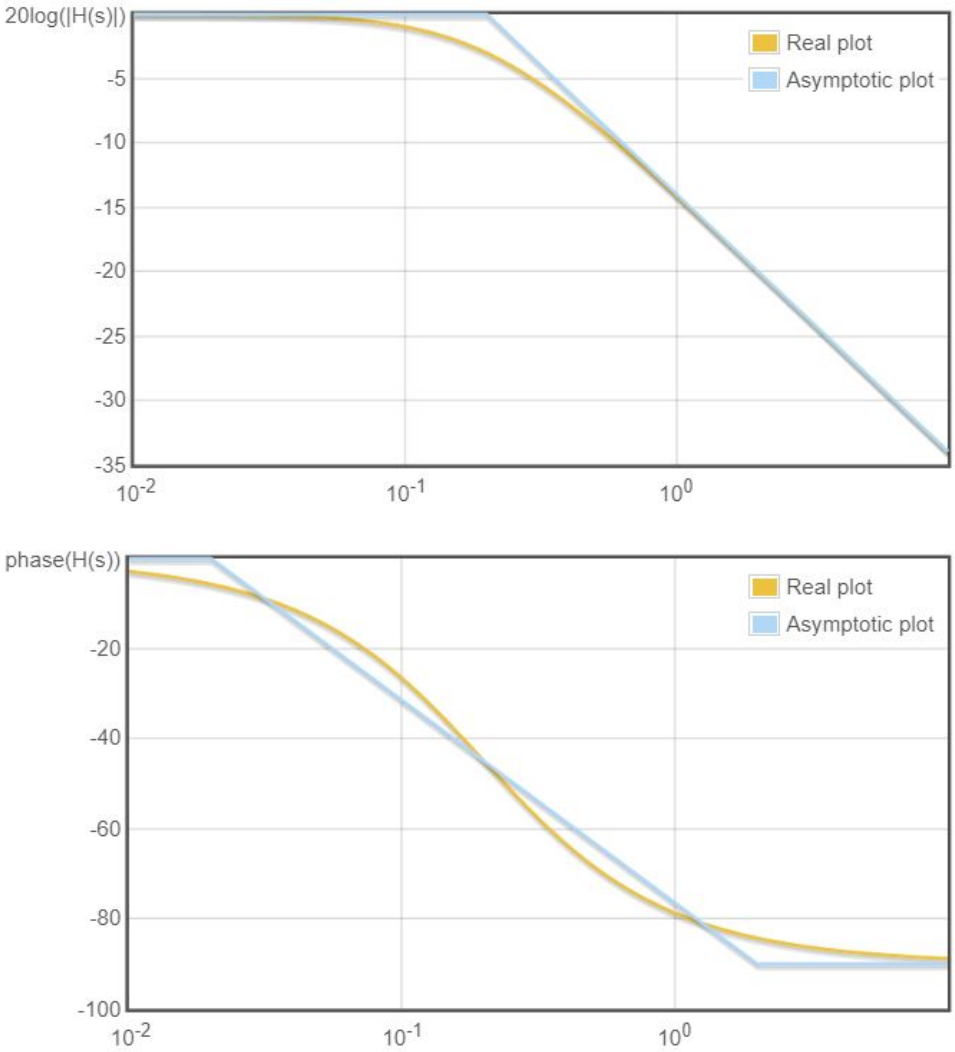


**Figure 7.1:** *Bode diagram for G(s) [W8]*

The most common way to implement a low-pass filter is with a RC circuit, where $\tau = RC \rightarrow \omega_0 = 1/RC$. However, these circuits filter high-frequency ripples in voltage, and the signal that needs to be filtered is current. For this reason, the parallel RC circuit will be implemented, instead of the series one, as they are equivalent following the conversion between the Thévenin and Norton's theorem. The parallel RC circuit can be seen in Figure 7.2

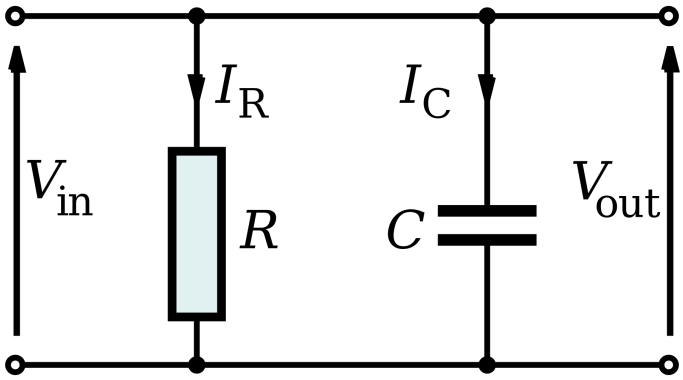


**Figure 7.2:** *Parallel RC circuit [W9]*

As these circuits are equivalent, $\tau = RC = 5$. Thus, the chosen values to implement the RC parallel circuit as the low-pass current filter are:

| Component | Size |
|---|---|
| Resistor | R = 1 kΩ |
| Capacitor | C = 5000 $\mu$F |

**Table 7.5:** *Low-pass current filter's sizing*

# Chapter 8

# Economic and environmental analysis

## 8.1 Budget

In this section an economic analysis of the project will be performed. It will be divided in two sections, a first one with the cost of realizing the study of modeling and sizing the robot's powertrain, and a second one, where the estimated cost of implementing the selected powertrain is found.

### 8.1.1 Cost of the project

The cost of realizing this study can be calculated considering the different costs related to the project. It will be divided in three types: personal, equipment and energetic costs. The licenses of the programs used and access to scientific articles can be considered costless as the license is already purchased by the university.

- **Personal cost**: The personal cost takes into consideration the hours of work of an engineer to do this study. The price set by hour will be of 8€, as it is the price recommended by the UPC for the work of an engineering student. However, if the project had been ordered to an engineering firm, the price paid by hour for a graduated engineer could be around 15€. The time put in the project can be divided in three major lines of work:

  - *Literature research*: Exhaustive literature research has been done in order to create the theoretical frame in which the project has been sustained. 35 articles/books have been referenced in this work, although many more have been researched and read but in the end haven't provided relevant information to the project. The approximate time taken to find, read and analyse the relevant information can be estimated to be around 2 hours for each article, giving a total of 70 hours.
  - *Data processing and simulation*: The processing of the data took approximately 4 hours. On the other hand, designing the simulations and optimizing its parameters has taken an average of 10 hours each simulation (the more complicated models more than that and the simpler ones less). As 4 simulations have been performed (without considering the one related to the actual state), the simulations have taken approximately 40 hours to do.
  - *Report elaboration*: From the 4 months of duration of the project, it is estimated that work has been put in the elaboration of the report in half of those days. This gives a total of 60 days. With a mean of 4 hours of dedication each day, the approximate time that has been needed to do the report elaboration is of 240 hours.

- **Equipment costs**: The main cost has been the need to buy a more powerful computer in order to be able to perform the simulations. The cost of the equipment can be calculated considering its useful life and amortization time, through equation 8.1. The initial value was 999.00€, and the useful life is considered to be 10 years. As it has been used for 3 months, the amortization time is 0.25 years.

$$Cost(€) = \frac{Initial\ value}{Useful\ life} \cdot Amortization\ time = \frac{999.00€}{10\ years} \cdot 0.25 \approx 25€ \qquad (8.1)$$

- **Energy costs**: The hours that the computer has been used are the same as the personal ones, with an addition of 10 extra hours for the time the computer was simulating (definitive simulations and small test to optimize the design of the

model). Considering that 25% of the time the laptop was charging, that the energy consumption when charging is of 0.1 kWh [W10] and taking an average price between high and low energy consumption prices of 0.09185 €/kWh [W11], the energy cost can be calculated as follows:

$$Cost(€) = (70+44+240+10)h \cdot 0.25 \cdot 0.1\ kWh \cdot 0.09185\ €/kWh = 0.84\ € \quad (8.2)$$

Thus, after breaking down the different costs related to the project, the total cost calculation can be seen in Table 8.1:

| Cost type | Activity | Dedication (h) | Price (€) |
|---|---|---|---|
| Personal cost | Literature research | 70 | 560.00 |
| | Data processing and simulation | 44 | 352.00 |
| | Report elaboration | 240 | 1920.00 |
| Equipment cost | Computer amortization | - | 25.00 |
| Energy costs | Computer charging | - | 0.84 |
| **TOTAL** | Total taxes (21%) | | 600.15 |
| | TOTAL PRICE | | **3457.99** |

**Table 8.1:** *Costs of the project*

### 8.1.2 Budget of the implementation

As the battery, driver and electric motor selected will be the ones already present in the actual state of the powertrain, their price does not reflect in the budget of the project. The prices of the FC components are obtained in $, but in the table the price has already been converted to €. On the other hand, the strategy found in [34] will be followed, and the PI controller will be implemented through a Programmable Logic Controller (PLC). The chosen one is the model *Mitsubishi Nexgenie 1000 PLC* [W12]. Also, the filter is

implemented through a 1 k$\Omega$ resistor of 1.12€ [W13] and a 5000 $\mu$F capacitor with a cost of 3.85€ [W14]; the cost of the filter is the sum of them both. The price of the new components of the powertrain, separated in groups, can be seen in the following table (with taxes already included in the price):

| Group | Component | Price (€) |
|---|---|---|
| FC components | Fuel Cell *Protium-150* | 3530.78 |
| | 400 l hydrogen storage tank | 871.72 |
| | Pressure regulator PR-30 | 317.89 |
| | 250 W FC Stack humidifier | 403.99 |
| | FC Diode [W15] | 0.14 |
| DC-DC Booster | Diode [W15] | 0.14 |
| | Inductor [W16] | 89.35 |
| | Capacitor [W17] | 4.19 |
| | Contrallable PWM generator [W18] | 0.40 |
| | MOSFET [W19] | 1.18 |
| | PLC | 283.00 |
| Other components | Lowpass filter | 4.97 |
| **TOTAL** | | **5507.75** |

**Table 8.2:** *Powertrain's cost*

## 8.2 Environmental impact

In order to analyse the impact this project has had in the environment a comparison between the initial and final state will be performed. Initially, an industrial mobile robot worked with an electric powertrain, with a small-capacity battery acting as its only source of power. The robot had a small autonomy, just a little over 1 hour, so it had to be recharged with great frequency. With the implementation of the FC as a complementary source of power, the robot achieves two full working days without charging. Considering the length of a workday as 8 hours and that in the initial state the

robot spent as much time operating as it did recharging, the robot spent 4 hours active and 4 hours recharging in 4 different times. The project has doubled the operating time of the robot, as it has enough endurance to go through the whole day, but also has reduced the energy consumption from recharging in 8 times. Also, although the scope of the project is small and not intended to gain worldwide recognition, having a small impact in whoever it reaches to increase the perception of the need to leave behind the conventional transportation systems and gain confidence in alternative propulsion systems can be beneficial for the environment.

On the other hand, the environmental cost of realizing the project is linked with the energy costs commented in the previous section. The computer has been used an estimated amount of 364 h. Taking into consideration that 25% of that time the computer was charging, and taking an average energy consumption of 0.1 kWh:

$$E_{consumed}\ (kWh) = 364\ h \cdot 0.25 \cdot 0.1\ kWh = 9.1\ kWh \tag{8.3}$$

# Chapter 9

# Conclusions

This project has performed an assessment of the most optimal way to implement a hybrid powertrain in a real industrial mobile robot. The powertrain designed consists in the combination of a fuel cell and the existing robot's battery as parallel sources of power to feed the electric motor's needs. The project can be considered successfully finished as the objectives proposed initially have been achieved. Therefore, several conclusions can be extracted from this work.

In the first place, an introduction to the actual state of the automotive and industrial equipment industry has been done. The different major propulsion systems have been presented and its strengths and weaknesses identified, as well as the role they can play in the incoming future. Thus, the underlying environmental problems of the conventional combustion engines have been commented, and an analysis of the different alternative propulsion systems has been performed. The focus has been put on battery-electric powertrains and hybrid configurations, and the drawbacks that need to be overcome in order to have a worldwide adoption of these greener propulsion systems.

One of the most promising hybrid configurations consist of combining a fuel cell with an energy storage system, as it overcomes the limitations of the actual battery-electric powertrains, while minimizing the high environmental damage the conventional powertrains do. Therefore, the different ways to implement this hybrid system have been

studied and afterwards tested in a real application. The testing has been performed in an industrial mobile robot, which is initially operating with an electric powertrain with a small-capacity battery working as its only power source. Using *Matlab's Simulink* module, passive, semi-active and full-active configurations have been tested, depending on the control system of the configuration and sizing of its elements. The optimal solution has been selected following the optimization criteria stated in section 6.1, taken into consideration constructive, performance and component degradation aspects.

Although the passive architecture presents excellent results in the performance of the powertrain, with low hydrogen consumption and high autonomy, the integration of the fuel cell and the battery had some requirements impossible to fulfill with the components found in the market. On the other hand, the full-active configuration presented improvements in the constructive aspects as the battery and fuel cell could be designed independently from the load, but its performance and component degradation parameters were poor when compared to the other architectures presented. The battery's depletion rate was high, and the control of the DC bus not effective, as it was not possible to stabilize the voltage of the DC bus to 44 V, as the load profiles were irregular and fast-changing.

Therefore, the decided model has been the semi-active configuration, with a DC-DC boost converter between the FC and the DC bus, which has allowed a precise control of the system and safe-operating conditions in the fuel cell. Initially, a 50 W FC has been tested, but has resulted to be not powerful enough, which has lead to insufficient robot's autonomy. Thus, the selected fuel cell has been the *Protium-150*, a 150 W model. The fuel cell won't have to work at full-power, and will normally operate below the 100 W of power. The selection of this fuel cell has been done because the price of this 150 W FC was lower than the price of a 100 W FC from another brand. Additionally, it can provide extra power if it is needed in future applications. The higher power of the fuel cell has lead to higher hydrogen consumption rates. However, the contribution of the battery is lower, leading to a minimization of the battery's degradation and an optimization of the robot's autonomy.

# Acknowledgements

First and foremost, I would like to express my deepest gratitude to my project tutor, Ramon Costa-Castelló, for giving me the opportunity of taking part of this challenging project. Not only has he been such a great guide, but he has also motivated me greatly by expressing its interest in the project's development and challenging me with new objectives throughout the work.

Furthermore, I would like to express my most sincere gratitude to my family, friends and every single person who has shown interest in the project and encouraged me throughout these months. I really appreciate their constructive criticism, or just the fact of being there to listen to me, which has been essential for my personal motivation and improvement.

# Bibliography


[1] Barbir Frano. *PEM Fuel Cells: Theory and Practice*. Elsevier B.V, 2005.

[2] Ron Bousso. BP energy outlook sees global fossil fuel demand falling for first time this year. *Institute for Energy Economics and Financial Analysis*, 2020.

[3] Jens Burchardt, Patrick Herhold, Joonas Päivärinta, and Stefan Schönberger. Have We Passed Peak Demand for Fossil Fuels? *BCG*, sep 2020.

[4] Vicente Roda, Javier Carroquino, Luis Valiño, Antonio Lozano, and Félix Barreras. Remodeling of a commercial plug-in battery electric vehicle to a hybrid configuration with a PEM fuel cell. *International Journal of Hydrogen Energy*, 2018.

[5] Mark A. Delucchi and Timothy E. Lipman. *Lifetime Cost of Battery, Fuel-Cell, and Plug-in Hybrid Electric Vehicles*. Elsevier B.V, 2010.

[6] Shailendra Jain and Lalit Kumar. Fundamentals of Power Electronics Controlled Electric Propulsion. In *Power Electronics Handbook*. 2018.

[7] EG&G Technical Services. *Fuel Cell Handbook (7th edition)*. National Energy Technology Laboratory, 2004.

[8] J. H. Hirschenhofer, D. B Stauffer, R. R. Engleman, and M. G. Klett. *Fuel Cell Handbook (4th edition)*. Federal Energy Technology Center (FETC), 1998.

[9] Daisie D. Boettner and Michael J. Moran. Proton exchange membrane (PEM) fuel cell-powered vehicle performance using direct-hydrogen fueling and on-board methanol reforming. *Energy*, 2004.

[10] M. H. Eikani, A. Eliassi, N. Khandan, and V. R. Nafisi. Design and fabrication of a 300W PEM fuel cell test station. *Procedia Engineering*, 2012.

[11] Mounir Nasri, Inga Burger, Schier Michael, and Horst E. Friedrich. Waste heat recovery for fuel cell electric vehicle with thermochemical energy storage. *2016 11th International Conference on Ecological Vehicles and Renewable Energies, EVER 2016*, 2016.

[12] O. S. Ijaodola, Zaki El- Hassan, E. Ogungbemi, F. N. Khatib, Tabbi Wilberforce, James Thompson, and A. G. Olabi. Energy efficiency improvements by investigating the water flooding management on proton exchange membrane fuel cell (PEMFC). *Energy*, 2019.

[13] Julio Luna, Ramon Costa-Castelló, and Stephan Strahl. Chattering free sliding mode observer estimation of liquid water fraction in proton exchange membrane fuel cells. *Journal of the Franklin Institute*, 2020.

[14] Hiroshi Ito, Tetsuhiko Maeda, Akihiro Nakano, and Hiroyasu Takenaka. Properties of Nafion membranes under PEM water electrolysis conditions. *International Journal of Hydrogen Energy*, 2011.

[15] Lei Chen, Yi Fan Wang, and Wen Quan Tao. Experimental study on the effect of temperature and water content on the thermal conductivity of gas diffusion layers in proton exchange membrane fuel cell. *Thermal Science and Engineering Progress*, 2020.

[16] M. Han, J. H. Xu, S. H. Chan, and S. P. Jiang. Characterization of gas diffusion layers for PEMFC. *Electrochimica Acta*, 2008.

[17] Lei Xing, Weidong Shi, Huaneng Su, Qian Xu, Prodip K. Das, Baodong Mao, and Keith Scott. Membrane electrode assemblies for PEM fuel cells: A review of functional graded design and optimization. *Energy*, 2019.

[18] Fuxiang Huang, Diankai Qiu, Shuhuai Lan, Peiyun Yi, and Linfa Peng. Performance evaluation of commercial-size proton exchange membrane fuel cell stacks considering air flow distribution in the manifold. *Energy Conversion and Management*, 2020.

[19] Mauro Carignano, Vicente Roda, Ramon Costa-Castello, Luis Valino, Antonio Lozano, and Felix Barreras. Assessment of Energy Management in a Fuel Cell/Battery Hybrid Vehicle. *IEEE Access*, 7, 2019.

[20] Mauro G. Carignano, Ramon Costa-Castelló, Vicente Roda, Norberto M. Nigro, Sergio Junco, and Diego Feroldi. Energy management strategy for fuel cell-supercapacitor hybrid vehicles based on prediction of energy demand. *Journal of Power Sources*, 360, 2017.

[21] Yujie Wang, Zhendong Sun, and Zonghai Chen. Development of energy management system based on a rule-based power distribution strategy for hybrid power sources. *Energy*, 175, 2019.

[22] Kevin Kendall and Nathan Jinlei Shang. *Hydrogen utilization: benefits of fuel cell–battery hybrid vehicles*. INC, 2020.

[23] Eduardo López González, Jaime Sáenz Cuesta, Francisco J. Vivas Fernandez, Fernando Isorna Llerena, Miguel A. Ridao Carlini, Carlos Bordons, Emili Hernandez, and Alberto Elfes. Experimental evaluation of a passive fuel cell/battery hybrid power system for an unmanned ground vehicle. *International Journal of Hydrogen Energy*, 44(25), 2019.

[24] P. Di Trolio, P. Di Giorgio, M. Genovese, E. Frasci, and M. Minutillo. A hybrid power-unit based on a passive fuel cell/battery system for lightweight vehicles. *Applied Energy*, 279(July):115734, 2020.

[25] Souleman Njoya Motapon, Louis A. Dessaint, and Kamal Al-Haddad. A comparative study of energy management schemes for a fuel-cell hybrid emergency power

system of more-electric aircraft. *IEEE Transactions on Industrial Electronics*, 61(3), 2014.

[26] Saurabh Kumar, Rajat Kumar, and Navdeep Singh. Performance of closed loop SEPIC converter with DC-DC converter for solar energy system. *2017 4th International Conference on Power, Control and Embedded Systems, ICPCES 2017*, 2017-Janua(March), 2017.

[27] Damien Guilbert, Arnaud Gaillard, Ali Mohammadi, Abdoul N'Diaye, and Abdesslem Djerdir. Investigation of the interactions between proton exchange membrane fuel cell and interleaved DC/DC boost converter in case of power switch faults. *International Journal of Hydrogen Energy*, 40(1), 2015.

[28] Jérôme Bernard, Sebastien Delprat, Felix N. Büchi, and Thierry Marie Guerra. Fuel-cell hybrid powertrain: Toward minimization of hydrogen consumption. *IEEE Transactions on Vehicular Technology*, 58(7), 2009.

[29] Jorge Garcia, Pablo Garcia, Fabio Giulii Capponi, and Giulio De Donato. Analysis, modeling, and control of half-bridge current-source converter for energy management of supercapacitor modules in traction applications. *Energies*, 11(9), 2018.

[30] Akash Pathak and Vikas Sahu. Review & study of bidirectional of DC-DC converter topologies for electric vehicle application. *International Journal of Science,Engineering and Technology*, 3(6), 2015.

[31] Simona Onori, Pierfrancesco Spagnol, Vincenzo Marano, Yann Guezennec, and Giorgio Rizzoni. A new life estimation method for lithium-ion batteries in plug-in hybrid electric vehicles applications Pierfrancesco Spagnol Vincenzo Marano Yann Guezennec and Giorgio Rizzoni. *Int. J. Power Electronics*, 4(3), 2012.

[32] P. Wang, L. Yang, H. Wang, D. M. Tartakovsky, and S. Onori. Temperature estimation from current and voltage measurements in lithium-ion battery systems. *Journal of Energy Storage*, 34(November 2020), 2021.

[33] Chen Yu Chen, Jian Hao Su, Hafiz Muhammad Ali, Wei Mon Yan, and Mohammad Amani. Effect of channel structure on the performance of a planar membrane humidifier for proton exchange membrane fuel cell. *International Journal of Heat and Mass Transfer*, 163, 2020.

[34] Dubey. H Ramavatar. S, Sharma. A. PLC Based Pid Implementation in Process Control of Temperature Flow and Level. *International Journal of Advanced Research in Engineering and Technology (IJARET)*, 6(1), 2015.

# Web References

[W1] https://www.fuelcellstore.com/fuel-cell-stacks/medium-power-fuel-cell-stacks/greenhub-2-pro-500

[W2] https://www.fuelcellstore.com/fuel-cell-stacks/5w-100w-fuel-cell-stacks/protium-50

[W3] https://www.fuelcellstore.com/fuel-cell-stacks/5w-100w-fuel-cell-stacks/greenbox-2-100

[W4] https://www.fuelcellstore.com/fuel-cell-stacks/medium-power-fuel-cell-stacks/protium-150-fuel-cell-stack

[W5] https://www.fuelcellstore.com/hydrogen-equipment/hydrogen-storage/my-h2-300-hydrogen-storage

[W6] https://www.fuelcellstore.com/hydrogen-equipment/hydrogen-storage/cl-400-metal-hydride

[W7] https://www.fuelcellstore.com/hydrogen-equipment/humidification-systems/fuel-cell-stack-humidifier-250w

[W8] http://www.onmyphd.com/?p=bode.plot.online.generator

[W9] https://en.wikipedia.org/wiki/RC_circuitParallel_circuit

[W10] https://smarterbusiness.co.uk/blogs/how-much-energy-do-my-appliances-use-infographic

[W11] https://tarifasgasluz.com/comparador/precio-kwh

[W12] https://www.indiamart.com/proddetail/nexgenie-1000-plc-19556466955.html

[W13] https://www.mouser.es/ProductDetail/KOA-Speer/RN73H2BTTD1001B10/?qs=sGAEpiMZZMtlubZbdhIBIC1okK3GxFAVM3YojsRo%252B2s%3D

[W14] https://www.mouser.es/ProductDetail/Nichicon/UXY1V502MHW/
?qs=sGAEpiMZZMsh%252B1woXyUXj6NiChfwzFay6k9SCuf4gj0%3D

[W15] https://www.mouser.es/ProductDetail/Vishay-Semiconductors/BAV20-TR?qs
=W9YKNzyuRaYLJRe6jQ1L4A%3D%3Dmgh=1vip=1gclid=Cj0KCQiA3Y-
ABhCnARIsAKYDH7s2HY5jzFgFTvIo4tDmgDvXDfXsf7U2RMo697sWPO3ej74_9Bo5KhYaAr94EALw_w

[W16] https://www.mouser.es/ProductDetail/Hammond-Manufacturing/195T5/
?qs=sGAEpiMZZMv126LJFLh8y2NIeaEvvx3Dt4fkdNgTy2o%3D

[W17] https://www.mouser.es/ProductDetail/United-Chemi-Con/EGVD500ELL202MM30H/
?qs=sGAEpiMZZMvwFf0viD3Y3YB0YelrAivsgrZTxDYmHunh7%2FY81ZmzCQ%3D%3D

[W18] https://www.mouser.es/ProductDetail/ON-Semiconductor/NCP4328ASNT1G/
?qs=xGcJQ%252BnsJwuysiuO%252BfAHwQ%3D%3D

[W19] https://www.mouser.es/ProductDetail/Vishay-Siliconix/
IRFR010PBF-BE3/?qs=zW32dvEIR3sojEq2SMtqHw%3D%3D

# List of Figures

# List of Tables